UNIVERSITÀ DELLA CALABRIA

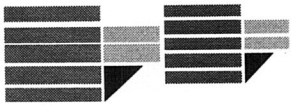

UNIVERSITÀ DEGLI STUDI DELLA CALABRIA
DIPARTIMENTO DI FISICA

BERNARDINO TELESIO – DOCTORATE SCHOOL OF SCIENCE AND TECHNIQUE

TESI DI DOTTORATO DI RICERCA IN FISICA DEI SISTEMI COMPLESSI

CICLO XXIV

SETTORE DISCIPLINARE
02/B1

Electronic and vibrational properties of ultrathin layers adsorbed on metal surfaces

DIRETTORE DELLA SCUOLA

Prof. Roberto Bartolino

COORDINATORE

Prof. Vincenzo Carbone

SUPERVISORE

Prof. Gennaro Chiarello

DOTTORANDO

Antonio Raimondo Marino

ANNO ACCADEMICO 2010/11

Acknowledgements

I wish to express here my gratitude to my supervisor, Prof. Gennaro Chiarello, for giving me the opportunities for cultural and human growth and the chance to learn from his expertise in the field. His willingness to answer all the questions I have had and his ability to recognize interesting research topics at an early stage have been indispensable for the results presented in this thesis.

I have also benefited a lot from numerous interesting discussions with colleagues from the SPES group, special thanks in this regard go to Antonio Politano who has always been prepared to answer a diversity of scientific questions and whose help was essential for the development of this work.

I am deeply indebted and grateful to Salvatore Abate, Myrsini Antoniou, Tommaso Caruso, Giovanni Desiderio, Vincenzo Formoso and Alfonso Policicchio for their ongoing support of my work, their stimulating discussions and keen suggestions, for creating a wonderful place to work.

The work with them has not only scientifically been fruitful, but it has also substantially enriched the experience of the past years. Thank you very much for the science and the fun.

This experience will be one of the most important and significant landmarks of my life.

CONTENTS

1 Introduction

On December 1959, in a famous and almost prophetic speech at Caltech, entitled "There is plenty of room in the bottom"[1], Richard Feynman, as a matter of fact, gave rise to the global research in nanoscience. He predicted exciting new phenomena that might revolutionize science and technology and affect our everyday lives, if only we could get precise control over matter, down to the atomic level:

«I would like to describe a field, in which little has been done, but in which an enormous amount can be done in principle. This field is not quite the same as the others in that it will not tell us much of fundamental physics (in the sense of, "What are the strange particles?") but it is more like solid-state physics in the sense that it might tell us much of great interest about the strange phenomena that occur in complex situations. Furthermore, a point that is most important is that it would have an enormous number of technical applications.

What I want to talk about is the problem of manipulating and controlling things on a small scale ».

The evolution predicted by Feynman could hardly be realized if it had not found a fertile ground due to the scientific and technological discoveries in the field of condensed matter physics and physical-chemistry, since the year 1940-50. Indeed, by the mid-1960s, technological innovation had progressed to the point that apparatus for generating Ultra High Vacuum (UHV 10^{-8}- 10^{-11} mbar) was available and could be combined in commercial instrumentation with electron, ion, and photon sources, versatile sample manipulators, and detectors for the measurement of scattered electron, photon, and ion beams.

[1] Feynman, R. P. There's plenty of room at the bottom. *Eng. Sci.* 23, 22–36 (1960).

A UHV environment is essential for surface science experimentation because UHV pressures are required for a surface to remain stable for the time required (i.e., hours) to characterize its composition and structure. Moreover, in low-energy range (1-10^2 eV) the inelastic-collision mean free paths for electrons are only a few angstroms, leading to the most important conclusion that electrons elastically scattered by or emitted from the solid must have come from the top few atomic layers. This combination of readily available technology for electron scattering and emission experiments in UHV, single crystal samples, and the insight that these experiments probe the surface rather than the bulk of a solid set off an explosion of activity, beginning in the late 1960s, that defined surface science research as we know it today.

Surfaces and interfaces are everywhere. They are found in systems as simple as a piece of metal in a vacuum, and as complex as biological cells and living organisms. They define a boundary with the surrounding environment and influence interactions with that environment. Today both the atomic composition and the atomic geometries of single crystal solid surfaces (and of ordered adsorbed overlayers thereupon) can be determined routinely by surface-sensitive electron spectroscopy in UHV environments. Dynamics of the evolution of simple diffusion, growth, and chemical reactions is taken as given. Moreover, surfaces, as entities unto themselves, are no longer interesting objects of study. What is of interest is what they reveal, e.g., about the nature of nanostructures; what they do, e.g., catalyze highly complex reactions; and what they can be used for, e.g., as templates for a new generation of computers or the basis for a complex technologies like semiconductor nanoelectronics fabrication. These complementary developments are different aspects of nanotechnology, which aims to create

and use structures, devices and systems in the size range of about 0.1–100 nm (covering the atomic, molecular and macromolecular length scales).

On this length scales, matter exhibits surprising properties such as atoms or molecules ability of self-assembly at well-defined surfaces. Self-organized growth and self-assembly at surfaces can serve as an efficient and versatile tool for creating low-dimensional nanostructures, i.e., systems in zero, one, and two dimensions. Dimensionality is one of the most defining materials parameters; the same chemical compound can exhibit dramatically different properties depending on whether it is arranged in a 0D, 1D, 2D, or 3D crystal structure. (e.g. quantum points or carbon nanoaggregates – nanotubes and nanowires, fullerenes, graphene…). While quasi 0D, quasi 1D and of course 3D crystal structures have been and are widely studied, the research on two dimensional crystals has been minimal until the recent (2004) experimental realization of two dimensional atomic crystals [1].

The new millennium led us into the "age of designer materials", when complex materials are designed to have desired properties, with both basic and technological applications. Energy production and storage could benefit from, e.g., new generations of improved catalysts with a reduction in noble metal concentration, new fuel cells (also biofuel), new batteries of advanced design, new lightweight nanostructured solids able to ensure an efficient hydrogen storage. Moreover, low-cost photovoltaic solar cells based on nanomaterials are being developed.

The application of this new technologies in almost all fields of human activity, may soon allow us detachment from traditional energy sources with significant consequences for environmental protection and for our own survival.

In this thesis, high-resolution electron energy loss spectroscopy (HREELS) was used to investigate both the vibrational and electronic properties of ultrathin layers grown on metal substrates and their interaction with reactive species such as carbon monoxide, oxygen, and water.

In chapter 2, we introduce our measurement techniques, in chapters 3, 4 and 5, low energy electron diffraction (LEED) and HREEL spectroscopy has been used for studying monolayer graphene epitaxially grown on Pt(111) surface. Graphene layers were grown on the surfaces of many transition metals upon annealing in a hydrocarbon atmosphere. What is nowadays a technique, was an unwanted side effect in catalytic processes, as it lead to the passivation of catalysts, known as poisoning. The chemical deposition of carbon on metal substrates has been extensively studied from the 1970s to 1990s [2-7]. A major motivation for studying these graphite films was the passivation of catalysts by carbon films known as poisoning, but the properties of graphene were not investigated in detail. The main scientific interest are the consequences of the unique band structure of graphene. The high mobility of electrons in graphene and the strong electric field effect encourage work to realize graphene-based electronics [8-15].

Graphene is lightweight, inexpensive, robust, chemically stable. Moreover, the use of graphene for transparent conducting electrodes [16-18], to realize photosensitive transistors [19], ultracapacitors [20, 21], or novel chemical sensors [22-27] is envisioned. Due to the increasing importance of graphene, it is desirable to obtain a thorough understanding of the structure of graphene on metals and of its interplay with the underlying substrate. Graphene is manufactured mainly in three ways: by exfoliation from highly oriented pyrolytic graphite (HOPG) [28-34], by the epitaxial growth in silicon carbide [35-54] and by the epitaxial growth on metals [55-84]. Exfoliation of

graphene was the basis for the exploration of the exciting electronic properties of graphene. They were primarily explored with transport measurements of devices built on flakes of exfoliated graphene on SiO_2. Nevertheless there appears to be consensus, that for future scientific exploration and technological applications, epitaxial growth of high quality graphene over large areas is mandatory.

Last chapter, HREELS has been used to investigate the adsorption and co-adsorption of oxygen and CO on the $Pt_3Ni(111)$ surface and, for the sake of comparison, on the Pt(111) surface. The adsorption of chemical species onto metallic substrates has attracted considerable interest in recent years for both fundamental interest and technological applications [85-87]. The presence of adsorbed atoms significantly changes the physical and chemical properties of the substrate. Understanding the electronic properties of surfaces and interfaces would imply the tailoring of more selective catalysts and an improvement of electronic devices. Also the investigation of bimetallic systems is currently the topic of interest in surface and catalytic science. A number of interesting phenomena such as segregation, faceting, reconstruction and chemical oscillations, which have direct correlation with the atomic scale modifications of these surfaces are emerging in this field. Most real catalysts consist of alloys of 3*d*, 4*d* and 5*d* elements [88-91]. Generally, these systems are characterized by a superior chemical activity and selectivity with respect to the pure elements [92].

2 Experimental methods

2.1 Ultra High Vacuum chamber

In Figure 2.1 is shown the Ultra High Vacuum (UHV) chamber (with a base pressure of $5 \cdot 10^{-9}$ Pa) used for our experiments.

Our system is a stainless steel vacuum chamber with a variety of pumps attached, which allows us to obtain UHV. The pumps used on our system include a scroll pump, two turbo pumps, a titanium sublimation pump and an ion pump. It is equipped with an electron analyser (Phoibos 100, Specs), a high-resolution electron energy loss spectrometer (Delta 0.5, Specs, Figures 2.7, 2.8), an apparatus for low-energy electron diffraction, a quadrupole spectrometer, and an ion gun for sputtering. Leak valves are used for controlled gas inlet in the UHV chamber.

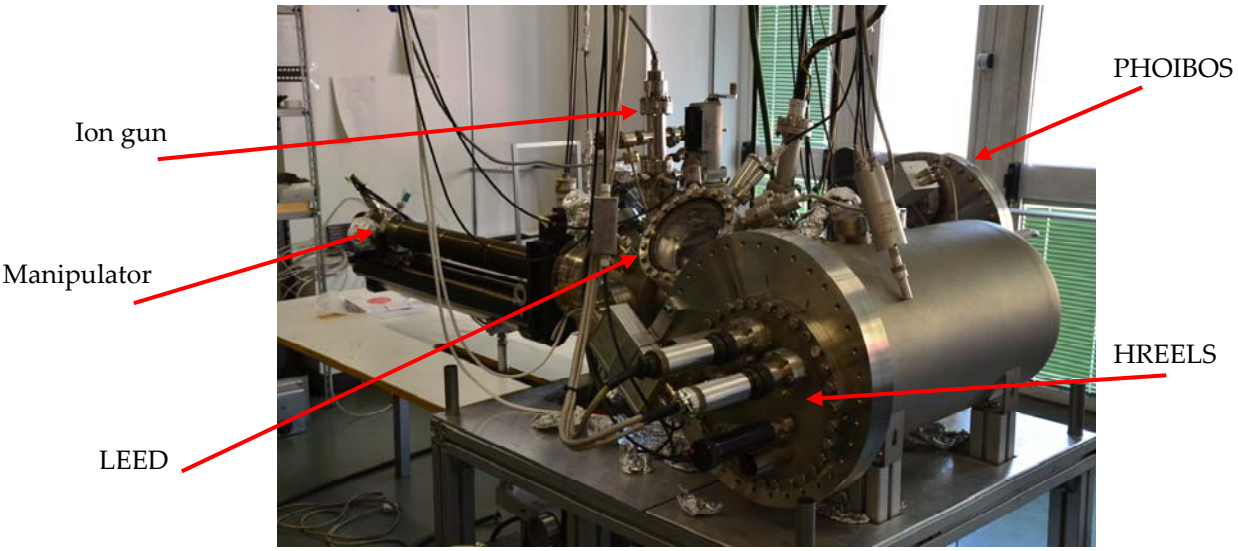

Figure 2.1: UHV chamber used for experiments. SPES-Lab. UNICAL.

Auger electron spectroscopy (AES) and low-energy electron diffraction (LEED) were used as control techniques for checking the cleanliness of the order of the surface.

The sample was a single crystal of Pt(111), delivered from MaTecK GmbH (Germany). The substrate was cleaned by repeated cycles of ion sputtering and annealing at 1300 K. Surface cleanliness and order were checked using Auger electron spectroscopy (AES) and low-energy electron diffraction (LEED) measurements, respectively.

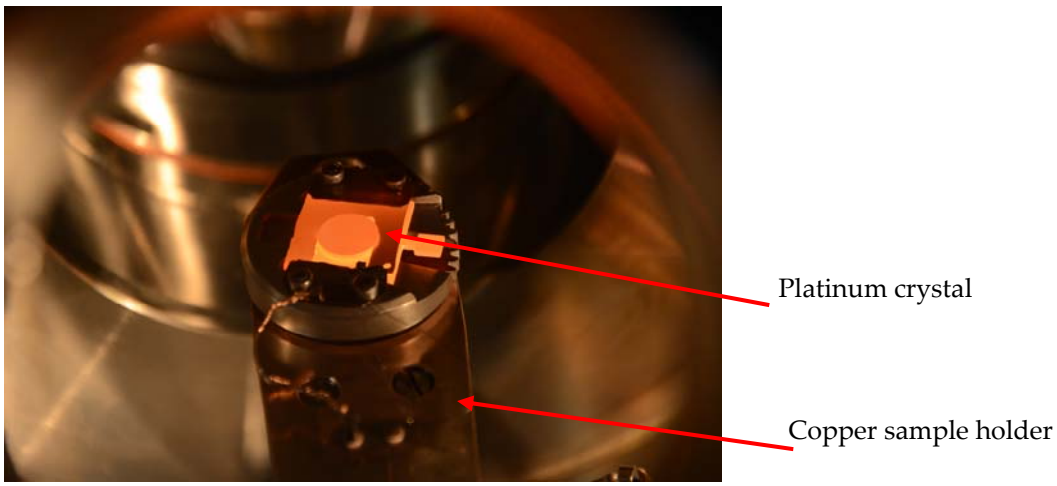

Figure 2.2: Sample during an annealing cycle.

2.2 The EELS technique

EELS (Electron energy loss spectroscopy) is an experimental technique that permit the study of materials through the analysis of their electronic and vibrational excitations. In contrast to infrared spectroscopy, EELS is not limited by strict dipole selection rules, which often hinder observation of important modes and adsorbates. In EELS both long-range *dipole* and short-range *impact* scattering mechanisms are operable and they may be effectively studied as a function of scattering angle and impact energy. Information

obtained from EELS ideally complements data obtained with other surface spectroscopies, and offers ease of interpretation for the experimentalist.

In this spectroscopy, a monochromatic electron beam is sent to the surface of a solid material, these primary electrons are partially inelastically scattered and their kinetic energy distribution is analyzed using an electron energy analyzer [93], the energy losses are due to the excitation of electronic and vibrational transition of the investigated materials and so provide a tool for analysing them. The EELS technique can be used in various configurations by changing the geometrical and physical parameters. For example different spectra and information can be obtained by changing the electronic energy or the incidence angle of the impinging primary beam, or the angle of analysis of diffused electrons [93].

The various excitations in a EEL spectrum cover a wide energy range which extends from some meV, as for phonons and vibrations of atoms or molecules adsorbed onto the surface, some eV, as for interband transitions and plasmonic excitations, up to hundreds of eV, as for the excitations of core electrons [94] (figure 2.3).

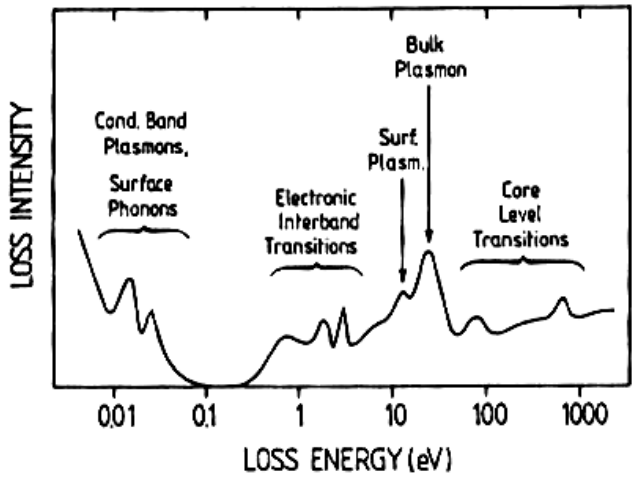

Figure 2.3: Regions of characteristic losses. Taken from [94].

Energy losses are due mainly to three processes:

1) excitations of network vibrations of atoms on the clean surface (optical phonons surface, acoustic phonons surface) and / or vibrations of atomic and molecular species adsorbed on the surface;

2) excitations of valence band transitions that can be divided into single particles electronic excitations (inter-band and intra-band excitations) and collective excitations (surface, volume and interface plasmons);

3) excitations of core levels electrons to conduction band levels.

The mentioned excitations hold a very large energy range, which extends from around tens meV (for phonons) up to a few thousands eV needed to excite core electrons to states above the Fermi level.

Thus, EELS plays an important role in the investigation of surface chemical reactions [95-106] and dynamic screening properties [59, 107-116] of metal systems.

The great diffusion of this technique in the last two decades is mainly due to the development of a new generation of high-resolution EEL spectrometers by prof. Harald Ibach [117, 118], whose resolution ranges from 0.5 to 5 meV. This allows HREELS to have an energy resolution similar to inelastic helium atom scattering [119-124] and optical techniques as infrared absorption spectroscopy [125-128] or second-harmonic generation [129-132]. The recent development of novel spectrometers for spin-polarized EELS [133, 134] is expected to further contribute to the diffusion of this spectroscopy.

The analysis of kinetic energy of electrons inelastically back-scattered provides information about excited modes at the surface. Electrons scattered from the sample are analyzed as a function of $E_{loss} = \Delta E = E_p - E_s$, where E_{loss} is the energy lost by electrons, E_P is the primary electron beam energy, and E_s is the energy of scattered electrons. If the electron excites a surface mode

$\hbar\omega_0$, after the interaction with the sample its energy will be $E_s = E_p - \hbar\omega_0$. Hence, if electrons lost E* they will give rise to loss peaks at energy E_p-E*.

In inelastic processes the energy change should equal the quantum energy of an electronic or vibrational surface mode, by respecting conservation laws of energy and wave-vector parallel to the surface.

$$\begin{cases} E_{loss} = E_p - E_S & (2.1) \\ \hbar\vec{q}_{\parallel} = \hbar(\vec{k}_i \sin\theta_i - \vec{k}_S \sin\theta_S) & (2.2) \end{cases}$$

Where $q_{\parallel}$ is the parallel momentum transfer, $\vec{k}_i$ is the wave-vector of incident electrons, $\vec{k}_s$ is the wave-vector of scattered electrons, θ_i and θ_s are the angles formed with the normal to the surface by incident and scattered electrons, respectively (figure 2.3).

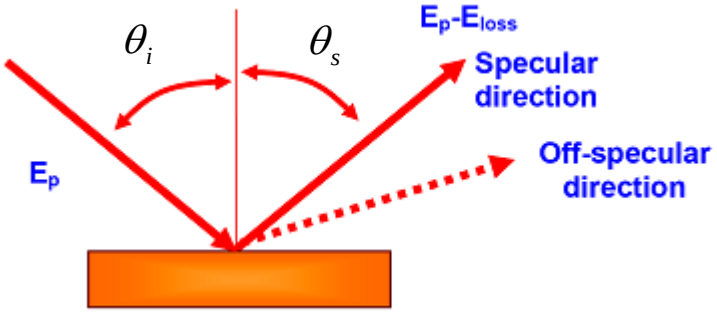

Figure 2.4: Scattering geometry in HREELS experiments

Thus an expression linking $q_{\parallel}$ with E_p, E_{loss}, and θ_i, θ_s could be obtained:

$$q_{\parallel} = \frac{\sqrt{2mE_p}}{\hbar}(\sin\theta_i - \sqrt{1 - \frac{E_{loss}}{E_p}}\sin\theta_S) \quad (2.3)$$

Likewise, it is possible to obtain the indeterminacy on $q_{\parallel}$, that is the window in the reciprocal space which also depends on the angular acceptance of the apparatus α [135], usually ranging between 0.5 and 1.0 degrees:

$$\Delta q_{\|} = \frac{\sqrt{2mE_p}}{\hbar}(\cos\theta_i - \sqrt{1-\frac{E_{loss}}{E_p}}\cos\theta_S)\cdot\alpha \quad (2.4)$$

Thus $\Delta q_{\|}$ is minimized for low impinging energies and for grazing scattering conditions.

Three scattering mechanisms for impinging electrons are possible: *dipole*, *impact* and *resonant scattering* [93]. The last mechanism is prevalent for molecules in gaseous phase (see Ref. [93] for more details) and thus it is not important for plasmonic excitations.

Concerning *dipole scattering*, it is worth remembering that the Coulombian field produced by incoming electrons interacts at long range (about 100 Å) with the surface. Loss events may occurs both before and after diffusion from the surface [135], as shown in figure 2.4.

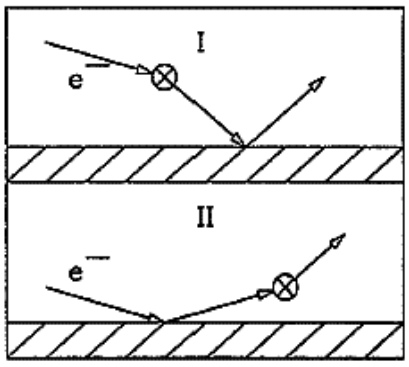

Figure 2.5: Possible loss events in dipole scattering. The loss event may occur before or after the impact with the surface. Taken from Ref. [135].

According to Mills [136], the differential cross section $d^2S/d\omega d\Omega$, is given by:

$$\frac{d^2S}{d\omega d\Omega} = \frac{(mev_{\perp})^2}{2\pi^2\hbar^5\cos\theta_i}\frac{k_s}{k_i}\frac{P(q_{\|},\omega)}{q_{\|}^2}\frac{\left|v_{\perp}q_{\|}(R_s+R_i)+i(R_s-R_i)(\omega-v_{\|}q_{\|})\right|^2}{\left[(v_{\perp}q_{\|})^2+(\omega-v_{\|}q_{\|})^2\right]^2} \quad (2.5)$$

where $v_{\|}$ are $v_{\perp}$ the parallel and perpendicular components of the velocity of impinging electrons with respect to the surface, respectively, and $P(q_{\|},\omega)$ is the surface loss function. R_i and R_s are the amplitude of complex reflectivity for initial and final energies. The maximum inelastic scattering

occurs for $\omega = v_{\|} q_{\|}$, in correspondence of a minimum in the denominator of (2.5). Such condition corresponds to the interaction of electrons with partial waves with phase velocity $\omega / q_{\|} = v_{\|}$. By defining θ as the deviation from trajectory of electrons inelastically scattered from specular direction, thus for $\hbar\omega << E_p$ and $\theta << 1$, the denominator of (2.5) may be written as:

$$\left(v_{\perp} q_{\|}\right)^2 + (\omega - v_{\|} q_{\|})^2 = 4E_i^2 \left(\theta^2 + \Psi_E^2\right) \cos^2 \theta_i \quad (2.6)$$

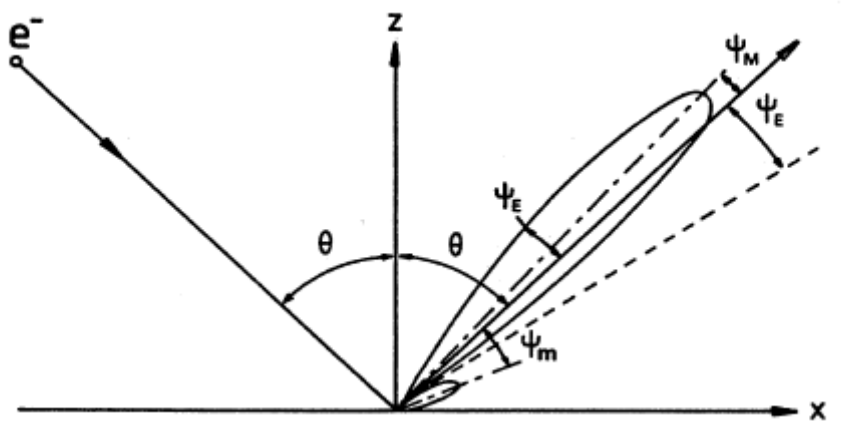

Figure 2.6: Schematic plot of the kinematic factor in the dipole scattering probability function, showing that the inelastically scattered electrons are confined to two lobes near the specular reflection direction. Taken from [137].

where $\Psi_E = \hbar\omega / 2E_p$. The equation (2.6) determines the angular dependence of dipole scattering and its concentrations in a lobe with semi-amplitude Ψ_E along specular directions. Dipole scattering dominates for small transfer momenta.

As shown in figure 2.6, a principal maximum exists (which corresponds to the condition $\omega = v_{\|} q_{\|}$), even if a secondary maximum also exists.

For short-range interactions *impact scattering* occurs. Within this scattering mechanism, electrons are diffused in every possible solid angle, even beyond the incidence plane. Both perpendicular and parallel

component of the wave-vector (with respect to the sample normal) are not conserved. As a consequence of such complexity, theory which describes such interactions is not deeply developed. The cross section is defined as [93]:

$$\frac{d\sigma}{d\Omega} = \frac{mE_p \cos^2\theta_s}{2\pi^2\hbar^2 \cos\theta_i} |M|^2 \quad (2.7)$$

where M is the matrix element for the transition and m is the mass of electrons. The cross section presents only minimal changes with scattering angle.

2.3 HREEL Spectrometer

We used an instrument manufactured by SPECS GmbH under licence of Forschungszentrum Jülich, Germany, distributed worldwide under the name DELTA 0.5. This spectrometer, designed by prof. Harald Ibach and shown in figures 2.7-2.8, is constituted by a two-step monochromator and by a rotating analyser which the peculiarity of having 151° cylindrical deflectors. This results in an ultimate resolution of 0.5 meV and a significant increase of intensity in the high resolution range.

The basic concept of the DELTA 0.5 spectrometer is a fixed double stage monochromator and a rotatable single stage analyser. In order to allow the probing of the largest possible fraction of the surface BZ the maximum rotation angle of the DELTA 0.5 analyzer stage was increased to > 90°. The impact energy is variable from 0 to 250 eV.

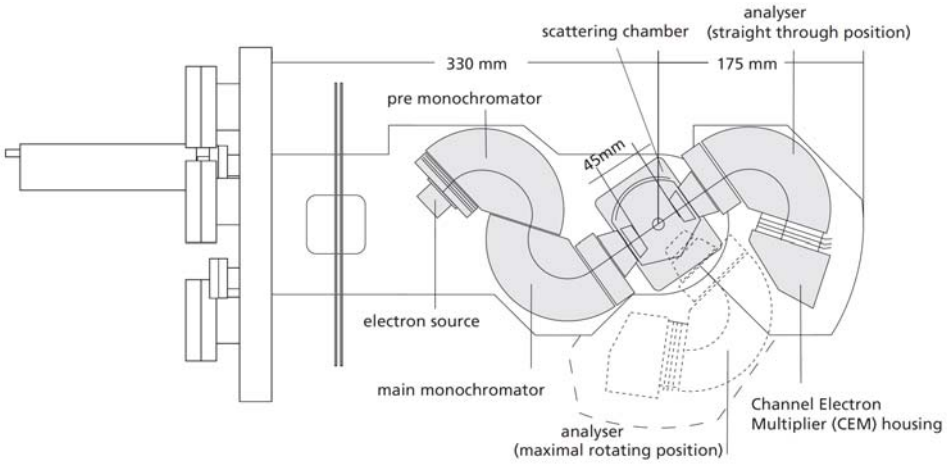

Figure 2.7: HREEL spectrometer Delta 0.5, designed by prof. Harald Ibach.

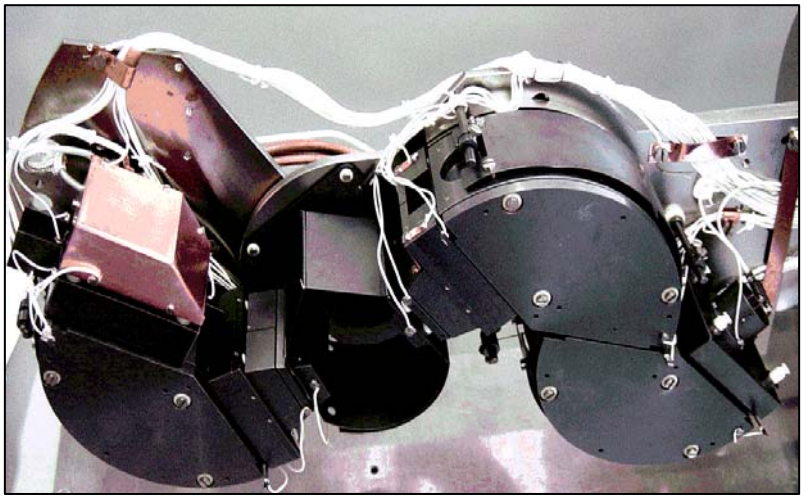

Figure 2.8: (SPES Lab-UNICAL) HREEL spectrometer in the straight-trough position. It has a double-step monochromator and a single-step analyzer. Its ultimate energy resolution is 0.5 meV.

2.4 The LEED technique

Low energy electron diffraction (LEED) is the principal technique for the determination of surface structures. The method exploits the wave-like nature of electrons originally proposed by Louis de Broglie in 1923 [138] and experimental confirmed by Davisson and Germer in 1927 [139, 140].

In LEED, electrons are accelerated towards the sample by means of an electron gun. The filament of the electron gun is held at a negative potential V_{fil} with respect to ground so that electrons leave the gun with a kinetic energy eV_{fil}. By adjusting the potential of the filament, different kinetic energies of the incident electrons can be obtained.

The LEED optics consists of a series of four hemispherical grids and a phosphor-coated hemispherical screen [141], as shown in figure 2.9.

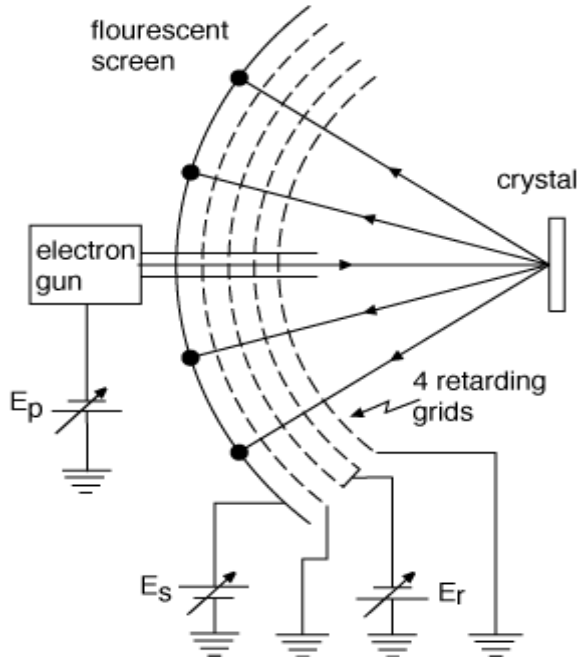

Figure 2.9: Schematic of the LEED optics.

To perform LEED measurements, electrons, emitted from the electron gun, are scattered by the sample towards the LEED optics. The first grid is normally kept at ground potential to create a region free of electric fields. The second and the third grids are held at a potential close to the potential of the filament. Therefore, these grids act as a filter to prevent inelastically scattered electrons from passing to the phosphor screen. The fourth grid is normally kept at ground potential. The screen for LEED is coated by phosphor and it is normally held at a potential between 3 and 7 kV, so that the diffracted

electrons have enough kinetic energy to excite transitions in the phosphor to emit visible light.

During a typical LEED experiment, a beam of low energy electrons (20 – 300 eV), with a wavelength $\lambda \cong$ (1-3) Å , strikes the sample at normal incidence. Low energy electrons have wavelengths comparable with interatomic distances of a crystal lattice and can therefore give rise to diffraction. The technique is thus sensitive to the surface as electrons penetrate into the solid for a few tens of Ångstrom. The electrons beam may be equally regarded as a succession of electron waves incident normally on the sample. These waves will be scattered by regions of high localised electron density, i.e. the surface atoms, which can therefore be considered to act as point scatterers.

When the electrons, elastically backscattered from the sample, strike the screen, they cause the phosphor to glow, revealing a pattern of dots which is the diffraction pattern. Since the electrons behave as waves, they produce an image that represents the reciprocal lattice of the crystal. The recording and analysis of the diffraction pattern can suggest us the arrangement of the atoms on the surface, i.e. the Bravais lattice of the surface and the size of the unit cell. The sharpness of the pattern is related to the extent of order (or conversely, disorder) of the atoms on the surface.

The condition for constructive interference for a diffraction experiment is that the difference in distance from one source to another is equal to an integer multiple of the wavelength,

$$\left|\vec{r}_1\right| - \left|\vec{r}_2\right| = n\lambda \,.$$

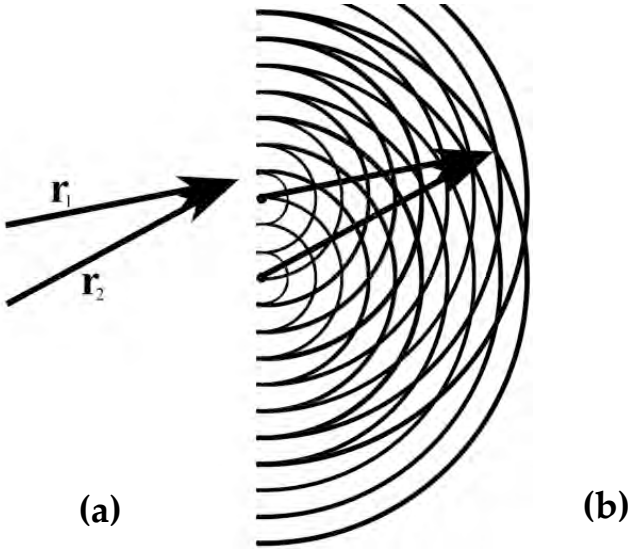

Figure 2.9: Schematic of (a) the vectors $\vec{r}_1$ and $\vec{r}_2$ from the two wave sources To a point of constructive interference and (b) the super-positioned wave crests.

It is from this constructive interference relation that we are able to view the two-dimensional reciprocal lattice of the crystal's surface. A plane wave is defined by

$$\Psi(r,t) = Ae^{i\left(\vec{k}_0 \cdot \vec{r} - \omega t\right)},$$

where $\vec{k}_0$ is the wave vector and ω is the angular frequency. Then the wave function of a scattering event with single point results in a spherical wave that can be given by

$$\Psi = f\frac{A}{D}e^{i\left(\vec{k} \cdot \vec{D} - \omega t\right)},$$

where D is the radial distance from the scattering point and *f* is the scattering power, for atoms it is also known as the atomic form factor.

The atomic form factor is the scattering amplitude of the outgoing spherical wave. It can defined as

$$f(Q) = \int_0^\infty \rho(r) e^{i\vec{Q} \cdot \vec{r}}\, dr,$$

where $\rho(r)$ is the spatial density of the scattering atom and $\vec{Q}$ is the momentum transfer.

If there are two scattering events separated in space then the resulting scattering wave function can be approximated as

$$\Psi = f\frac{A}{D}e^{i\vec{k}\cdot\vec{D}}\left[e^{i\vec{s}\cdot\vec{r}_1} + e^{i\vec{s}\cdot r_2}\right],$$

where $\vec{r}_1$ and $\vec{r}_2$ are the position vectors of the two scattering points relative to the origin, and $\vec{s}$ is the scattering vector defined as

$$\vec{s} = \vec{k} - \vec{k}_0 .$$

Note that is assumed that *D* is much larger than the distance between the points $\vec{r}_1$ and $\vec{r}_2$, therefore the denominator of the amplitude can be approximated to *D* alone. This can be generalized to scattering from *n*-bodies by

$$\Psi = f\frac{A}{D}e^{i\vec{k}\cdot\vec{D}}\sum_n e^{i\vec{s}\cdot\vec{r}_n} .$$

A real crystal lattice is defined as [142]:

$$\vec{R} = l_1\vec{a} + l_2\vec{b} + l_3\vec{c} ,$$

where $\vec{a}$, $\vec{b}$ and $\vec{c}$ are the lattice vectors. Scattering events from this lattice results in the wave function

$$\Psi = f\frac{A}{D}e^{i\vec{k}\cdot\vec{D}}\sum_{l_1,l_2,l_3} e^{i\vec{s}\left(l_1\vec{a}+l_2\vec{b}+l_3\vec{c}\right)} .$$

The condition for constructive interference is that the sum must be finite which means that $\vec{s}$ must be simultaneously satisfy the following three conditions:

$$\vec{s}\cdot\vec{a} = h2\pi ,$$

$$\vec{s}\cdot\vec{b} = k2\pi ,$$

$$\vec{s}\cdot\vec{c} = l2\pi .$$

ehere *h*, *k*, *l* are integers.

Since the reciprocal lattice for the surface of the crystal is defined by

$$\vec{G} = n_1\vec{a}^* + n_2\vec{b}^* + n_3\vec{c}^*,$$

and using the orthogonality condition between the reciprocal lattice vectors and the real lattice vectors, the following relationship holds:

$$\vec{G}\cdot\vec{R} = n_1\vec{a}^*\cdot l_1\vec{a} + n_2\vec{b}^*\cdot l_2\vec{b} + n_3\vec{c}^*\cdot l_3\vec{c}\,.$$

Substituting the definition of each reciprocal lattice vector yields:

$$\vec{a}^*\cdot\vec{a} = \frac{2\pi}{\Omega_c}\left(\vec{b}\times\vec{c}\right)\cdot\vec{a} = 2\pi,$$

$$\vec{b}^*\cdot\vec{b} = \frac{2\pi}{\Omega_c}\left(\vec{c}\times\vec{a}\right)\cdot\vec{b} = 2\pi,$$

$$\vec{c}^*\cdot\vec{c} = \frac{2\pi}{\Omega_c}\left(\vec{a}\times\vec{b}\right)\cdot\vec{c} = 2\pi\,.$$

Since n_1, n_2, n_3, l_1, l_2 and l_3 are integers the reciprocal lattice satisfies the condition for constructive interference.

3 Quasi-freestanding graphene on Pt(111)

3.1 Peculiarities of graphene

Graphene is nothing more than a single atomic layer of graphite. Intense research on the outstanding properties of graphene was initiated in 2004, when graphene and several 2D materials were observed by Geim et al. [1] at Manchester University. From then on, theoretical and experimental efforts enabled one to unravel some of the unique physical properties of graphene [143-146]. Before the discovery of graphene it was always assumed that two-dimensional crystals could not exist due to the Mermin-Wagner theorem [147] which states that long-range order is destroyed at any finite temperature due to divergent contributions from thermal fluctuations. The discovery of graphene obviously required an explanation and nowadays it is believed that small height fluctuations, or ′ripples′ [62, 148-151], in the carbon sheet suppress the thermal fluctuations making graphene a stable crystal even at finite temperatures [149] (Figure 3.1).

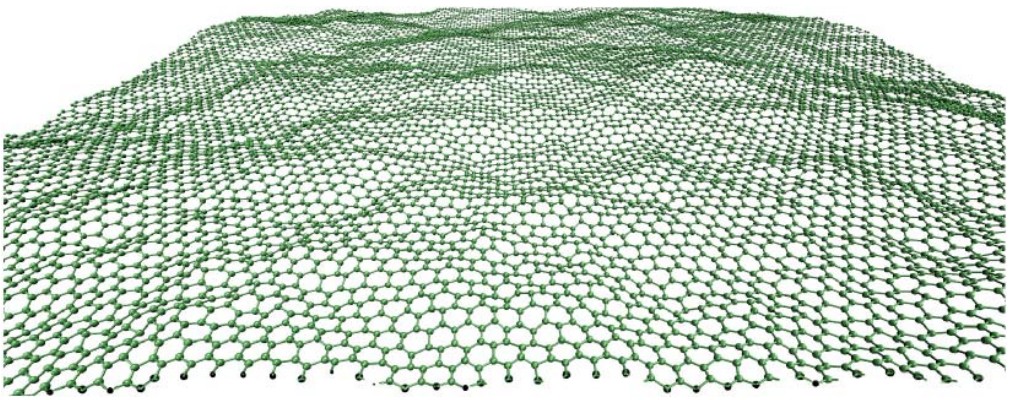

Figure 3.1: Graphene is a single sheet of carbon atoms packed in a honeycomb lattice. Sheets are rippled at any finite temperature to ensure structural stability. Shown is a simulation of a graphene sheet performed on the basis of the LCBOPII empirical potential.

Since its discovery graphene has attracted an enormous amount of scientific interest, mainly because of its unusual electronic properties. The unique two-dimensional honeycomb lattice (made up of two interpenetrating triangular lattices) and the monoatomic thickness [152] results in a linear energy band dispersion, that allows charge carriers to behave as massless Dirac fermions. Essentially, the electron transport is governed by Dirac's relativistic equation since the electrons move through the material at a significant fraction of the speed of light (the speed of light replaced by an effective speed of about 10^6 ms^{-1}). This is due to the theoretical π-band structure of graphene because it develops the Dirac cone at the k-points of the Brillouin zone (Figure 3.2), well described by the electronic structure of a perfect, flat, freestanding and infinite graphene crystal in vacuum, which causes the energy of the charge carriers to be directly proportional to their momentum instead of the usual classic result, energy being proportional to the square of the momentum.

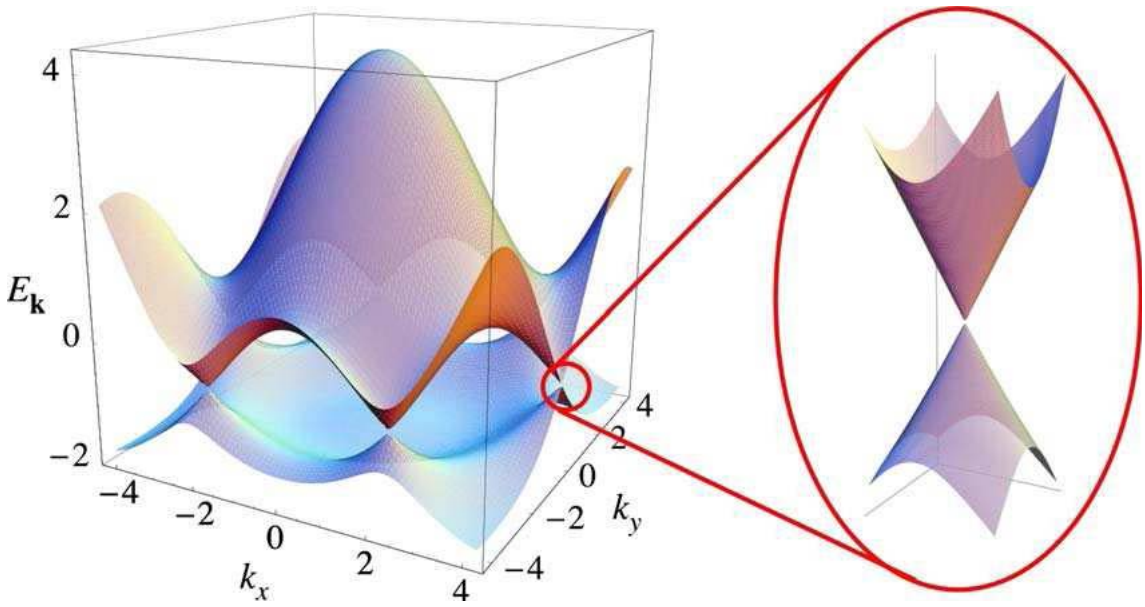

Figure 3.2: (a) The band structure of graphene (only π-band). The energy is given in units of t. The bands cross the Fermi level at the K-points. A zoom in is shown in (b).

It is evident that the remarkable properties of graphene can lead to interesting new applications.

With the fundamental limitations of silicon-based electronics in sight, it is time to look for other materials to continue the advancement in electronic applications. Graphene might be a good candidate because it obviously possesses many properties that make it interesting to use in electronics: it has high mobility charge carriers, even at high carrier concentrations, and exhibits ballistic transport on a submicrometer level, even at room temperature. However, the actual use of graphene in practical electronics is still very limited.

Therefore, due to the increasing importance of graphene, it is desirable to obtain a thorough understanding of the structure of graphene on metals and of its interplay with the underlying substrate.

3.2 Structure of graphene on Pt(111)

The graphene-metal interface is a model system where the interaction between the graphene π-bands and the metal bands can be investigated. This has relevance to contacting of graphene with metal electrodes. The carbon hybridization and also the epitaxial relationship with the metal substrate were proposed to influence the contact transmittance [153, 154] and cause local doping of graphene [155, 156]. A variety of situations regarding the interplay of graphene and its metal support is realized depending on the support material. One type with strong bonding between metal graphene and a typical metal-graphene distance smaller then a metal-metal bond (around 1.4°A– 2.2°A) and one with weak bonds and a typical metal-graphene distance which is much larger then the bonds between the substrate atoms (around 3.2°A– 3.7°A).

The difference in bonding also reflects in the phonon modes of graphene. A softening of the phonon modes indicating weakened C-C bonds is observed

in the case of strong binding, whereas in the case of weak binding the phonon frequencies stay close to the bulk values known from HOPG [152]. The electronic structure ranges from almost no interaction in the case of Pt(111) [81, 157] to deep a modification in the case of a graphene monolayer on Ni(111) [158-161] or Ru(0001) [162-164].

Using chemical vapour deposition (CVD) to grow graphene on metals recently was found to yield large graphene sheets of uniform monoatomic thickness [61, 151, 157-159]. This form of epitaxy, which occurs through ethylene decomposition on the uncovered parts of the metal substrate, by nature limits the thickness of the graphene sheets to a single atomic layer on some metals, in contrast to e.g. sublimation of Si on SiC substrates [41, 42, 160-162]. Epitaxy thus appears to be the route of choice for fabrication of large graphene sheets.

The initial methods of preparation of graphene by peeling graphite or vaporizing SiC suffered from an inherent lack of control and were not scalable and they have been replaced almost universally by methods to grow controlled epitaxial graphene on different substrates. The epitaxial growth of large, highly perfect graphene monolayers is indeed a prerequisite for most practical applications of this "wonder" material [143], but also, the possibility to produce single layers of graphene has permitted the exploration of a fascinating world of physical phenomena in two dimensions [14, 163-170]. Most of these epitaxial graphene layers are spontaneously nanostructured in a periodic array of ripples by the Moiré patterns caused by the difference in lattice parameter with the different substrates such as Ru(0001) [61-64, 76, 80, 171-175] , Ir(111) [65, 71, 165, 167, 183-187] or Pt(111) [58, 59, 68, 77, 81, 171]. The careful characterization of these superlattices is important because nanostructuring graphene (in superlattices, stripes or dots), in turn, may reveal new physical phenomena and

fascinating applications [189-192]. In addition, it is crucial to understand the interaction of graphene with the surfaces of substrates of different nature (oxides, semiconductors or metals), as well as with adsorbed molecules, in view of the relevance of metallic contacts, and the sensitivity of the conduction properties of graphene to gating materials and doping by adsorbed molecules [22, 27]. All these topics can be characterized in detail in what has become on of the benchmarks for epitaxial graphene: a self-organized, millimeter large, periodically "rippled" epitaxial monolayer of graphene grown by soft Chemical Vapor Deposition under Ultra High Vacuum (UHV) conditions on single crystal metal substrates with hexagonal symmetry. The superb control that allows the UHV environment facilitates the characterization of the system down to the atomic scale.

3.2.1 Low Energy Electron Diffraction measurements

Among graphene systems, the epitaxial growth of monolayer graphene (MLG) on Pt(111) is particularly interesting [68, 77, 81, 193, 194] as a consequence of the weak graphene-Pt interaction [172], in contrast with MLG grown on other transition-metal substrates [62, 178]. In fact, the graphene-Pt distance (3.31 Å) lies close to the *c*-axis spacing in graphite.

For platinum the lattice constant is $a = 3.92$ Å and the nearest neighbour distance between atoms is $d = 2.77$ Å. For graphene the lattice constant is $a = 2.46$ Å and the nearest neighbour is $d = 1.42$ Å. As can be seen from a comparison of the close-packed layer of atoms of the Pt(111) surface and the honeycomb structure of graphene, they both have hexagonal symmetry. This similarity should make Pt(111) a natural fit for growing well-ordered graphene on the surface. However, the presence of a difference in lengths of the lattice constants, results in a mismatch of approximately 11%.

Such system is ideal for a study of phonon modes and elastic properties due to the absence of corrugation of the graphene overlayer found on other substrates [151, 172-174] which has been demonstrated [172] to be caused by the hybridization with the substrate. The growing strength of hybridization is accompanied by a gradual change in graphene morphology from nearly flat for MLG/Pt(111) to strongly corrugated in MLG on other substrates [172]. Thus, MLG on Pt(111) behaves as nearly-flat free-standing graphene, as also confirmed by angle-resolved photoemission spectroscopy experiments [81].

Graphene was obtained by dosing ethylene onto the clean Pt(111) substrate held at 1150 K. At a certain temperature, the hydrocarbon is catalytically dissociated and hydrogen desorbs, remaining carbon adsorbed species can then form graphene. Moreover, the high temperature of the sample during depositions favours the increase of the size of monolayer graphene islands [83] and allows maintaining the substrate clean so as to avoid any contaminant-induced effect on graphene growth. The completion of the first layer was reached upon an exposure of $3 \cdot 10^{-8}$ mbar for ten minutes (24 L, 1 L=$1.33 \cdot 10^{-6}$ mbar·s). After removing the C_2H_4 gas from the chamber the temperature was held at 1150 K for further 60 seconds.

The attained LEED pattern (shown in figures 3.3, 3.4) is essentially similar to that one reported in Ref. [68]. The ring pattern indicates the existence of different domains. Nonetheless, preferred orientations aligned with the substrate (R_0) are clearly distinguished. The presence of well-resolved spots in the LEED pattern is a clear fingerprint of the order of the MLG over-structure, also evidenced by the high electron reflectivity of the obtained surface (even higher with respect to the bare Pt substrate).

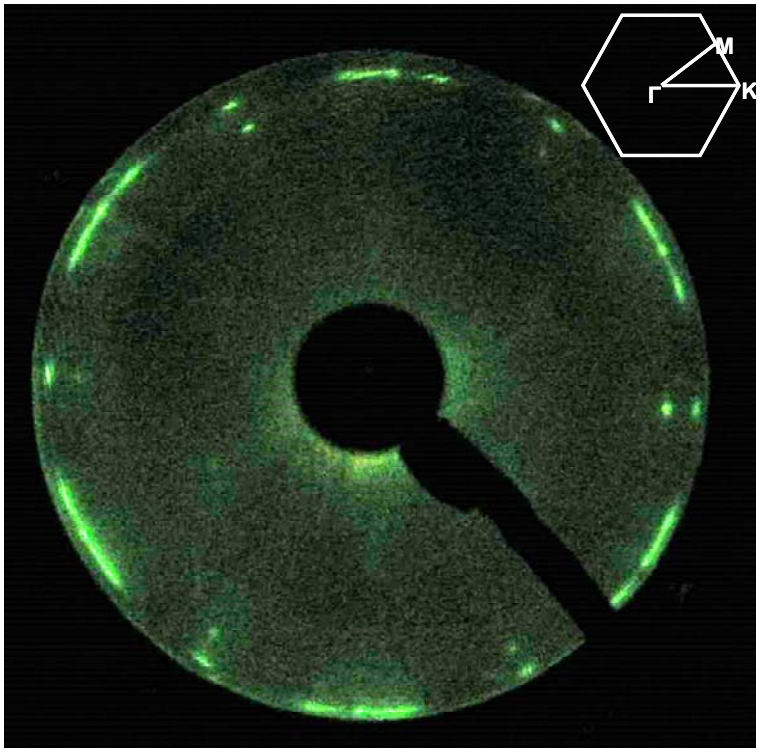

Figure 3.3: LEED pattern of graphene on Pt(111),
recorded at E_P = 74.7 eV and for a sample temperature of 100 K.

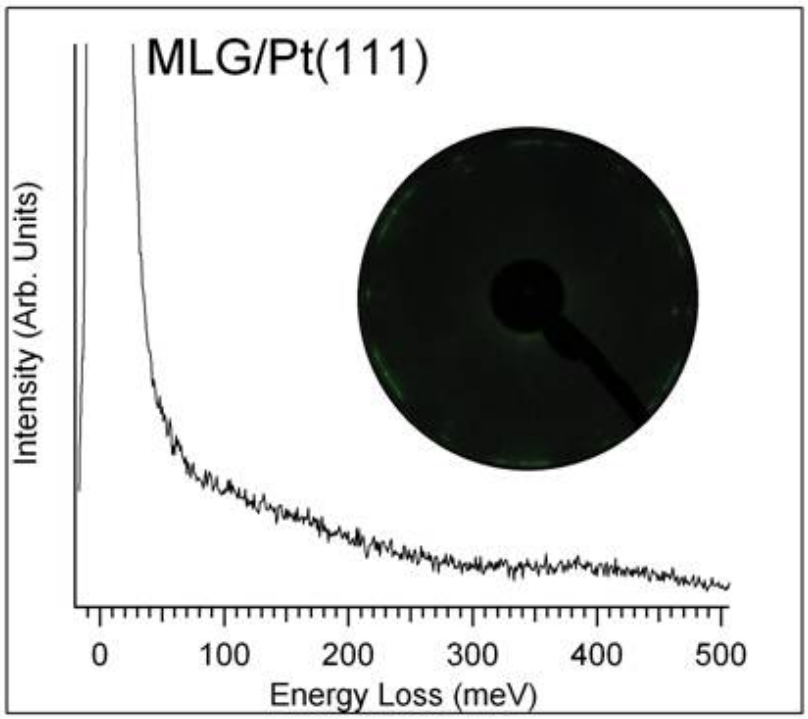

Figure 3.4: HREEL spectrum of MLG/Pt(111), recorded with an impinging energy of 4 eV and in specular scattering conditions.
In the inset the LEED pattern recorded with E_P=74.7 eV is reported.

Despite the presence of other domains, the predominance of R_0 in the whole sample has been clearly inferred by the analysis of phonon dispersion measurements performed along the $\overline{\Gamma}-\overline{\mathrm{K}}$ and the $\overline{\Gamma}-\overline{M}$ directions (inset of figure 3.3).

3.3 Phonons dispersion

The dynamics of atoms at surfaces plays an important role in many chemical and physical processes. In particular, lattice vibrations can afford essential information on many physical properties, such as thermal expansion, heat capacity, sound velocity, magnetic forces, and thermal conductivity [175]. Recently, phonon modes of graphene sheets are attracting much attention [176] as they influence many of the novel and unusual properties of graphene [177].

Due to the high energy of phonon modes in graphitic materials, several techniques as inelastic helium atom scattering can not be used. Infrared or Raman spectroscopy can not probe the whole Brillouin zone, while neutron or inelastic ion scattering are not always applicable. Among various detection methods for phonon dispersion, HREELS is a powerful tool to gain knowledge on phonons in graphene.

Present HREELS measurements show the dispersion relation of phonon modes in MLG/Pt(111). Results have been compared with recent calculations in Ref. [178].

The energy resolution of the spectrometer was degraded to 4 meV so as to increase the signal-to-noise ratio of loss peaks. Dispersion of the loss peaks, i.e., $E_{loss}(q_{||})$, was measured by moving the analyzer while keeping the sample and the monochromator in a fixed position (See chap. 2). To measure the dispersion relation, values for the parameters E_p, impinging energy and θ_i , the incident angle, were chosen so as to obtain the highest signal-to-noise ratio. The primary

beam energy used for the dispersion, E_p=20 eV, provided, in fact, the best compromise among surface sensitivity, the highest cross-section for mode excitation and $q_{||}$ resolution.

All measurements were made at room temperature.

The phonon dispersion was measured along the $[\bar{2}11]$ direction of the Pt substrate which corresponds to the $\overline{\Gamma}-\overline{K}$ direction of the MLG.

Loss measurements of MLG/Pt(111) recorded at E_p=20 eV as a function of the scattering angle θ_s are reported in figure 3.5, while the dispersion relation $E_{loss}(q_{||})$ is shown in figure 3.7.

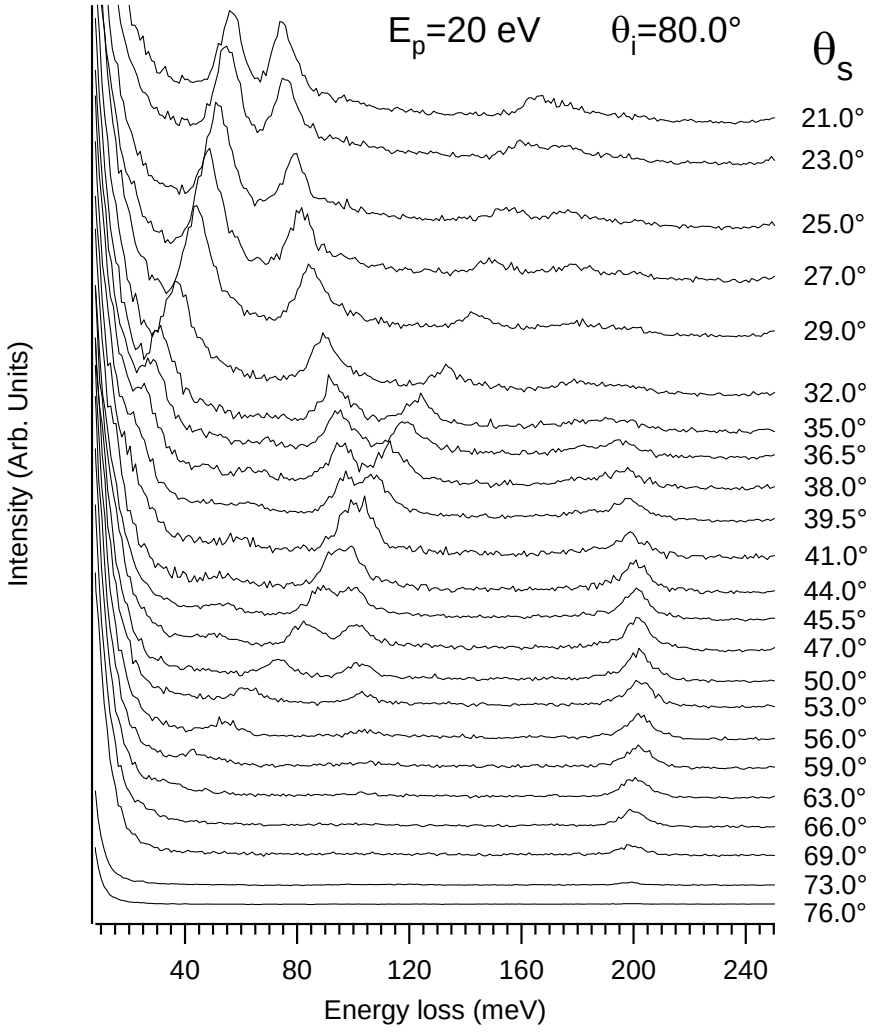

Figure 3.5: HREEL spectra for MLG/Pt(111) in the $\overline{\Gamma}-\overline{K}$ direction as a function of the scattering angle. The incidence angle is 80.0° and the impinging energy is 20 eV.

Measurements were repeated for several preparations of the MLG over-structure also by using different impinging energies and incident angles. All these experiments provided the same phonon dispersion. Such reproducibility further support the occurrence of a predominant graphene domain.

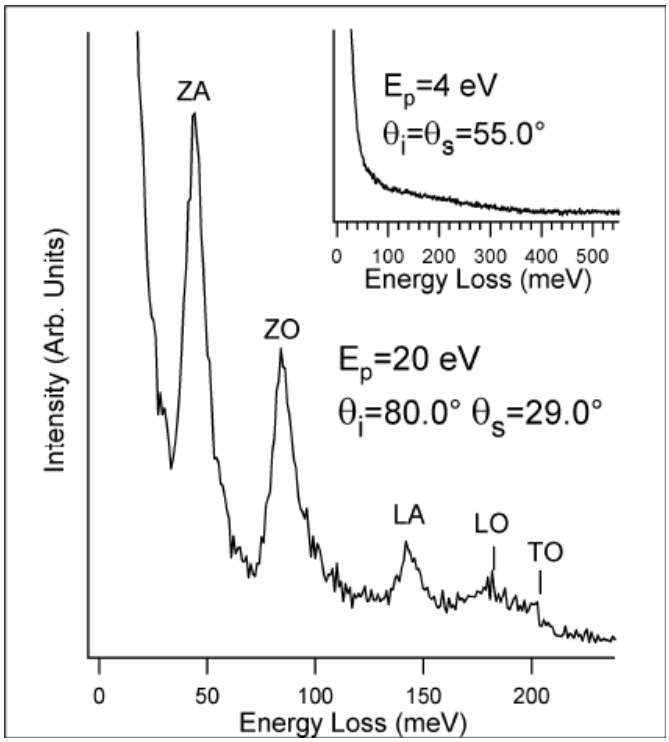

Figure 3.6: HREEL spectrum of the MLG/Pt(111) for an impinging energy of 20 eV. The incidence angle is 80.0° while the scattering angle is 29.0°. The inset shows the HREEL spectrum recorded for an impinging energy of 4 eV in the specular geometry with incidence angle of 55.0° (dipole scattering conditions). It is worth noticing that in scattering geometries near the specular conditions, the phonon modes of the graphene lattice cannot be detected, in agreement with results in Ref. [179]. On the other hand, the lack of vibrational bands in dipole scattering conditions (spectrum in the inset) ensures of the absence of contaminants or adsorbed functional groups on the bare graphene surface.

HREEL spectra show several dispersing features as a function of the scattering angle, all assigned to phonon excitations (figure 3.6). The energy and the dispersion of phonon modes indicate a negligible interaction between MLG and the underlying Pt substrate, in agreement with previous works [59, 68, 81,

177]. Accordingly, MLG may be considered as a quasi-freestanding sheet physorbed on the underlying Pt substrate.

As for graphite [201, 202], vibrations of the graphene lattice are characterized by two types of phonons: those ones vibrating in the plane of the sheet with transverse and longitudinal acoustic (TA and LA) and optical (TO and LO) branches, and those ones with vibrations out of the plane of the layer—the so-called flexural phonons (ZA and ZO). Modes classified with "T" are shear in-plane phonon excitations; "L" modes are longitudinal in-plane vibrations; while "Z" indicates out-of-plane polarization. In general, the ZO mode is significantly softened with respect to the other two optical modes, i.e. TO and LO. This is due to the higher freedom for atom motion perpendicularly to the plane with respect to the in-plane motion. All observed phonons are similar to those ones of bulk graphite.

This is quite expected for modes associated with vibrations of carbon atoms in the direction of the σ bonds, i.e. the LA and LO phonons (except a stiffening of the LO mode at $\bar{\Gamma}$ by 5 meV). In particular, a careful comparative analysis with respect to graphite showed a softening of the TA mode (with a maximum difference of 18 meV). On the other hand, by comparing the phonon dispersion relation of MLG/Pt(111) with that one recorded for MLG/Ni(111) [6, 180], we notice a significant energy shift by 10-15 meV at the $\bar{\Gamma}$ point for the ZA and ZO modes, which are connected to perpendicular vibrations of carbon atoms with respect to the surface. In particular, in MLG/Ni(111) the ZA phonon is stiffened while the ZO mode is softened with respect to MLG/Pt(111). This is caused by of the orbital mixing of the π-states of the MLG with Ni d-bands [157].

A particular attention should be devoted to the ZA phonon, as it was recently found that the ZA modes in suspended graphene carry most of the

heat [181]. It is a bending mode in which the two atoms in the unit cell are involved in an in-phase motion in the out-of-plane direction. At long wavelengths it bends the MLG sheet so as to induce rippling in graphene. While the TA and the LA phonons are characterized by a linear dispersion, the ZA mode has a quadratic dispersion near the $\overline{\Gamma}$ point (Figure 3.7), as also in layered crystals [182]. Its dispersion depends on the bending rigidity τ, which is an important parameter for mechanical properties of membranes:

$$\omega_{ZA}(q_{\parallel}) = \sqrt{\frac{\tau}{\rho_{2D}}}\left|\vec{q}_{\parallel}\right|^2$$

where $\rho_{2D} = 4m_C/(3\sqrt{3}a^2)$ is the two-dimensional mass density (m_C is the atomic mass of carbon atoms; a is the in-plane lattice parameter). We found that the bending rigidity τ could be estimated to be about 2 eV, in agreement with results in Ref. [183].

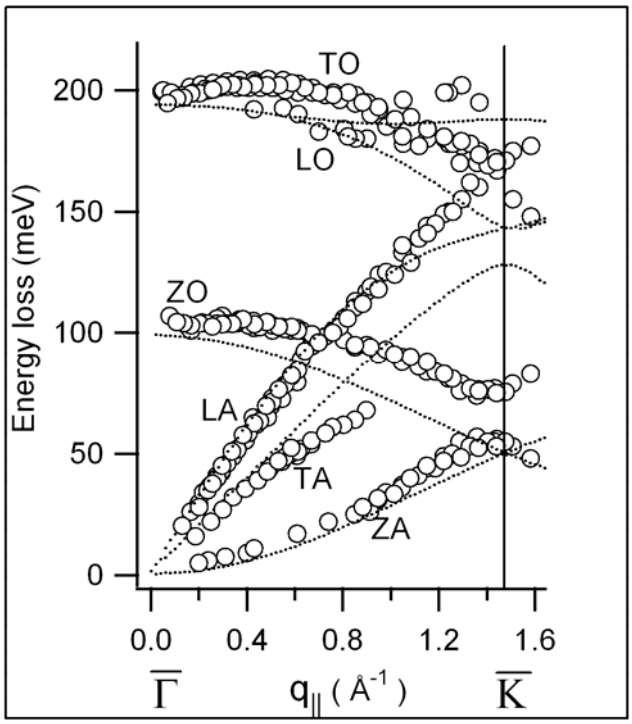

Figure 3.7: Dispersion relation for phonon modes in MLG/Pt(111) in the $\overline{\Gamma}-\overline{K}$ direction (empty circles). The dotted line represents the calculated phonon dispersion in Ref. [178]

The dispersion relation of phonons in MLG/Pt(111) have been compared with recent calculations for free-standing graphene derived from Long-range Carbon Bond Order Potential [178] (dotted line in Figure 3.7). In particular, we note an excellent agreement with calculations for the LA mode. The recorded dispersion for the flexural phonon ZA apparently does not match the behavior predicted by theory. However, it is worth remembering that the bending rigidity strongly depends on temperature and an increase by about 40% was found in the range 0-300 K[149]. The temperature dependence of the bending rigidity implies that also the ZA mode should depend on temperature. Hence, comparison of the calculated dispersion of ZA phonons at 0 K with experiments at 300 K is not straightforward.

Interestingly, the ZA/ZO degeneracy at $\overline{K}$, predicted by theoretical calculations for free-standing graphene [178] and bulk graphite [184], is lifted and a "gap" of 20 meV in MLG/Pt(111) appears. Allard and Witz demonstrated in Ref. [176] that this is a direct consequence of symmetry reduction in supported graphene systems. In fact, for free-standing graphene all carbon atoms of the graphene unit cell are equivalent, while for adsorbed graphene both atop and three-fold adsorption sites exist. Thus, some atoms are directly connected to the substrate while other ones are unconnected. In the ZA mode, the unconnected atoms are performing a perpendicular motion while the bonded atoms are at rest. For the ZO branch, the opposite occurs. This implies a higher energy for the ZA phonon. Thus, the ZA/ZO gap can be taken as a fingerprint for graphene adsorption on solid substrates, in fact, it occurs also for MLG/Ni(111) [3, 6]. By decoupling the MLG from the substrate through Ag intercalation, the gap can be removed [180, 185].

By contrast, the degeneracy of LA and LO phonons at $\overline{\mathrm{K}}$ was observed, even if the energy of such degenerate mode at $\overline{\mathrm{K}}$ is blue-shifted by 25 meV with respect to the calculated value in Refs. [186] and [178].

3.4 Kohn anomalies

Atomic vibrations could be screened by electrons and, moreover, screening can change rapidly for vibrations associated with high-symmetry points of the Brillouin zone. This phenomenon leads to an anomalous behaviour of the phonon dispersion around such points, which is called Kohn anomaly (KA)[187]. Their occurrence is completely determined by the shape of the Fermi surface.

Inelastic x-ray scattering experiments[188] that graphite exhibits two KAs for the $\overline{\Gamma} - E_{2g}$ and $\overline{\mathrm{K}} - A'_1$ modes. In details, only the highest optical branches (HOB) show KAs, which are evidenced in the phonon dispersion curve by two sharp kinks. Their existence is intimately related to the dispersion of the π bands around the high-symmetry point $\overline{\mathrm{K}}$.

With regard to graphene, several theoretical studies predicted the existence of KAs [189]. However, recently it has been demonstrated[176] that the electron-phonon coupling in epitaxial graphene systems can be strongly modified by the interaction with the underlying metal substrate. Allard and Wirtz [176], analyzing previous phonon measurements [6] performed on monolayer graphene (MLG) grown on a Ni(111) surface suggested a complete suppression of KAs for such system. Therein it was suggested that the absence of KAs in MLG/Ni(111) is caused by the hybridization of the graphene π-bands with the Ni d bands which lifts the linear crossing of the π bands at $\overline{\mathrm{K}}$.

Experiments on phonon dispersion showed that, in contrast with the case of MLG/Ni(111), KAs could be detected in MLG/Pt(111). We ascribe this finding

to the nearly quasi-freestanding behaviour of π bands in this system. Such results could be important to evaluate the interaction strength between the graphene layer and the underlying metallic substrate.

MLG/Pt(111) loss spectra around the high-symmetry point $\overline{\mathrm{K}}$ show (Figure 3.8) a softening by about 30 meV of the TO mode (characterized by A'_1 symmetry), which reaches a minimal loss energy at $\overline{\mathrm{K}}$ (172 meV).

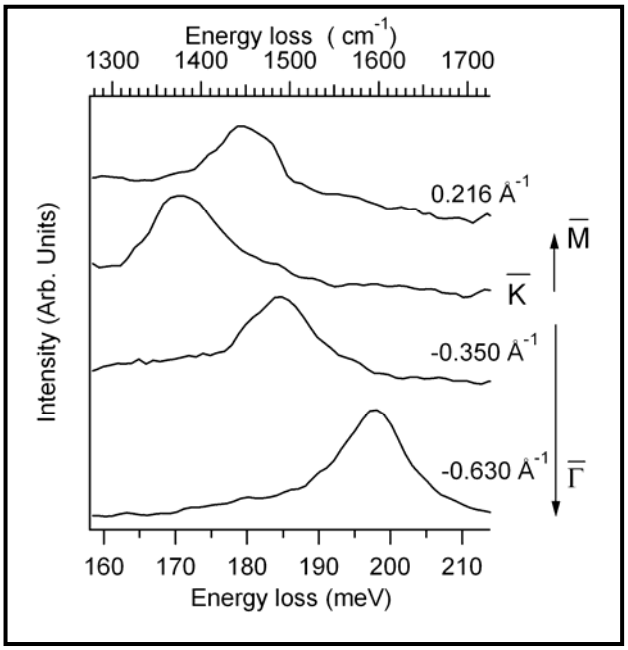

Figure 3.8: HREEL spectra for MLG/Pt(111) as a function of the scattering angle around the high-symmetry point $\overline{\mathrm{K}}$. The incident angle is fixed to 86.0° with respect to the sample normal. The impinging energy is 20 eV. All measurements have been carried out at room temperature.

Figures 3.9 and 3.10 report the dispersion relation of the HOB as a function of $q_{\parallel}$ around the $\overline{\mathrm{K}}$ and $\overline{\Gamma}$ symmetry points, respectively. The most striking feature of these dispersions is the discontinuity in the derivative of the HOB (A'_1 and E_{2g}, respectively) at $\overline{\mathrm{K}}$ and $\overline{\Gamma}$, which is a direct evidence of the existence of KAs. This should be put in relationship with the abrupt change in the screening of lattice vibrations by conduction electrons. On the other hand, for MLG/Ni(111), the dispersion of the HOB is almost flat at both $\overline{\mathrm{K}}$ and $\overline{\Gamma}$ symmetry points. This means that the interaction with the substrate leads to a

complete suppression of KAs, as a consequence of the strong hybridization of the graphene π-bands with Ni d-bands [155]. In fact, the hybridization induces around $\overline{K}$ the appearance of a "gap" of almost 4 eV between unoccupied and occupied π-bands.

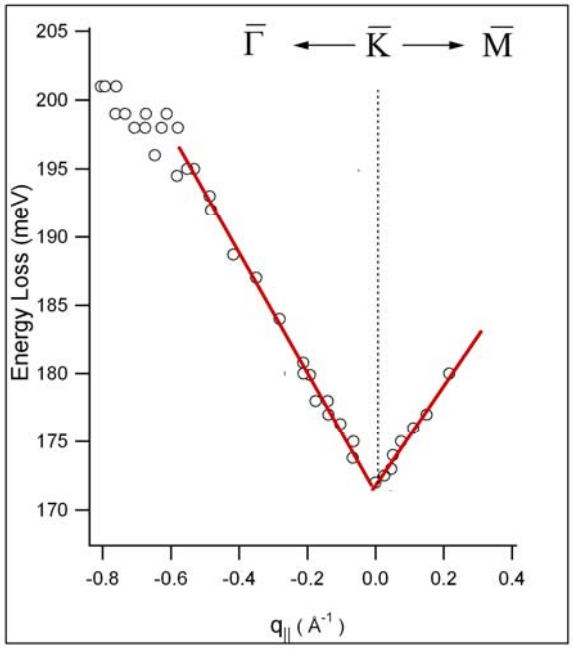

Figure 3.9: Graphene HOB in the nearness of the $\overline{K}$ of the Brillouin zone.

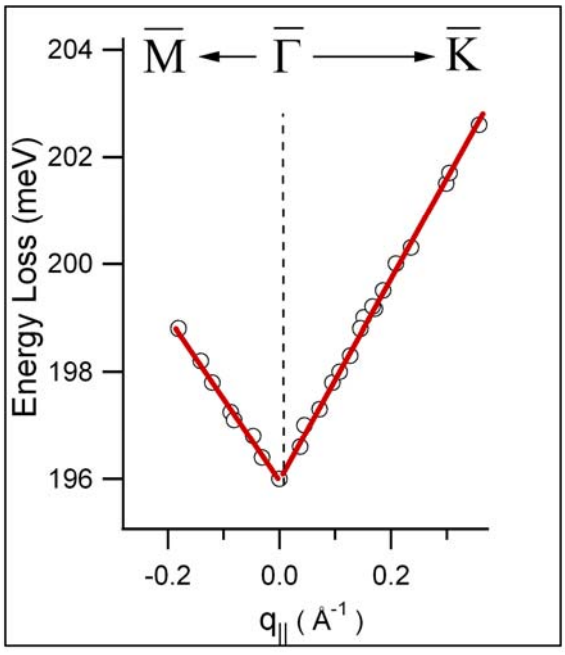

Figure 3.10: Graphene HOB in the nearness of the $\overline{\Gamma}$ of the Brillouin zone.

3.5 Conclusions

Lattice dynamics in quasi-freestanding graphene epitaxially grown on Pt(111) has been investigated by using high-resolution electron energy loss spectroscopy.

The phonon dispersion of MLG/Pt(111) resembles the behaviour reported for the pristine graphite, while the softening of out-of-plane modes occurs only MLG/Ni(111) and MLG/Ru(0001), that is for interacting graphene/metal interfaces, regardless of surface corrugation. Interestingly, the ZA/ZO degeneracy at $\overline{K}$ is generally lifted upon adsorption on a solid surface.

From experimental phonon dispersions, therefore it is possible to draw conclusions about the interaction strength in graphene/metal interfaces. Such investigation is of fundamental importance for graphene-based devices as both electronic and optical excitations can be scattered by phonon states or decay into vibrational excitations.

KAs have been revealed in phonon dispersion of MLG/Pt(111). We ascribe this finding to the nearly-freestanding behaviour of graphene epitaxially grown on Pt(111). Thus, from the experimental phonon dispersion, it is possible to draw conclusions about the interaction strength in graphene/metal interfaces. Such investigation is of fundamental importance to evaluate the quality of the contacts between metallic electrodes and graphene devices and, moreover, to understand the peculiar thermal properties of graphene.

4 Water adsorption on MLG/Pt(111)

4.1 Water adsorption

The adsorption of water on carbon species is a long-standing issue in surface science. Many investigations have been reported for graphite, nanotubes, fullerenes, diamond, active carbon, amorphous carbon and so on[190-193]. Such interest is motivated for practical interest ranging from biochemistry to nanotechnology and atmospheric science [190, 194-203]. Moreover, water interaction with graphene and nanotubes has been investigated in order to understand at molecular level hydrophobicity and water confinement.

Despite the notable significance of such topic, only a few dedicated experimental investigations [207-211] exist for water on graphene and therefore a full understanding is hitherto missing. In particular, theoretical interpretation of vibrational data (by infrared absorption spectroscopy, IRAS) is controversial. Many theoretical works use a molecular dynamics simulation with approximate water models which cannot properly reveal the geometrical arrangement of the water/graphene interface. On the other hand, experimental studies are complicated by the strong water-water interaction which leads to the formation of water clusters. This implies that the experimental investigation of water monomers adsorbed on the graphene surface to date is not achievable.

Vibrational spectroscopy is a powerful tool for studying adsorption at surfaces [93, 204, 205]. In particular, the analysis of the vibrational modes of

chemisorbed species is not only a fingerprint of the adsorbed chemical species but it also provides information on surface chemical bonds [98, 100, 103, 106, 206-211] and, moreover, on adsorption geometry [212].

Herein, we report on careful HREELS measurements on the early stages of water adsorption at 100 K on clean and alkali-doped quasi-freestanding monolayer graphene (MLG) epitaxially grown on Pt(111). The preferential adsorption geometry favoured in the first steps of water interaction with the pristine graphene sheet is the two-leg, i.e. circumflex water molecules on the graphene sheet. For higher coverage, one-leg water adsorption occurs, with the formation of OH···π complexes. As regards water interaction with the potassium-doped MLG, a dissociative adsorption is deduced by the presence of K-OH and C-H vibrations. We can therefore assert that alkali-induced water dissociation may lead to the partial hydrogenation of graphene.

4.2 Results and discussion

The possible adsorption geometries of water monomers on MLG/Pt(111) are depicted in Figure 4.1. The structures are described by water orientations (a: circumflex; b: OH···π; c: coplanar; and d: O-down structures).

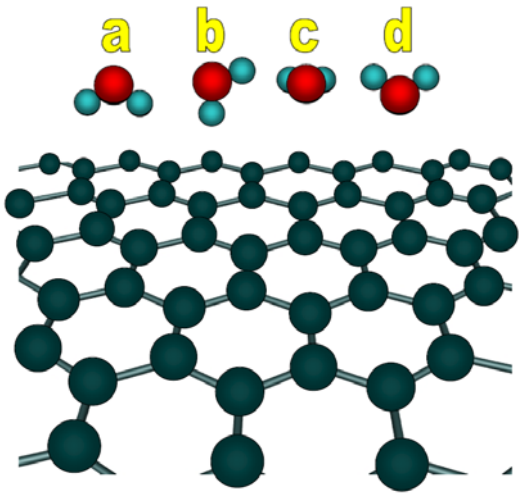

Figure 4.1: The four (a-d) possible orientations of the water molecules with respect to the graphene lattice.

Several calculations for water on graphene [219, 220] have reported that the OH···π complexes (geometry b, with one OH pointing towards the surface and the other OH being oriented along the surface) are up to 2 kJ/mol less stable than the circumflex complexes (geometry a, E_{int}= -15.0 kJ/mol[213], where E_{int} is the interaction energy value of a single water molecule with graphene). On the other hand, the O-down structure (geometry d) is energetically the least favorable (E_{int} =-8.8 kJ/mol [213]). The coplanar structure (geometry c) with interaction energy of -10.8 kJ/mol [213] can be viewed as a transition between the circumflex and O-down stationary structures on the global water-graphene potential energy surface. It is worth mentioning that the OH···π structure above the C atom has been found [213] to be more stable with respect to the one above the center of the six-member ring.

In summary, only two different orientations of the water molecules are expected to be observed. We refer to "one-leg" adsorption [214] the structure of OH···π complexes (geometry b) and with "two-leg" adsorption [214] the structure a in which the water is located over the center of a hexagon ring with the two hydrogens equidistant from carbon atoms. Vibrational spectra, recorded as a function of water coverage (up to saturation), were inspected (Figure 4.2) in order to distinguish fingerprint for one-leg and two-leg water adsorption.

The vibrational spectrum may be divided into four major regions (see Ref. [215] for a review): frustrated translations around 30 meV; frustrated rotations, i.e. librations at 100-110 meV; H_2O deformations, i.e. the scissoring band centered around 200 meV; and O-H stretching modes around 400-460 meV. Instead, the vibrational band around 500 meV should be assigned to a combination mode of the O-H stretching and the libration modes.

At the lowest coverage (up to 0.25 ML), the loss spectra, in figure 4.2, show well-distinct and intense bands in the region of frustrated translations (29 meV) and librations (91 meV). Instead, the scissoring and the O-H bands exhibit weaker intensities. The O-H band shows two features at 414 and 428 meV ascribed to symmetric and anti-symmetric stretching vibrations, respectively[222, 223].

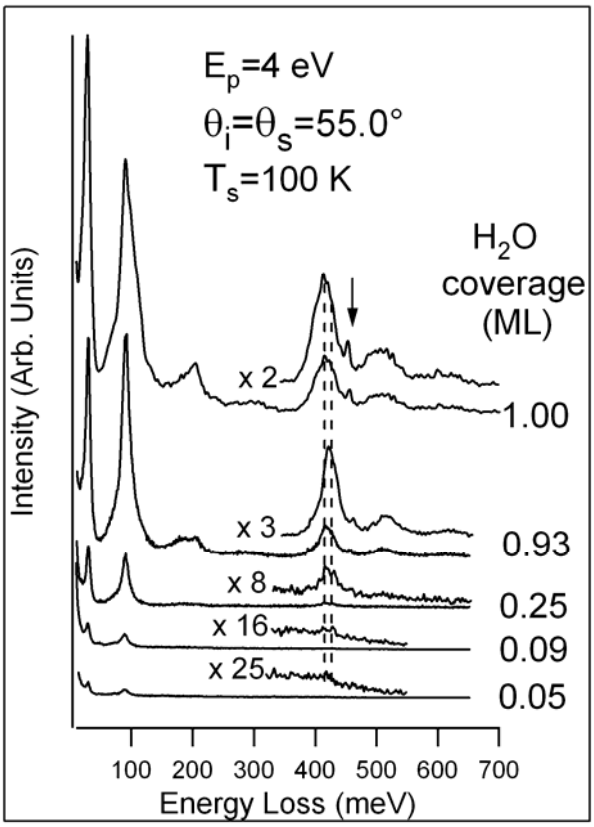

Figure 4.2: HREEL spectra for MLG/Pt(111) exposed to different amounts of H_2O. Both measurements and exposures were carried out at 100 K.

With increasing the water coverage (0.65 ML, top panel of Figure 4.3 and the two outermost spectra in Figure 4.2 for 0.93 and 1.00 ML) these two features merge into a broad O-H band. In addition, a narrow peak appears at 457 meV (spectra for 0.93 and 1.00 ML in Figure 4.2 and HREEL spectra in Figure 4.3). The intensity of such feature is maximum at ice saturation. By a comparison with existing calculations and measurements[60, 190, 216], the

peak at 457 meV has been assigned to O-H stretching in one-leg water molecules.

Such narrow feature and the broad O-H band, recognized from the vibrational spectra in Figure 4.2, originate from different surface chemical bonds of OH groups of water molecules. The free OH has the shortest bond length and the highest O-H vibrational frequency (457 meV). On the contrary, the strong H-bonded OH has the lowest frequencies (400-440 meV) but the largest bond length [216]. The hydrogen bonding polarizes so as the O-H bonds are lengthened [217] and this causes a red-shift of its stretching energy with respect to one-leg H_2O.

From the analysis of O-H mode, information about the adsorption geometry can be obtained[93]. On the basis of results in figure 4.2, we can conclude that in the initial stage water molecules adsorb only in the two-leg configuration.

Lin et al.[218] performed simulations on water clusters interacting with single-layer graphite (graphene) and they found that increasing the water cluster size from a monomer to a hexamer leads to a monotonous increase of the binding energy between the water clusters and the graphene surface. This implies that changes in the adsorption geometry occur. It has been suggested that, for increasing water coverage, only one OH bond points towards the graphene sheet [218] (one-leg adsorption). These theoretical findings are fully confirmed by our vibrational measurements. In particular, the peak at 457 meV in HREEL spectra for the saturated ice layer (outermost spectrum in Figure 4.2) is a direct evidence of the presence of non-hydrogen-bonded O-H bonds at the interface between water and epitaxial graphene. In fact, the frequency of the O-H stretching in one-leg water molecules is close to the frequency of O-H stretching in the gas-phase [193].

Kimmel et al. [219] studied MLG/Pt(111) with IRAS and concluded that the water film is rotationally aligned with graphene in spite of the weak interaction between the water film and the graphene sheet. They suggested that water on MLG/Pt(111) could form an ordered and crystalline ice film with the same hexagonal symmetry as the graphene substrate on which it grows. According to the structural model proposed therein on the basis of LEED and IRAS experiments, no dangling OH groups or lone pair electrons exist at the vacuum/ice and ice/graphene interfaces. However, present HREEL measurements strongly deviate from these conclusions. In particular, the presence of an intense and well-distinct vibrational fingerprint of free OH groups in Figures 4.2 and 4.3 (see also discussion of Figure 4.5 for the case of D_2O) clearly indicates that the model in Ref. [207] is inadequate to describe the geometrical structure of the ice film on MLG/Pt(111).

Although the graphene sheet is nearly-freestanding on Pt(111) [172], we could not exclude that the underlying Pt substrate could influence O-H bonds. As an example, the role of the substrate on water adsorption on graphene has been put in evidence in Ref. [220].

4.2.1 LEED analysis

LEED could provide important information about symmetry of the ice layers on the graphene sheet. In Figure 4.3 we report the LEED pattern for two different coverages of water on the graphene sheet, together with the corresponding vibrational spectrum. The LEED pattern does not change up to about 0.85 ML. At ice saturation, no structures in the LEED pattern could be recorded for impinging energies below 180 eV. For energies higher than 180 eV, impinging electrons penetrate underneath the outermost surface layer and therefore diffraction spots of the underlying Pt(111) could be recorded, in addition with very weak arcs characteristic of the MLG/Pt(111)

(see chap.3). We conclude that, in the present experimental conditions, water does not form ordered structures.

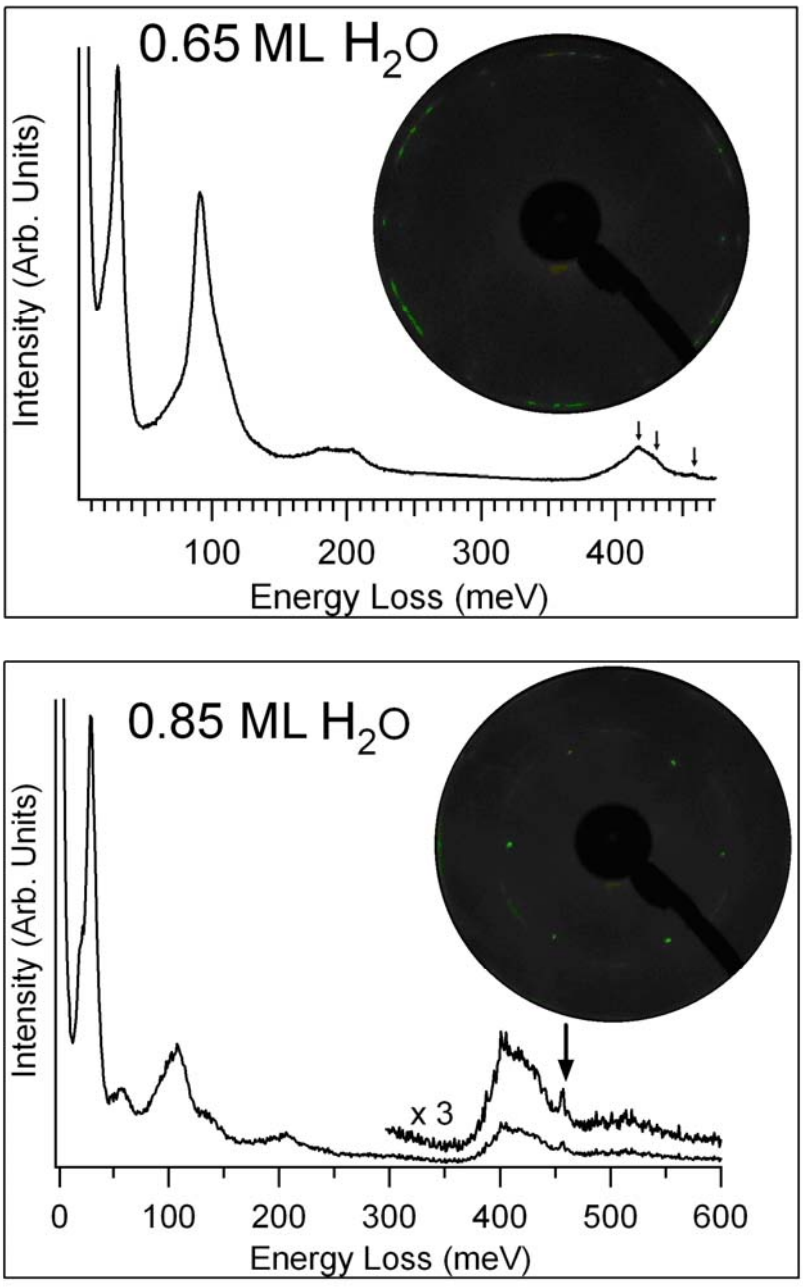

Figure 4.3: (top panel) LEED pattern, shown with its corresponding vibrational spectrum measured for an impinging energy of 4 eV, for 1.70 ML ice on MLG/Pt(111). The LEED pattern has been recorded for E_p=74.7 eV; (bottom panel) The LEED pattern for bilayer ice, recorded for E_p=198.5 eV. The corresponding HREEL spectrum shows a well-distinct non-H-bonded O-H vibration at 457 meV, evidenced with an arrow.

4.2.2 Desorption experiments

In figure 4.4 we report vibrational spectra for 0.40 ML ice annealed at 120 (second spectrum) and 140 K (outermost spectrum in the same figure), respectively. Upon annealing at 120 K, about 70% of water molecules desorbs. Interestingly, all bands broadened upon annealing very likely due to an increase of the disorder in the ice layer. The O-H band red-shifted by 5 meV as a consequence of the annealing-induced weakening of the O-H bond. Hence, there is a direct evidence that the O-H bond softens before ice desorption.

By heating the sample to 140 K, ice completely desorbed from MLG, as indicated by the featureless HREEL spectrum.

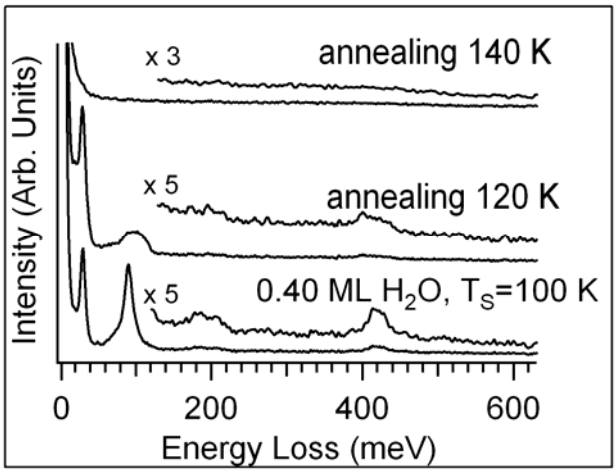

Figure 4.4: HREEL spectra recorded for 0.80 ML ice on MLG/Pt(111) prepared at 100 K, successively annealed at 120 (second spectrum) and 140 K (outermost spectrum), respectively. All measurements have been carried out at 100 K.

4.3 D_2O interaction with graphene

We have also performed measurements for D_2O-exposed MLG/Pt(111) (Figure 4.5). Apart from the isotope shift, the same vibrational features of figure 4.2 (for H_2O) have been observed. In particular, a vibrational mode due to non-D bonded D_2O molecules was recorded at 337 meV. Upon

annealing at 120 K, some D_2O molecules desorb (about 65%), as suggested by the overall decrease of the intensity of vibrational bands. It should be noted that the annealed sample shows clear frequency shifts. The centroid of the broad O-D band shifts from 312 down to 302 meV, while a red-shift by 4 meV is recorded for the libration band. This is a consequence of the softening of O-D bonds upon annealing. The feature of non-D bonded D_2O disappear in the annealed sample. Thus, such species desorbs first than bonded OD groups.

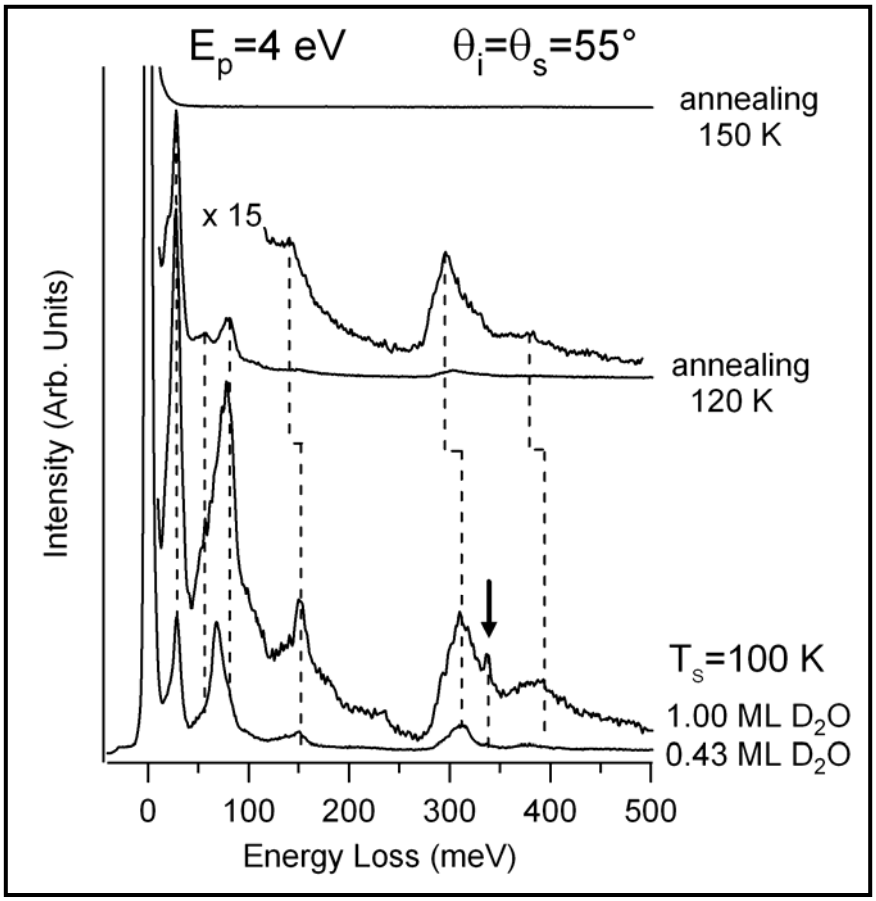

Figure 4.5: HREEL spectra for MLG/Pt(111) covered with 0.43 (bottom spectrum) and 1.00 ML (second spectrum) of D_2O, respectively. The latter surface has been successively annealed to 120 (third spectrum from the bottom) and 150 K (outermost spectrum), respectively. All measurements and exposures were carried out at 100 K.

The desorption of D_2O is complete by heating the sample to 150 K. In fact, no vibrational features are present in the outermost spectrum of Figure 4.5. It should be noticed that the authors of Ref. [219] do not observe the feature at 457 meV for H_2O/MLG/Pt(111) (Figure 4.5) in their IRAS experiments while a small feature at 337 meV was recorded for D_2O/MLG/Pt(111) but it was not discussed.

4.4 Water adsorption on graphene at room temperature

Water molecules adsorbed on graphene act as dopants without remarkable changes in electron mobility [27, 221]. However, recently, it has been reported that water adsorption could change photoemission spectra of air-exposed graphene samples [222]. Moreover, a tunable band gap of about 0.2 eV can be opened by controlled adsorption of water molecules [223]. The hydrolysis products could be used for functionalizing graphene in order to create graphene field-effect transistors [227, 230].

Figure 4.6 shows that the HREEL spectrum attained after exposing the pristine MLG (spectrum a) to 10^5 L (1 L=$1.33 \cdot 10^{-6}$ mbar·s) of water molecules at room temperature (spectrum b). Vibrational bands centered at 91, 180, and 360 meV were recorded. Interestingly, the latter two peaks indicate the occurrence of water dissociation as they are well known to be unambiguous fingerprint of the formation of C-H bonds [224]. They are assigned to the bending and stretching vibrations of C-H, respectively. More in details, the energy of the C-H stretching indicates the formation of a sp^3 bond. In fact, such mode is expected around 375–380 and 360–365 meV for the sp^2 and sp^3 hybridization, respectively [225].

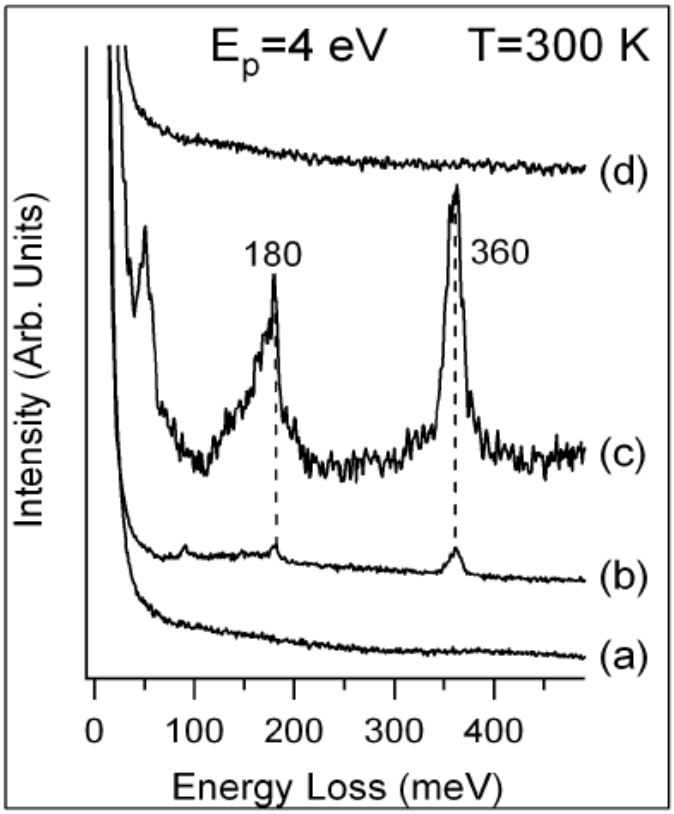

Figure 4.6: HREEL spectra acquired in the specular geometry (incidence angle 55° with respect to the sample normal) for (a) MLG/Pt(111) , successively exposed to 10^5 L of H_2O at 300 K (spectrum b) and annealed at 450 K (spectrum d) . The spectrum (c) has been recorded for the same surface of the spectrum (b) but for an off-specular geometry (scattering angle 49°) . The beam energy Ep is 4 eV. All measurements have been performed at room temperature.

The absence of vibrational modes of OH groups at 415-450 meV [98, 101] indicates that their adsorption energy is positive in the presence of co-adsorbed H atoms on the MLG sheet, i.e. such species are not stable at 300 K.

The intensity of vibrational features significantly increased in off-specular scattering geometry (spectrum c of the same Figure). This is a consequence of the weak oscillating dipole of chemisorbed H atoms [226] against the graphene sheet.

For the sake of completeness, it is worth mentioning that losses at 50 meV (spectrum c) and 91 meV (spectrum b) of Figure 4.6 should be assigned to phonon modes of the hydrogenated surface [227].

Due to the high dissociation barrier for water molecules, we are led to suggest that water dissociation should occur on defects of the graphene lattice. Likewise, it has been demonstrated that water can dissociate at vacancy defects on graphite following many possible reaction pathways [228-230], some of which have activation barriers lower than half the value for the dissociation of bulk water. However, we could not exclude that the dissociation could be driven by the catalytic activity of the underlying Pt substrate. As an example, the role of the substrate on water adsorption on graphene has been put in evidence in Ref. [220]. Water reactivity strongly depends on both the substrate underneath the graphene sheet as well as the amount and type of defects. Adsorbates desorb from MLG upon annealing at 450 K, as evidenced by the lack of vibrational modes in the annealed surface (spectrum d of figure 4.6).

In figure 4.7 we show the effects of H_2O exposure on the optical phonon modes of MLG. The pristine graphene (middle spectrum) is characterized by the presence of out-of-plane (ZO) and longitudinal (LO) optical phonons at 104 and 202 meV, respectively. After water adsorption and dissociation, the intensity of these modes strongly decreased (topmost spectrum of Figure 4.7). The band at 175-180 meV is due to the C-H stretching mode.

It is worthwhile mentioning that photoemission spectroscopy (PES) experiments on an air-exposed MLG/Au/Ni(111) sample [222] reported a strong reduction of the intensity from the graphene π bands. The intensity decrease was tentatively assigned to adsorbate water from the atmosphere.

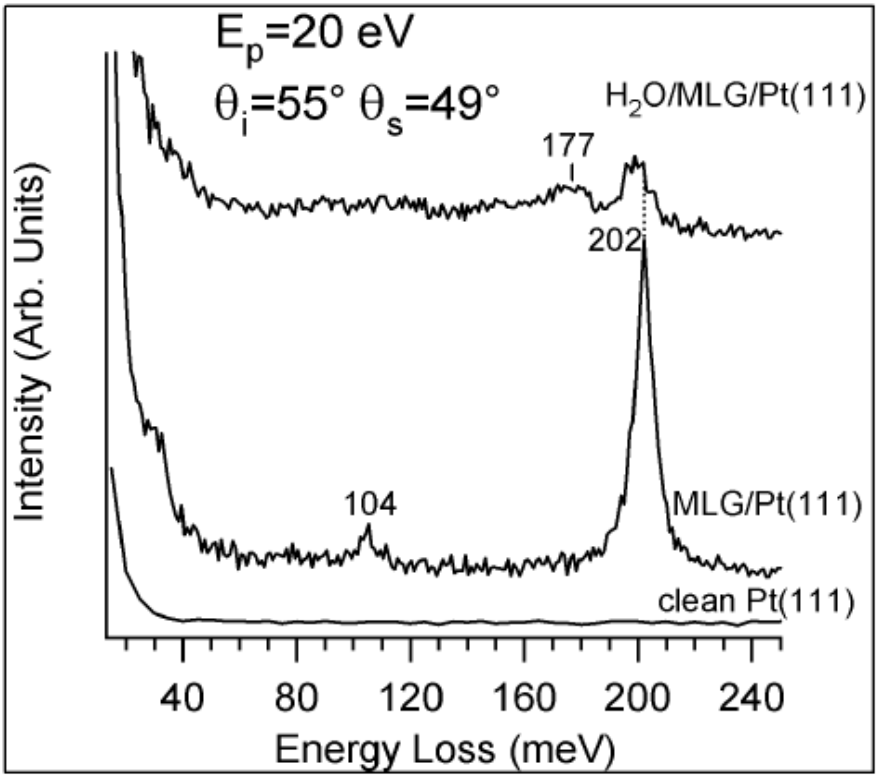

Figure 4.7: HREEL spectrum of the clean Pt(111) substrate (bottom spectrum) and for the MLG/Pt(111) (middle spectrum) and the H2O/MLG/Pt(111) (topmost spectrum) surfaces. Optical phonon modes could be detected only for impact scattering conditions, i.e. off-specular geometries. All measurements have been performed at room temperature.

4.5 Water interaction with alkali-doped graphene

Compared to the comprehensive studies on ions in bulk water, much less is known about the behaviour of ions on a hydrophobic surface. The structure and dynamics of interfacial water may strongly depend on the presence of ions at surfaces [231]. Alkali metal atoms easily ionize in the adsorbed phase [102, 213, 239, 240]. Recently, it has been demonstrated that potassium readily donates electrons to graphene [232]. Thus, alkali doping offers an opportunity for investigating water interaction with ionic species at graphene surface.

Meng et al. [231, 233] simulated the dynamics of hydration shell formation and the interaction of alkali metal ions on a hydrophobic single-sheet graphite (graphene) surface using ab-initio quantum molecular dynamics simulations at an ion coverage of $1.2 \cdot 10^{18}$ atoms/m^2. They found that two-dimensional shell structures were formed in the initial stage of hydration and that a potassium ion was always present at the surface, while the sodium ion was dissolved in the water/graphene interface. Moreover, water molecules seem to mediate an effective ion-ion interaction, which prevents nucleation of K.

Hence, it is particularly interesting the case of K doping. Experiments on the adsorption of K on MLG on a metal surface has been recently carried out by Starodub et al. [234]. It was found that, contrary to the case of graphite [235], K atoms do not intercalate underneath the graphene sheet [234], but form an overlayer on the graphene surface. Similar results have been reported for Rb and Cs [36] on MLG/6H-SiC(0001).

Thus, K-doped MLG/Pt(111) provides an ideal playground for investigating water interaction with ions at an hydrophobic surface. We have studied the adsorption of water on K-doped graphene. In details (Figure 4.8), the MLG/Pt(111) surface precovered by 0.08 (bottom spectrum) and 0.25 ML (top spectrum) of K, respectively, was exposed to 20 L of water.

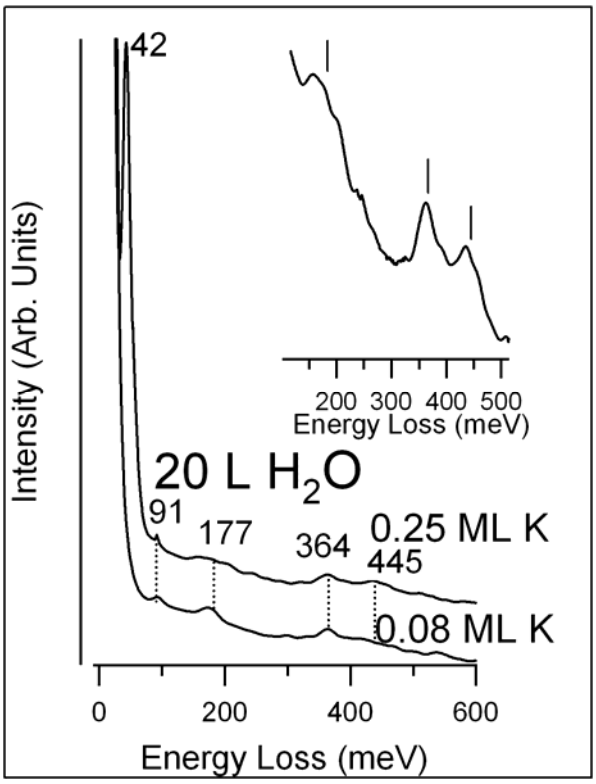

Figure 4.8: HREEL spectra for 0.08 and 0.25 ML of K adsorbed on MLG/Pt(111) and successively exposed to 20 L of H_2O at 100 K.
The inset shows a magnification of the outermost spectrum (0.25 ML K).

Vibrational bands centered at 91, 177, 364, and 445 meV were recorded in both loss spectra reported in Figure 4.6. Interestingly, the bands at 177 and 354 meV indicate the occurrence of water dissociation as they are well known to be fingerprint of the formation of C-H bonds [224]. They are assigned to the bending and stretching vibrations of C-H, respectively. More in details, the energy of the C-H stretching indicates the formation of a sp3 bond. In fact, such mode is expected around 375–380 and 360–365 meV for the sp2 and sp3 hybridization, respectively [225].

Alkali atoms are known to be extremely reactive toward water molecules[60-62]. The partial electron transfer from the π orbitals of graphene to unoccupied valence bands of the alkali-metal ion is expected to change the oxidation number and the chemical reactivity of alkali species.

Thus, very likely such phenomenon plays a pivotal role in the K ions-induced water dissociation at the hydrophobic graphene surface.

For the sake of completeness, it is worth mentioning that loss at 92 meV in the bottom spectrum should be assigned to phonon modes of the single-side hydrogenated surface [227] while the weak band centered around 445 meV should be assigned to the O-H stretching of residual adsorbed hydroxyl groups[98, 215]. On the other hand, the peak at 42 meV in the K-saturated H2O/MLG/Pt(111) (0.25 ML of K) should be assigned to a vibration of K atoms against OH groups in K(OH)x complexes.

Results in Figure 4.8 provide a novel mechanism for attaining a partial graphene hydrogenation by water dissociation on K/graphene at 100 K.

However, the role of K atoms in the dissociation process is expected to be predominant. Moreover, we would like to point out that alkali interaction with co-adsorbed molecules has been demonstrated to be short-ranged[50,78].

4.6 Conclusions

We have studied water interaction with clean and K-doped quasi-freestanding graphene on Pt(111) at 100 K. On pristine graphene, water adsorption does not occur for sample temperature higher than 130 K. Loss measurements demonstrate that at the lowest coverages water molecules adsorb in the two-leg configuration. For increasing water coverage, we found that the adsorption of one-leg H_2O takes place. Present results agree with recent theoretical works, which thus provide a satisfactory description of the adsorption geometry at the water/graphene interface, and, in particular, of the water orientation on graphene. On the other hand, our results disagree with findings in Ref. [207] for the same system. In particular, the presence of

non-H-bonded OH species is not consistent with the new ice polymorph proposed therein for the present system.

Water exposure at room temperature of MLG/Pt(111) could lead to the formation of C-H bonds. Such finding gives a response to previous results of Ref. [222]. Dehydrogenation is possible upon annealing at 450 K. On the other hand, no dissociation was observed at 100 K. Water dissociation could also afford interesting pathways to produce hydrogen. Moreover, water-induced hydrogenation of graphene should be taken into account in engineering graphene-based devices which should work at atmospheric pressure and at room temperature.

Moreover, we find that water adsorption on K-modified graphene is dissociative, as evidence by the existence of C-H bending and stretching modes in the vibrational spectrum. This provides a new method for modifying the interfacial properties of graphene by adsorption of atomic and molecular species.

5 Electronic collective excitations

5.1 Introduction

Low-energy collective excitations in graphene are attracting much interest in recent years [166, 234-251] as they influence many of the peculiar properties of graphene samples. In particular, the dispersion and damping of plasmons in epitaxial graphene have recently been studied for the case of graphene deposited on SiC(0001) [236, 237] and Ir(111) [238]. The understanding of plasmonic excitations of graphene plays a key role in tailoring the properties of novel graphene-based devices [239].

Indeed, many of the peculiar graphene's properties are related to its electronic collective excitations [59, 237, 238, 240-253], even if their understanding is still missing. In particular, it is essential to shed the light on plasmon modes in graphene/metal interfaces to understand dynamical processes and screening in such systems.

The electronic structure of MLG on Pt(111) resembles that of isolated graphene[10]. In particular, the linear dispersion of π bands in the so-called Dirac cones, which gives rise to many manifestations of massless Dirac fermions, is preserved. Angle-resolved photoemission spectroscopy (ARPES) experiments[10] do not show any remarkable hybridization of graphene π states with metal *d* states. They just represent a superposition of graphene and metal-derived states, with minimal interaction between them. The MLG on Pt(111) is hole doped by charge transfer to the Pt substrate [254]. The Fermi energy E_F of the graphene layer shifts 0.30 ± 0.15 eV below the Dirac-

energy crossing point of the bands, with the Fermi wave vector k_F = 0.09 Å^{-1}. Epitaxial graphene on Pt(111) thus behaves as an ideal 2D system, sustaining a purely 2D electron gas (2DEG) system whose collective excitations (plasmon modes) are able to propagate along the sheet. The dielectric response of the 2DEG system is determined by plasmon dispersion, which could be measured by high-resolution electron energy loss spectroscopy.

The 2D plasmon, characterized by its square-root-like dispersion, has been predicted [255] and observed in metal layers on semiconductors [256, 257]. On the other hand, the acoustic surface plasmon (ASP) with a linear dispersion was demonstrated to exist on semiconductor quantum wells with two interacting quantum well minibands [258]. Successively, ASP has been experimentally revealed on Be(0001) [259] and on noble-metal surfaces [260, 261]. The acoustic-like dispersion is a consequence of the combination of the nonlocality of the 3D response and the spill-out of the 3D electron density into the vacuum, both providing incomplete screening of the 2D electron-density oscillations [271].

Previous measurements on MLG/SiC(0001) showed a nonlinear dispersion for the sheet plasmon in MLG. Such behaviour could be described by the Stern's model [255]. It is interesting to study the behaviour of collective excitations of MLG grown on a metal substrate in order to shed light on the screening mechanisms of the sheet plasmon in the presence of an underlying metal substrate. Present measurements by HREELS show a linear dispersion for the sheet plasmon in MLG/Pt(111). Our results indicate that the sheet Plasmon of MLG survives up to a high energy, i.e., 3 eV. This is a consequence of the fact that intraband excitations have negligible influence on the propagation of the plasmon mode. On the other hand, the dispersion curve of the sheet Plasmon overlaps with the continuum of interband

transitions above the Fermi wave vector. This broadens the plasmon peak but does not cause its disappearance (in agreement with predictions in Ref. 5), in contrast with the behaviour found for ordinary sheet plasmons in 2DEG and ASP.

5.2 Evidence for acoustic-like plasmons

To measure plasmon dispersion (see chap. 2), values for the parameters Ep, impinging energy, and θi , the incident angle, were chosen so as to obtain the highest signal-to-noise ratio. The primary beam energy use for the dispersion, Ep = 7–12 eV, provided, in fact, the best compromise among surface sensitivity, the highest cross section for mode excitation and momentum resolution.

To obtain the energies of loss peaks, a polynomial background was subtracted from each spectrum. The resulting spectra were fitted by a Gaussian line shape (not shown herein). All measurements were made at room temperature.

Measurements were performed for both symmetry directions (Γ–K and Γ–M), but no remarkable differences were recorded as a consequence of the existence of differently oriented domains on the sample, as observed in previous low-energy electron microscopy experiments [81]. Loss measurements of MLG/Pt(111) recorded as a function of the scattering angle θs are reported in figure 5.1. HREEL spectra show a low-energy feature which develops and disperses up to 3 eV as a function of the scattering angle. This resonance exhibits a clear linear dispersion and its frequency approaches zero in the long-wavelength limit. We assign it to the sheet plasmon of MLG, in agreement with theoretical [246, 252, 262-264] and experimental [236-238, 265, 266] results.

The dispersion of the sheet plasmon for MLG on SiC(0001) well agrees with Stern's [255] prediction ($\omega \propto \sqrt{q_{\|}}$). However, the plasmon dispersion recorded in our experiments (Fig. 2) is well described by a linear relationship, as in the case of ASP on bare metal surfaces [259-261]:

$$\hbar\omega_{2D} = Aq_{\|}$$

where $A = 7.4 \pm 0.1\ eV{\cdot}\mathring{A}$.

The sheet plasmon with a linear dispersion owes its existence to the interplay of the underlying metal substrate with the π-charge density in the MLG in the same region of space. It resembles the ASP in metal surfaces that support a partially occupied surface state band within a wide bulk energy gap [267, 268].

The nonlocal character of the dielectric function [269] and the screening processes in graphene [241, 270] prevent the sheet plasmon from being screened out by the 3D bulk states of Pt(111).

Recently, Horing [253] predicted that the linear plasmon in graphene systems may arise from the Coulombian interaction between the native sheet plasmon ($\omega \propto \sqrt{q_{\|}}$) in MLG and the surface plasmon of a nearby thick substrate hosting a semi-infinite plasma. Calculations taking into account the electronic response of the Pt substrate could in principle put this effect in evidence, but this is not trivial due to the existence of a Moiré reconstruction in the MLG lattice on top of the Pt(111) substrate. The slope of the dispersion relation of the sheet plasmon in MLG/Pt(111) and the ones of acoustic-like excitations provide information about group velocities of the plasmon mode. We found that the group velocity of the sheet plasmon in MLG/Pt(111) ($1.1 \pm 0.2 \times 10^6$ m/s) is similar to the ones calculated for ASP [268, 271]. The group velocity of the sheet plasmon in MLG/Pt(111) is about 2 orders of magnitude lower than the speed of light, thus its direct excitation by light is not possible.

However, nanometer-size objects at surfaces, such as atomic steps or molecular structures, can allow coupling between sheet plasmon and light.

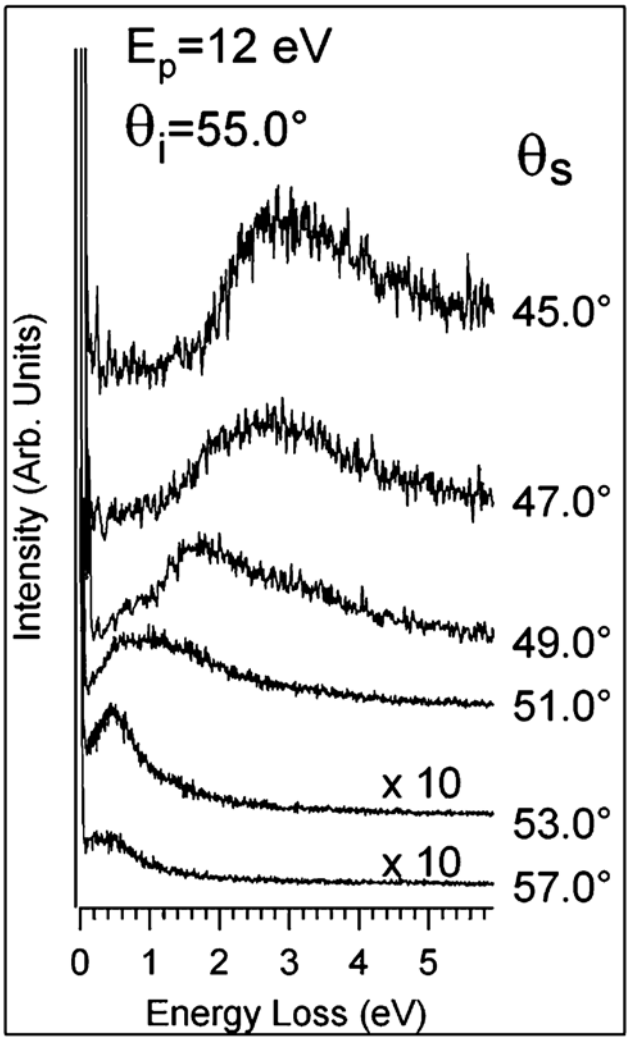

Figure 5.1: HREEL spectra of MLG/Pt(111) acquired as a function of the scattering angle. The incident angle is 55.0◦. The impinging energy *Ep* is 12 eV.

The linear behaviour of its dispersion implies that both phase and group velocities of the collective excitation are the same, so signals can be transmitted undistorted along the surface. Hence, this finding could be of significant importance in future graphene-based nano-optical devices, especially if we have in mind that the Moiré pattern of MLG on metal substrates offers a naturally nanostructured system [62, 150, 151, 272].

In figure 5.2, we also show the electron-hole continuum or single-particle excitation (SPE) region, which determines the absorption (Landau damping) of the external field at given frequency.

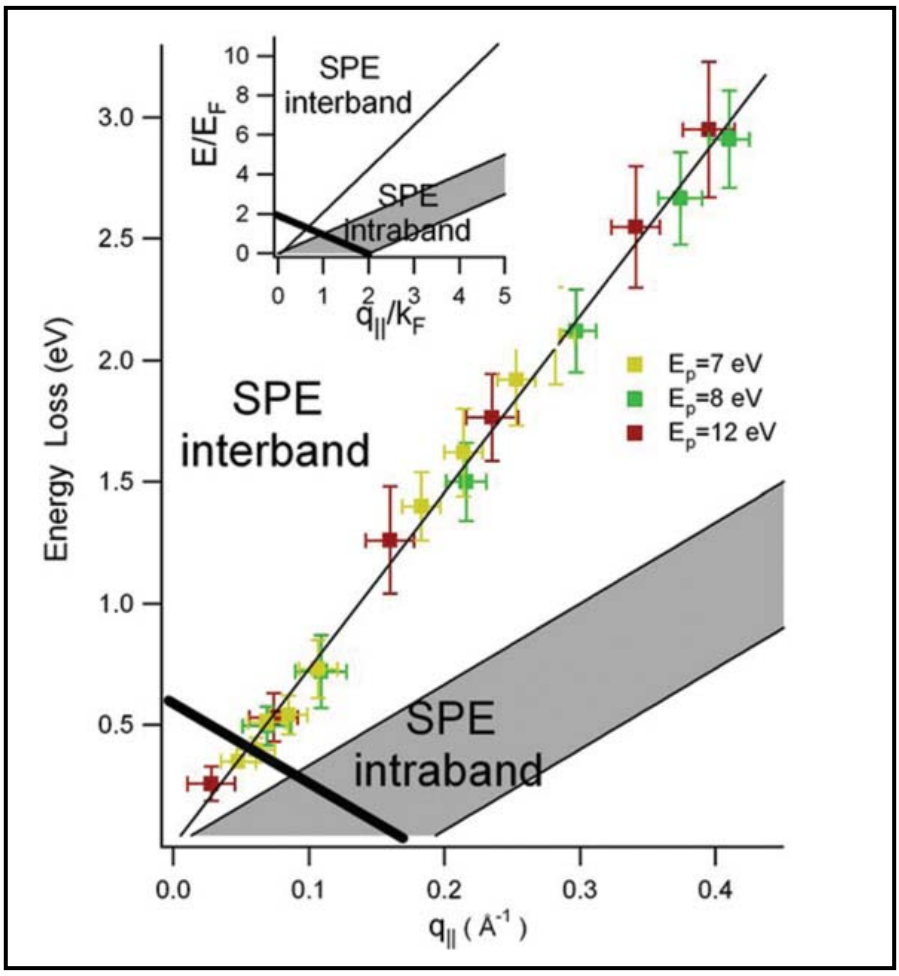

Figure 5.2: Plasmon dispersion in MLG/Pt(111). Data have been acquired for three different impinging energies. The thin solid line represents the best fit for experimental points. The dashed area indicates the continuum of intraband SPEs. The thick solid line represents the boundary for the continuum of interband SPEs. The plasmon mode enters the Landau damping regime by interband electron-hole excitations when its dispersion relation intercepts the boundary for the continuum of interband SPEs. In the inset, the curves are reported with respect to the dimensionless units E/EF and $q_{\parallel}/kF$.

It was calculated on the basis of results in Refs. [262-264] by substituting the values of E_F and k_F for MLG/Pt(111) obtained by ARPES [81]. For a normal 2D system, only indirect transition is possible within the band. However, for graphene, both intraband and interband transitions are possible, and the boundaries are given in figure 5.2. Due to the phase-space restriction, the interband SPE continuum has a gap at small momenta.

For $q_{\|} = 0$, the transition is not allowed at $0 < E < 2E_F$. If the collective mode enters the SPE continuum, the plasmon mode can be damped. The plasmon lies inside the interband SPE continuum, thus decaying into electron-hole pairs, above the Fermi wave vector. Plasmon can propagate without damping only in the region (see fig. 5.2) not included in the continuum of SPE (interband and intraband). Such considerations are fully confirmed by the analysis of the full-width at half maximum (FWHM) of the plasmon peak as a function of both $q_{\|}$ [Figure 5.3(a)] and the plasmon energy [Figure 5.3(b)]. Landau damping for the MLG sheet plasmon occurs for momenta above the Fermi wave vector (about 0.09 $Å^{-1}$) and for energies above 0.5 eV, as revealed by the sudden increase of the FWHM. Interestingly, the sheet plasmon does not enter into the intraband SPE continuum and it exists for all wave vectors. By contrast, for ASP, Landau damping occurs via intraband transitions and the plasmon mode exists only up to a few hundreds meV [259-261]. On the other hand, for MLG on SiC(0001), the FWHM continuously increases with the momentum [236, 273]. For such system, it has been shown [236] that the existence of steps or grain boundaries is a source of strong damping, while the dispersion is rather insensitive to defects.

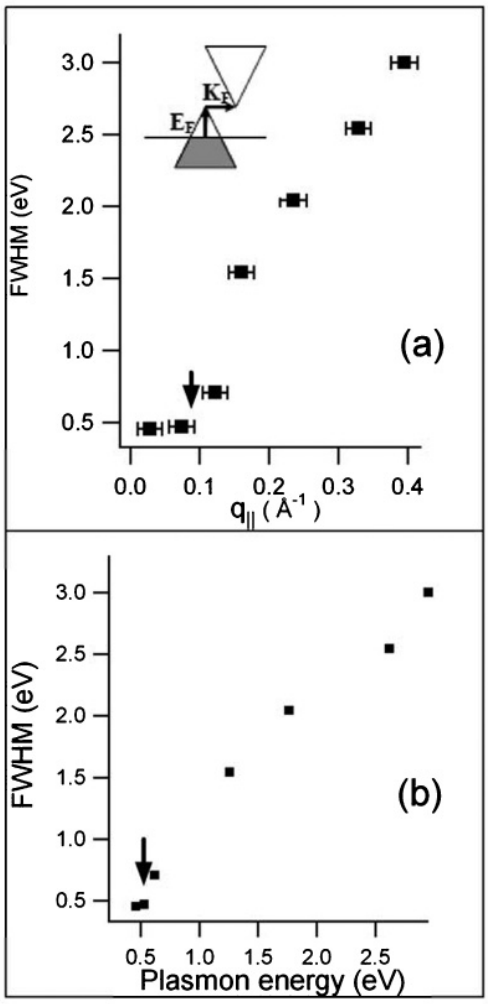

Figure 5.3: FWHM of the plasmon peak as a function of (a) the parallel momentum transfer $q_{||}$ and of (b) the plasmon energy. The inset in the top panel shows the origin of interband SPEs from π to π^* bands. The Fermi wave vector represents the onset where plasmon enters the damping region.

5.3 Dispersion and damping processes of π plasmon

The electronic response of graphene systems is related to the collective excitations of the electrons which combine in-plane and inter-plane interactions. Herein we want to investigate the nature and the dispersion of π plasmon in MLG grown on a metal substrate. The π plasmon is a sensitive probe of the graphene band structure near the Fermi level [274]. Its physical origin is the electric dipole transition between the π energy bands ($\pi \rightarrow \pi^*$) mainly in the region of the M point of the Brillouin zone of graphitic systems

[21-25]. Recently, it has been demonstrated [241] that in the presence of a free-electron substrate the plasmonic excitation of the graphene sheet are nearly completely quenched, as a consequence of the dynamical Coulomb interaction between induced charges in the substrate and graphene. However, in the case of graphene on Ni(111), the π plasmon was found to exist [275, 276]. It is thus interesting to characterize the π plasmon mode also in the case of a graphene sheet weakly bonded to the metal substrate, as occurs for MLG/Pt(111).

5.3.1 Results and discussion

HREELS measurements show a quadratic dispersion for the π plasmon in MLG/Pt(111), in contrast with results obtained for MLG/6H-SiC(0001) [266] and calculations for free-standing graphene [277] and in agreement with very recent findings for MLG/Ni(111) [276]. However, the quadratic coefficient of the dispersion relation of π plasmon in MLG/Pt(111) is higher by a factor ~8 with respect to the case of MLG/Ni(111) while it is similar to the value reported for graphite.

Moreover, we found that the plasmon peak is blue-shifted by about 1.5 eV with respect to free-standing graphene and MLG/6H-SiC(0001). The presence of the metal substrate also decreases the lifetime of the plasmonic excitation, as evidenced by a careful analysis of its damping processes.

To measure the dispersion relation, primary beam energies, Ep=30-70 eV, were used. Spectra recorded for MLG on Pt(111) with the substrate oriented in the $\overline{\Gamma}-\overline{M}$ direction are reported in figure 5.4a (for a primary energy Ep of 70 eV) and 5.4b (for Ep=30 eV). A peak showing clear dispersion from 6.2 to 8.2 eV has been recorded as a function of the parallel momentum transfer $q_{\parallel}$. It has been assigned to π plasmon of graphene, in

agreement with previous experimental [276, 284-286] and theoretical [29] works.

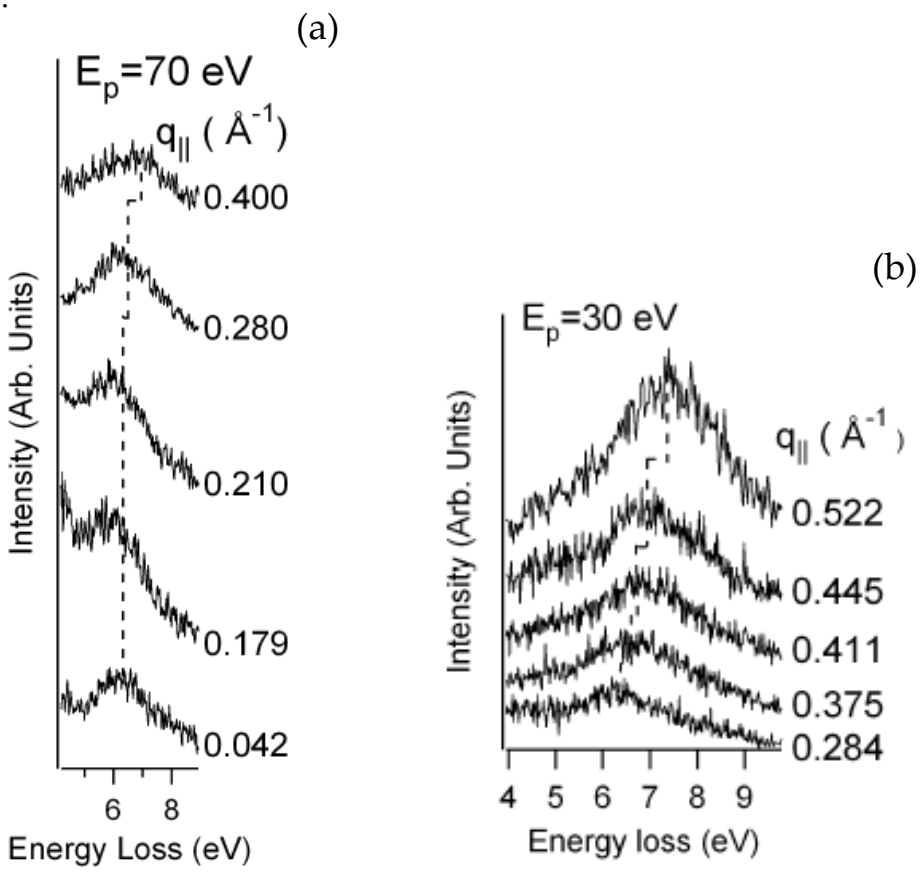

Figure 5.4: HREEL spectra for MLG/Pt(111) as a function of the parallel momentum transfer $q_{||}$. (a) Loss spectra acquired by using an impinging energy of 70 eV and an incidence angle of 65°. (b) Spectra acquired with an impinging energy of 30 eV and an incidence angle of 55°. It is worth mentioning that, due to the very weak intensity of loss peaks (≈10^{-4} with respect to the intensity of the elastic peak), an acquisition time of several hours has been required for each spectrum to reach a sufficient signal-to-noise ratio. All measurements were made at room temperature.

The intensity of the backscattering yield around the π plasmon energy versus the off-specular angle clearly demonstrates that the plasmon mode has a dipolar nature because it is nearly peaked in the specular direction [108, 135].

The measured dispersion curve $E_{loss}(q_{||})$ in figure 5.5 was fitted by a second-order polynomial given by:

$$E_{loss}(q_{//}) = E_{loss}(0) + Aq_{//}^2 = E_{loss}(0) + \alpha \frac{\hbar^2}{m} q_{//}^2$$

Where $E_{loss}(0) = (6.2 \pm 0.1) eV$, $A = (4.1 \pm 0.2) eV \cdot \text{Å}^2$, $\alpha = 0.53$.

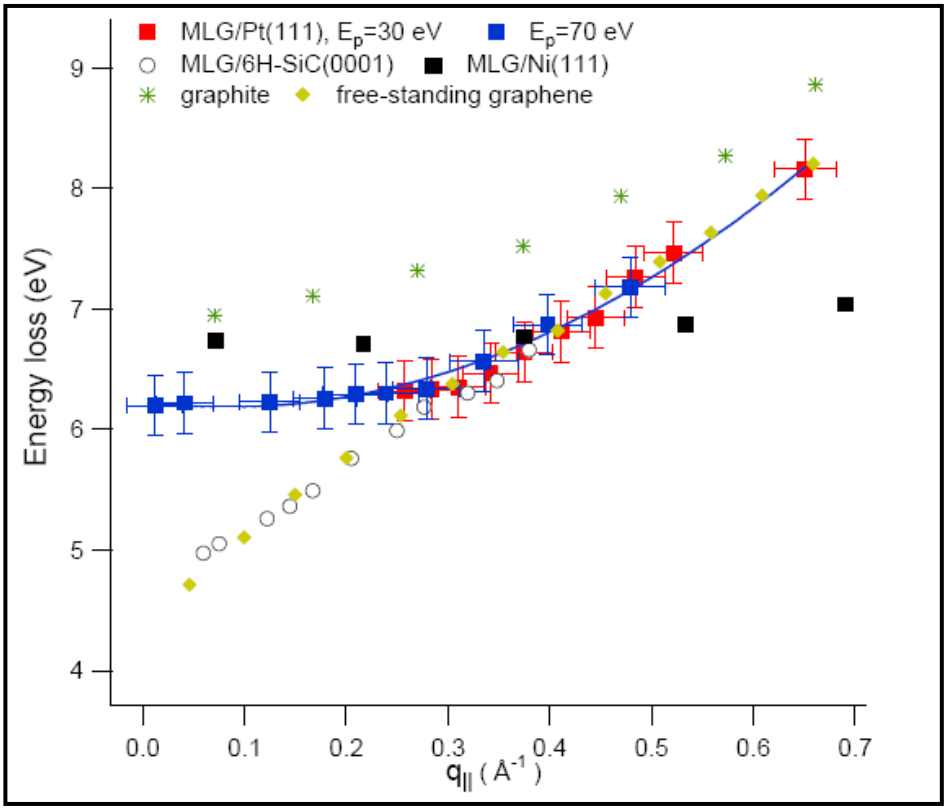

Figure 5.5: Dispersion relation of the π plasmon for MLG/Pt(111) (our data, acquired for two different scattering geometries), MLG/Ni(111) (data taken from Ref. [276]), MLG/6H-SiC(0001) (data taken from Ref. [266]), graphite (data taken from Ref. [278]) and calculations for free-standing graphene (data taken from Ref. [286]).

The same measurements were repeated for the $\overline{\Gamma} - \overline{\text{K}}$ direction, giving a similar dispersion. This is a consequence of the existence on the sample of differently oriented domains with a preferential orientation aligned with respect to the substrate (chap. 3 [68]). These findings agree with the conclusions of previous low-energy electron microscopy experiments [81].

Important information on graphene systems is provided by the analysis of the frequency of the π plasmon in the long-wavelength limit ($q_{\parallel} \approx 0$),

reported in Table I for various carbon-based systems. It can be noticed that it ranges between 4.7 eV (free-standing graphene) [286] and 6.5-7.0 eV (graphite) [287-290].

	E_{loss} ($q_{\parallel}$=0) in eV	FHWM ($q_{\parallel}$=0) in eV
free-standing graphene, data taken from Refs. [249, 286] (calculations) and Refs. [61, 62] (experiment)	4.7 [31, 57, 58] ~6 [240]	0.45
MLG/6H-SiC(0001), data taken from Ref. [266]	4.9	0.95
VA-SWCNT, data taken from Ref. [31]	5.1	1.00
Bilayer graphene on SiC(0001), data taken from Ref. [266]	5.3	1.10
Magnetically-aligned bundled SWCNT, data taken from Ref. [279]	6.0	1.25
MLG/Pt(111) (our data)	6.2	1.40
Few-layer graphene on SiC(0001), data taken from Ref. [266]	6.3	1.70
Graphite, data taken from Refs. [278, 280-282]	6.5 [287, 290] ~ 7 [281, 282]	2.90
MLG/Ni(111), data taken from Refs. [275, 276]	6.7 [276] 7.5 [275]	~ 3

Table I: Energy and line-width of the π plasmon in the long wavelength limit (small momenta) for different systems.

As regards graphite, it is important to notice that π plasmon energy in the long-wavelength limit (small momenta) strongly depends on the modality of the EELS experiment. In fact, EELS measurements in the

reflection mode provide an energy of 6.5 eV [287, 290], while transmission measurements yield approximately 7 eV [288, 289].

Intermediate values have been recorded for vertically-aligned (VA) single-walled carbon nanotubes (SWCNT) [286] and MLG on 6H-SiC(0001) [266] (about 5 eV) and magnetically aligned bundles of SWCNT [279] (about 6 eV).

A HREELS investigation on graphene grown on 6H-SiC(0001) showed the existence of a blue-shift of the π plasmon energy [266] as a function of the number of graphene layers. In fact, it shifted from 4.9 (MLG) to 5.3 eV for bilayer graphene and to 6.2 eV for 3-4 layers of graphene.

The red-shift of the plasmon energy (at small momenta) when going from bulk graphite to quasi-two-dimensional graphene is caused by a decrease of the screening and of the interlayer coupling. This also influences the dispersion relation of the plasmon frequency. A linear dispersion was found for both VA-SWCNT [286] and MLG on 6H-SiC(0001) [266]. On the other hand, a quadratic dispersion has been recorded for bulk graphite [278], stage-1 ferric-chloride-intercalated graphite [283] and multilayer graphene on 6H-SiC(0001) [266]. For the latter case, it is clear that the realistic band structure of the system changes the dispersion of the π plasmon from linear to quadratic as a function of the number of graphene layers.

The dispersion relations that we obtained for MLG on Pt(111) (Figure 5.5) indicate a quadratic dispersion for the π plasmon. Even if a negligible hybridization between Pt and graphene states has been observed by angle-resolved photoemission spectroscopy measurements [81], the dispersion relation of the π plasmon is quadratic already for the MLG, as a consequence of the screening of the collective mode by the metal substrate. The screening in MLG on metal substrates is clearly more effective with respect to the case

of graphene layers grown on the semiconductor silicon carbide substrate. This should explain the quadratic dispersion recorded in MLG/Ni(111) (Ref. [276]) and MLG/Pt(111) (our data), in spite of the very different band structure of such two graphene/metal interfaces. We also remind that the plasmon dispersion in the long-wavelength limit is predicted to be quadratic with respect to momentum for the interacting electron gas [284].

Another issue to be considered is the interlayer coupling. Concerning supported graphene, the interlayer interaction varies as a function of the electron density in the layers. At higher electron density the overlap between orbitals of adjacent layers increases, thus increasing the interlayer coupling [285]. Hence, in principle the fact that MLG is hole-doped by charge transfer from the Pt substrate (Fermi level below Dirac point) [254] could influence the electronic response of the interface. As regards graphite, it is worth mentioning that its interlayer coupling is still under debate. Band structure calculations predicted an interlayer coupling much larger than the values deduced by c-axis conductivity measurements [286, 287].

A key factor in the propagation of the plasmonic excitation is its lifetime, which is limited by the decay into electron-hole pairs (Landau damping) [288]. The damping of the plasmon peak is clearly revealed by the trend of the full width at half maximum (FWHM) versus $q_{\parallel}$, reported in Fig. 5.6. The width of the plasmon rapidly increases with $q_{\parallel}$ due to the occurrence of Landau damping. It is worth remembering that, in contrast with the low-energy sheet plasmon [59, 236], the π-plasmon is a mode which lies inside the continuum of particle-hole excitations and therefore it will be damped even at $q_{\parallel} \rightarrow 0$ [240].

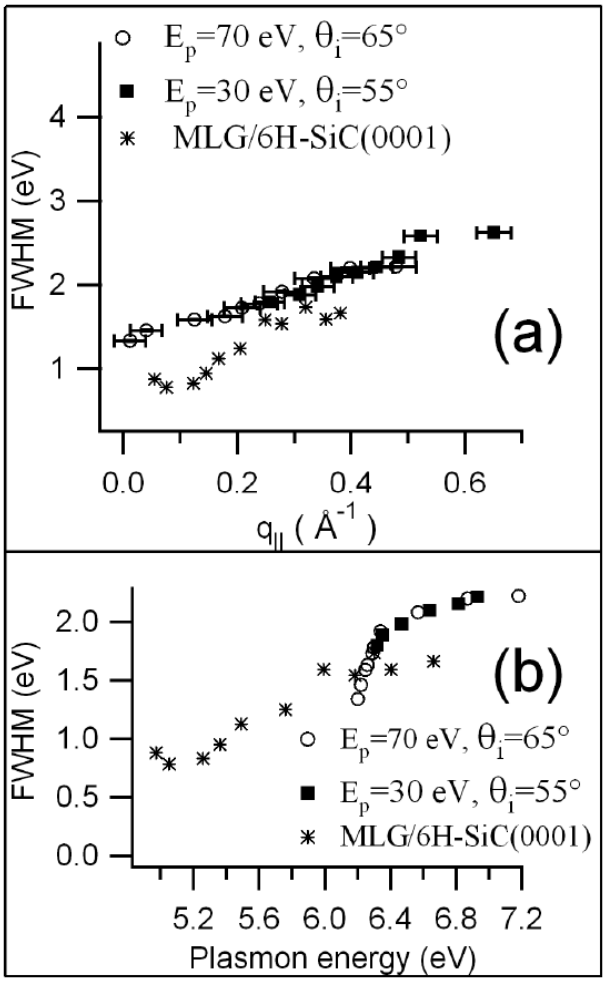

Figure 5.6: Behaviour of the FWHM of the π plasmon of MLG/Pt(111) acquired for two different scattering conditions as a function of (a) the parallel momentum transfer and (b) the plasmon energy. Data for MLG/6H-SiC(0001), taken from Ref. [266], are shown for a comparison.

On the other hand, the width of the π plasmon in MLG/6H-SiC(0001) initially decreased up to 0.1 Å^{-1}, followed by a steep increase as a function of $q_{\parallel}$. A similar behaviour has been recorded on graphite [278], where the turning point has been found at 0.3-0.4 Å^{-1}. The absence of a turning point in MLG/Pt(111) could be related to the nearly-linear dispersion of π bands in the Dirac cones [81]. Instead, substrate interactions in graphene on silicon carbide are known to distort the linear dispersion near the Dirac point in the first graphene layer [289]. They cause the appearance of a 260 meV energy gap and enhanced electron-phonon coupling [289]. This gap decreases as the

sample thickness increases and eventually approaches zero for multilayer graphene. The behavior of the FWHM as a function of the plasmon energy (Figure 4b) showed that for MLG/Pt(111) there is an enhanced broadening of the plasmon peak around 6.3 eV. These findings indicate that the Landau damping processes of the π plasmon in MLG/Pt(111) are mainly due to π-π^* interband transitions centered around 6.3 eV.

By comparing the FWHM in the long wave-length limit for various graphene systems (Table I), it is quite evident that the presence of out-of-plane decay channels reflects into a wider line-width of the plasmon peak, i.e. a shorter lifetime of the plasmon mode. As demonstrated for graphite [290], they cause additional damping of plasmons, which result in a more diffuse shape for the loss spectrum. As a matter of fact, the FWHM increases by a factor 6 from free-standing graphene to graphite.

Results for graphene on 6H-SiC(0001) showed that the π plasmon peak becomes broader and blue-shifted as the thickness of the epitaxial graphene increases. In fact, the π plasmon of 3–4 layer epitaxial graphene includes spectral contribution from both the out-of-plane and in-plane excitations of graphitic origin. This may be due to the three-dimensional band structure of graphite which allows interlayer coupling and out-of-plane excitation.

Moreover, it is worth noticing that the π plasmon in MLG/Pt(111) (our data) and MLG/Ni(111) [275, 276] has a shorter life-time (higher FWHM) than in MLG/6H-SiC(0001) and free-standing graphene as a consequence of enhanced screening by the metal substrate. This implies a broadening of the plasmon peak due to Landau damping via the creation of electron-hole pairs.

5.4 Conclusions

We have found a linear dispersion of the sheet plasmon in MLG on Pt(111), such behaviour is attributed to the nonlocal screening of the plasmon mode of MLG caused by the underlying Pt substrate. Due to its low energy and its linear dispersion, the sheet plasmon is expected to play an important role in graphene dynamics. This could be especially relevant for future graphene-based nano-optical devices, since the rippled, nanostructured surface of MLG on metal substrates (see Refs. [62, 151, 272]) provides an interesting scenario to couple acoustic surface plasmons and light. We have also shown that Landau damping occurs via interband transitions starting above the Fermi wave vector.

The π plasmon in MLG/Pt(111) has a quadratic dispersion, as in graphite but in contrast with results for MLG/6H-SiC(0001). Likewise, a quadratic dispersion has been found in MLG/Ni(111) but the quadratic coefficient differs by a factor 9. This is a consequence of the different electronic properties of MLG grown on Ni(111) (MLG strongly interacting with the substrate) and Pt(111) (Dirac cone preserved). A blue-shift by about 1.5 eV has been found with respect to the case of free-standing graphene and MLG/6H-SiC(0001).

We ascribe these results to the peculiar electronic properties of the MLG/Pt(111) interface. The system MLG/Pt(111) was characterized by a number of experimental techniques, indicating very weak interaction with the substrate, crucial for preservation of the astonishing intrinsic properties of graphene. It should be expected that the weak hybridization between graphene and Pt states and the graphene-Pt distance which resembles the interlayer distance in graphite would have implied that MLG/Pt(111) behaves as free-standing graphene. On the other hand, our findings indicate

that the screening by the underlying Pt substrate turns the dispersion of the π plasmon from linear to quadratic and it reduces plasmon life-time.

Thus, plasmon modes in MLG on Pt(111) could not be described by a model for quasi-two-dimensional electron gas, spatially-separated from the supporting substrate. In spite of the weak MLG-Pt interaction, π electrons behaves as an interacting electron gas. Our findings could be important for a more careful tailoring of the properties of graphene applications which are based on the propagation of plasmon modes.

6 CO and O_2 adsorption on $Pt_3Ni(111)$

6.1 Introduction

The investigation of the adsorption and dissociation of reactive chemical species on catalyst surfaces stand as one of the foremost aims of fundamental research in heterogeneous catalysis[85, 98, 103, 216, 231, 291-298]. In particular, the chemical reactivity of bimetallic surfaces has received considerable attention[299-305] as most real catalysts consist of alloys of 3*d*, 4*d* and 5*d* elements[88-91, 306-308]. Generally, these systems are characterized by a superior chemical activity and selectivity with respect to the pure elements[92, 299, 309]. For example, bimetallic catalysts play a key role in hydrogen low-temperature polymer electrolyte membrane fuel cells [310, 311].

Recently, it has been reported that the chemical activity of a $Pt_3Ni(111)$ surface towards the oxygen reduction reaction (ORR) is dramatically enhanced with respect to Pt/C catalysts and Pt(111) [312]. Such an enhanced reactivity is a consequence of the peculiar geometric arrangement of the topmost atomic layers of $Pt_3Ni(111)$ single crystals [313, 314]. Detailed investigation of $Pt_3Ni(111)$ crystals demonstrated that the first and third layers are Pt-rich while the second layer is Ni-rich [312, 315-317].

However, Pt-based surfaces are known to strongly react with CO [318-320]. This affects the activity of the catalyst surface by limiting the efficiency of the dissociation of O_2 molecules and consequently the rate of the ORR process.

In principle, the CO-induced poisoning effect could be significantly limited by CO oxidation, catalyzed by the Pt-M alloy (with M=V, Ti, Co, Fe, Ni). Hence, dedicated investigations on the adsorption of CO and oxygen and their co-adsorption on Pt-M surfaces are required in order to tailor more selective and effective catalysts for the ORR process.

Herein we report on a high-resolution electron energy loss spectroscopy (HREELS) investigation on the adsorption of O and CO and their co-adsorption on the $Pt_3Ni(111)$ surface. For the sake of comparison, selected adsorption experiments have been performed on the Pt(111) and Ni(111) surfaces.

We find that CO adsorbs in bridge and atop sites on both $Pt_3Ni(111)$ and Pt(111) surfaces with negligible differences as concerns vibrations. On the contrary, the vibrational spectra for oxygenated $Pt_3Ni(111)$ and Pt(111) surfaces exhibit significant differences as a consequence of the presence in the $Pt_3Ni(111)$ sample of a Ni layer underneath the outermost Pt layer. The oxidation of the Pt(111) substrate has a negligible effect on the adsorption of CO while the oxidation of the $Pt_3Ni(111)$ surface leads to a blocking of the bridge site for CO adsorption.

6.2 Results and discussion

6.2.1 CO adsorption

The loss spectra recorded by saturating the $Pt_3Ni(111)$ and Pt(111) samples at room temperature with an exposure of 10 L of CO (1 L=$1 \cdot 10^{-6}$ torr·s) are shown in the top panel of Figure 6.1. No appreciable differences between the results obtained for the two surfaces exist. The loss feature at 56 meV is due to the vibration of the whole CO molecule against the Pt(111) substrate [321-323]. Vibrational peaks at 230 and 258 meV arise from the intramolecular stretching vibration of CO adsorbed at bridge and atop sites, respectively, in agreement

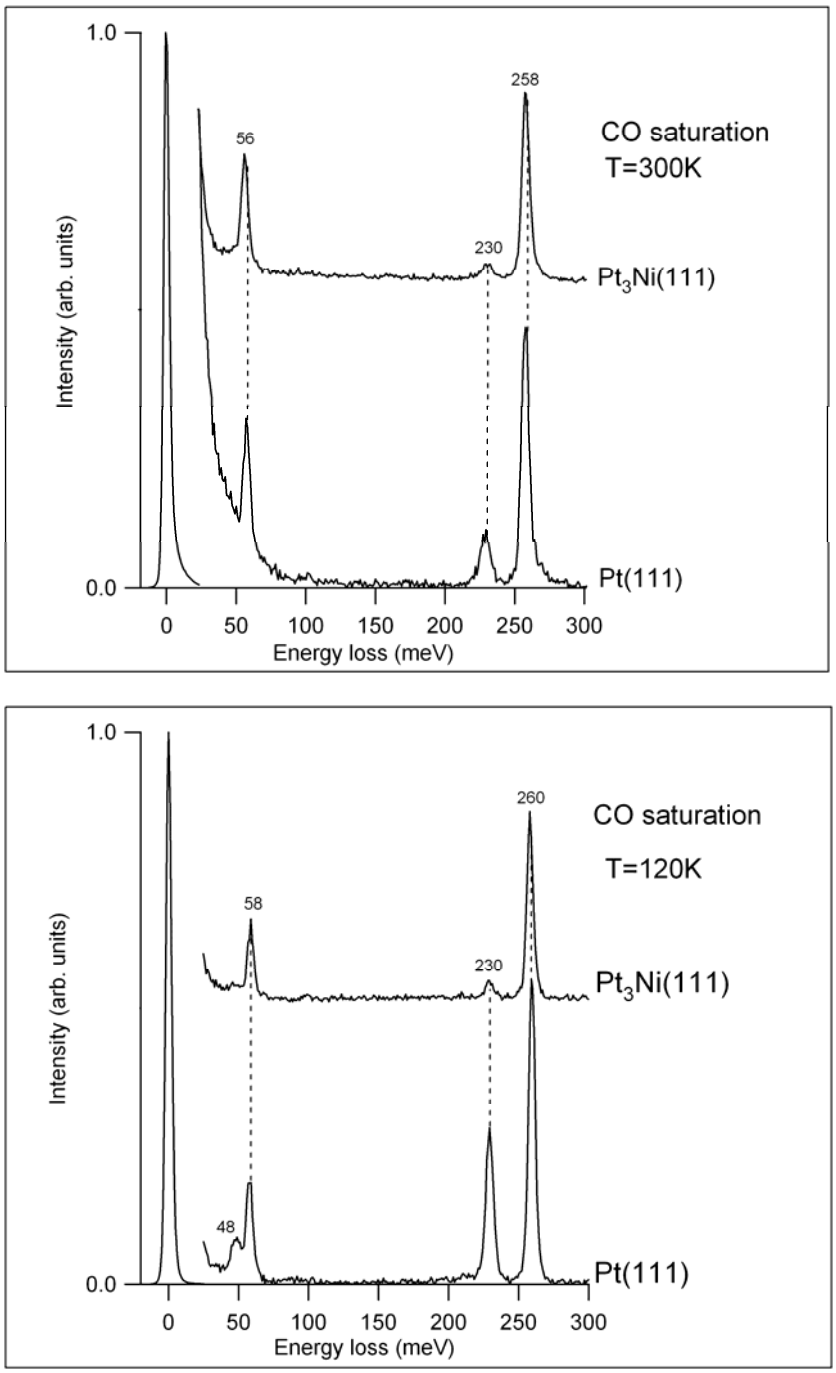

Figure 6.1: HREEL spectra for the CO-saturated Pt(111) and $Pt_3Ni(111)$ surfaces. Both measurements and exposures have been carried out at 300 K (top panel) and 120 K (bottom panel), respectively. Spectra have been recorded in specular geometry (incidence angle 55° with respect to the sample normal) and with a primary electron beam energy of 4 eV.

with previous results for CO adsorption on Pt(111) [324-326] and other transition-metal systems[101].

CO adsorption on the $Pt_3Ni(111)$ surface was also studied at 120 K (bottom panel of Figure 6.1). A preferential occupation of the atop site with respect to the bridge is observed. In particular, it is possible to clearly separate the vibration against the substrate of the whole CO molecule adsorbed at atop and bridge sites, recorded at 48 and 58 meV, respectively.

One of the reasons leading to the improved ORR of Pt_3M samples is their superior resistance to poisoning effect toward CO and OH in comparison to pure Pt [327, 328]. However, present results in UHV conditions demonstrate that both $Pt_3Ni(111)$ and Pt(111) surface strongly interact with CO molecules and, moreover, there are no noticeable differences between the two surfaces. Loss spectra of figure 6.1 also indicate that the first layer of $Pt_3Ni(111)$ is composed exclusively of Pt atom (Pt-skin), in agreement with results in Refs. [312, 313, 315, 329-333]. The possible modifications in the electronic structure of this Pt overlayer induced by Ni atoms located in the second layer do not affect CO adsorption. Density functional theory calculations showed that the interaction of adsorbates with Pt_3Ni alloy is notably weakened with respect to the pure Pt sample [332, 334]. This should be a direct consequence of the downshift of the localised d-band center in the alloy [332, 334]. However, such finding is not confirmed by present vibrational measurements as concerns CO adsorption.

6.2.2 Oxygen adsorption

Oxide layers play a fundamental role in several catalytic reactions[113, 335, 336]. Contrary to the common thought it is now accepted that CO oxidation is more effective on oxidized metal surfaces than on clean metal surfaces[337, 338]. Recently, it has been reported that oxide patches may be formed even at low temperature as reported for the case of the Ni(111) and Au/Ni(111) surfaces

exposed to oxygen at 100 K [339]. The oxide phase is active toward low-temperature CO oxidation. In the present study, oxide layers were obtained by exposing the $Pt_3Ni(111)$ surface to 100 L of O_2 at a sample temperature ranging from 400 to 900 K. The corresponding loss spectra, recorded at room temperature after O_2 exposure, are shown in Figure 6.2. Intense C-O vibrational bands (arising from residual CO in the chamber) are present in loss spectra for O_2 exposure at a sample temperature up to T=800 K. The contamination by CO molecules is expected to affect the adsorption and dissociation of O_2 molecules. Loss spectra for O_2 exposure of the $Pt_3Ni(111)$ substrate at lower sample temperature (400 and 500 K) show two weak features at 60 and 125 meV, respectively. While the peak at 60 meV can be assigned to O atoms in three-fold hollow sites vibrating against the Pt substrate[340, 341], the origin of the band at 125 meV is unclear. However, a discussion about this feature will be presented in the next subsection. By increasing sample temperature during O_2 exposure, the loss spectrum exhibits notable changes with the appearance of new and intense vibrational bands. The spectrum obtained for O_2 exposure at 800 K is dominated by an intense peak at 69 meV and less intense losses at 55, 116, and 138 meV. These three features further evolve by increasing the sample temperature during O_2 exposure and for T=900 K the loss spectrum show bands centered at 60, 84, 125, and 157 meV. The oxidation processes of a $Pt_3Ni(111)$ surface have been investigated in Ref. [342] by Menning et al. [316].

Therein the possible segregation of Ni atoms towards the first layer of the $Pt_3Ni(111)$ surface at 450 K has been suggested to occur. Actually, the presence of the loss peak at 69 meV (oxidation at T=800 K) seems to support these conclusions. As a matter of fact, the O-Ni vibration is expected at 70 meV in (111)-oriented surfaces [106, 343].

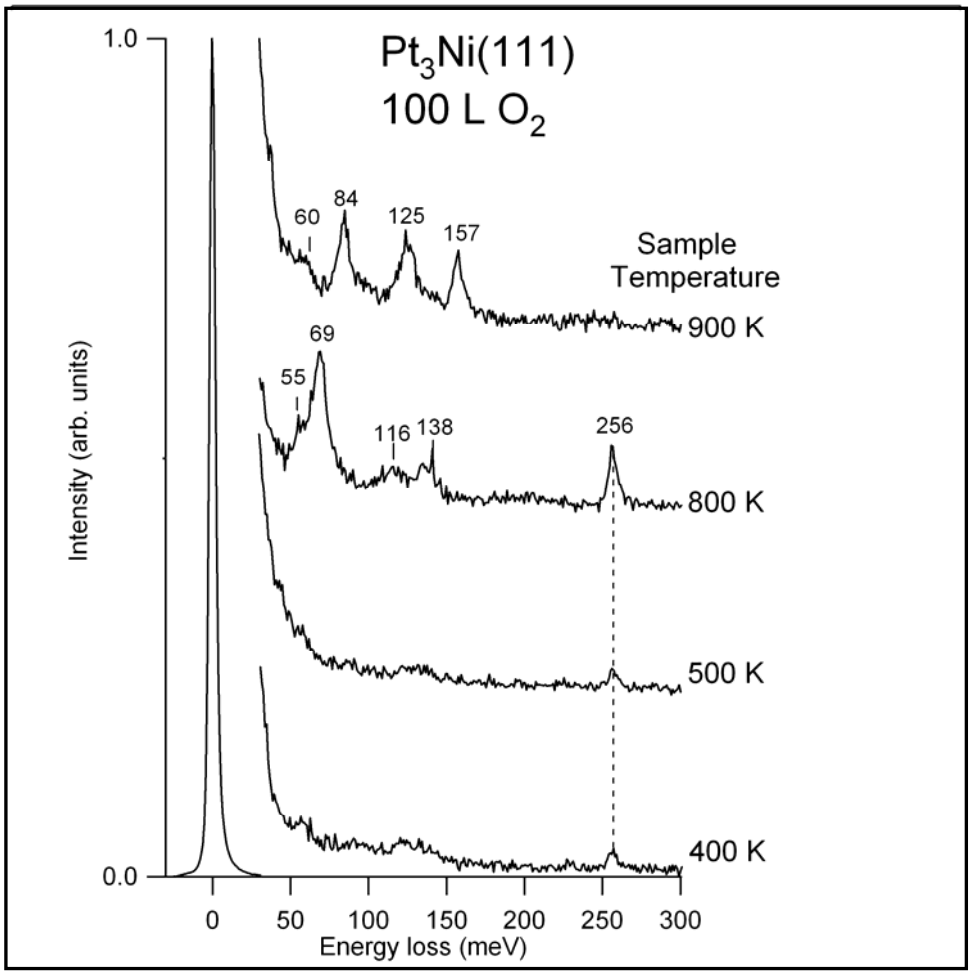

Figure 6.2: HREEL spectra recorded after the $Pt_3Ni(111)$ surface was dosed with 100 L of O_2 as a function of the sample temperature. Measurements have been carried out at 300 K.

However, it is worth noticing that the exact identification of vibrational peaks of surface oxides is quite difficult, as evidenced in Ref [344]. In fact, the spectrum obtained by surface oxidation at 900 K shows the same number of losses as that at 800 K but slightly shifted to higher energies. In our opinion such shift arises from changes occurring in the local atomic arrangement due to the formation of a surface oxide and, moreover, from possible lateral interactions among oxygen atoms. With the aim to gain useful information for a correct interpretation of losses peaks observed for $O/Pt_3Ni(111)$ surface we also

carried out loss measurements on Pt(111) and Ni(111) after their oxidation, respectively (Figure 6.3).

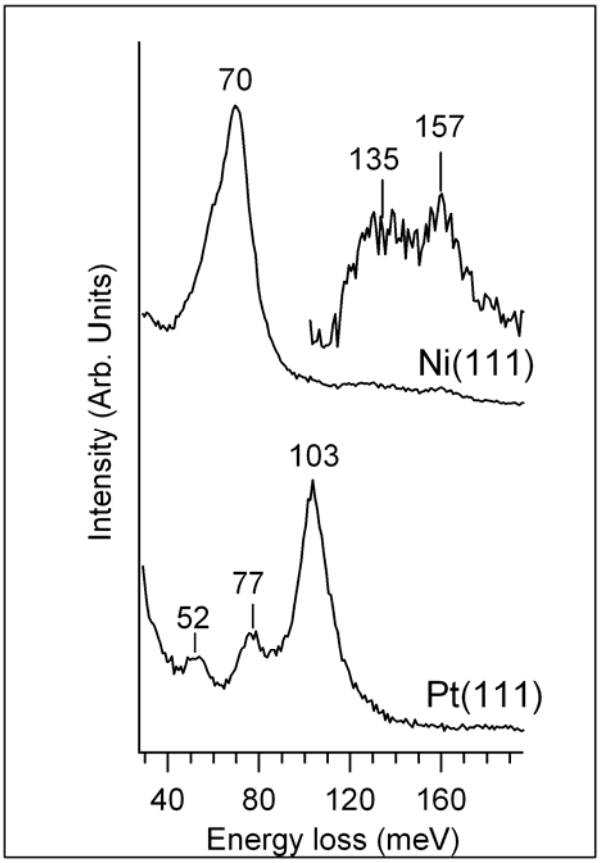

Figure 6.3: HREEL spectra for the oxidized Pt(111) and Ni(111) surfaces. Measurements have been carried out at room temperature.

Interestingly, the surface oxide formed on the Pt(111) surface shows essentially three losses at 52, 77, and 103 meV. The vibrational energies of these losses are slightly red-shifted with respect to the corresponding losses in the spectrum of O/Pt_3Ni(111). Instead, in the loss spectrum of O/Pt(111) there are no peaks in the region 138-157 meV. The spectrum taken on the O/Ni(111) surface (Figure 6.3) shows a peak at 70 meV due to the O-Ni vibration [102, 106, 343]. Particularly intriguing are the losses at 135 and 157 meV. The high energy of such features suggests a generic assignment to vibrational modes related to the presence of subsurface oxygen. Interestingly, they could be fingerprint for the

formation of d-holes, which takes place in the initial oxidation stage of the Ni(111) surface.

It has been demonstrated for O/Ag(001)[345] that the complex formed by the Ag^{2+} ion, two oxygen adatoms and one oxygen atom in the octahedral interstitial gives rise to a dipole active electron energy loss at 130 meV. Likewise, localised d-d transition within a complex formed by the Ni^{2+} ions, by one subsurface oxygen atom in the octahedral interstitial site and by two neighbouring oxygen adatoms could cause the appearance of loss peaks at 135 and 157 meV.

The presence of Ni^{2+} ions at the surface induced by subsurface oxygen could explain some of the peculiar catalytic properties of oxygenated nickel surfaces [346].

Likewise, we suggest that bands at 116-125 and 138-157 meV in figure 6.2 could arise from localized d-d transitions of Pt-O and Ni-O complexes.

On the basis of the results presented above, we suggest that the first layer of the $Pt_3Ni(111)$ crystal is composed exclusively of Pt atoms (Pt-skin) even after annealing at high temperature while Ni atoms reside in the layer underneath the outermost Pt layer. However, while we cannot find significant differences between the adsorption of CO on $Pt_3Ni(111)$ and Pt(111), on the contrary the adsorption of oxygen (both over-surface and subsurface) is strongly influenced by the electronic and geometric structure of the $Pt_3Ni(111)$.

6.2.3 CO and oxygen co-adsorption

The dissociation of oxygen molecules on metal surfaces is the limiting steps in several chemical reactions i.e. the ORR and the catalytic oxidation of CO. We have investigated how CO adsorbs and reacts with the oxygenated $Pt_3Ni(111)$ and Pt(111) surfaces. In our previous study of CO/O/Ni(111) we find

that oxygen do not interacts with a CO-precovered surface [347]. On the clean Ni(111) surface, both CO and oxygen occupy three-fold hollow sites and thus whenever these sites are occupied by CO molecules, oxygen do not adsorbs. By contrast, CO adsorption occurs on the oxygen–predosed surface and a change of site from three-fold to atop is observed [347]. In this study, an oxygenated $Pt_3Ni(111)$ surface (O_2 exposure at 900 K) was saturated with CO at room temperature (Figure 6.4). On this surface CO adsorbs only at atop site as evidenced by the C-O stretching at 258 meV and CO-substrate at 56 meV. Thus, pre-adsorbed oxygen block the bridge site which instead was occupied for the clean $Pt_3Ni(111)$ surface. Hence, this is the unique effect of pre-adsorbed oxygen on CO adsorption. The expected weakening of the CO-substrate bond due to CO-O lateral interaction [310] is not observed. It is interesting to notice that, contrary to the case of the $Pt_3Ni(111)$ surface, the adsorption of CO onto an oxygenated Pt(111) surface (Figure 6.5) is not at all influenced by pre-adsorbed oxygen. The single vibrational band at 107 meV of the oxygenated Pt(111) surface indicates the formation of a single type of oxide [341]. On both the clean and the O-precovered surface, CO molecules adsorb in bridge and atop sites. This could arise from the coexistence of part of surface that are covered by a surface oxide and part of the surface that are O-free. Thus, we have direct evidences that CO adsorbs differently on the oxidized $Pt_3Ni(111)$ and Pt(111) surfaces.

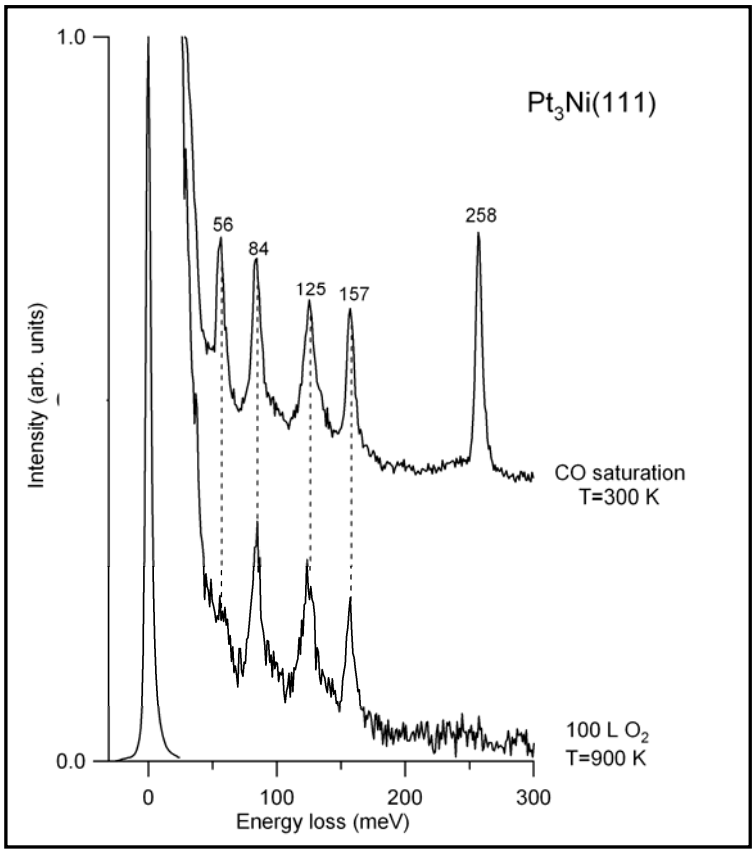

Figure 6.4: HREEL spectra for the Pt3Ni(111) surface exposed to 100 L of O2 at 900 K and successively saturated with CO at 300 K.

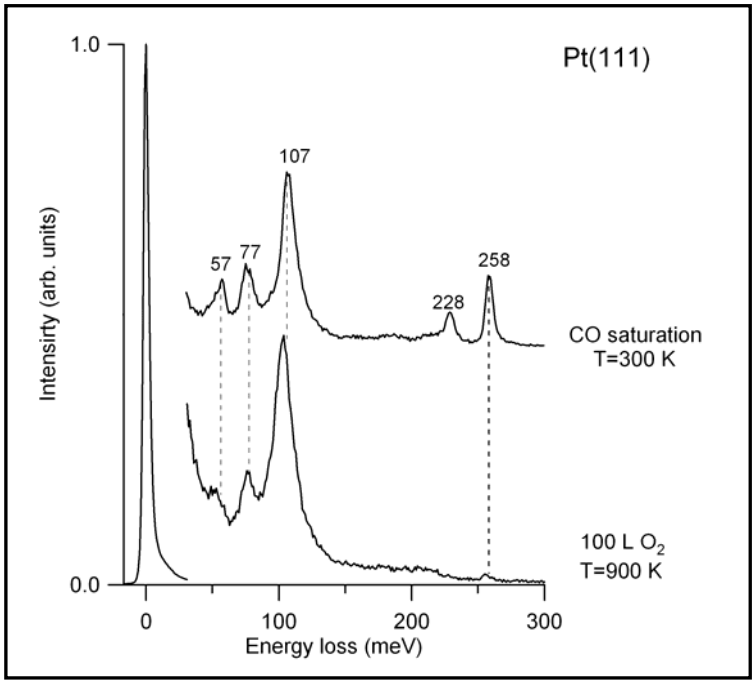

Figure 6.5: HREEL spectra for the Pt(111) surface exposed to 100 L of O_2 at 900 K and successively saturated with CO at 300 K.

6.3 Conclusions

In this investigation we have shown that CO adsorbs without appreciable differences on $Pt_3Ni(111)$ and Pt(111). The vibrational results indicate that the first layer of the $Pt_3Ni(111)$ surface is composed of Pt atoms and, moreover, that the presence of Ni atoms in the second layer has modest influence on the C-O chemical bond. On the contrary, the geometrical structure of the $Pt_3Ni(111)$ alloy has a great influence on the oxidation process at high temperature. In particular, for the $Pt_3Ni(111)$ surface, the occupation of the bridge sites of the Pt first layer and the presence of subsurface oxygen (on the Ni atoms) are identified. The population of the bridge sites in $Pt_3Ni(111)$ is further confirmed by the adsorption of CO. In fact, in the oxidized $Pt_3Ni(111)$ surface CO adsorbs only at atop site. On the contrary, on both clean Pt(111) and oxidized Pt(111), CO molecules occupy bridge as well as atop sites.

7 Summary

HREELS has proved a powerful and versatile technique for understanding the adsorption, catalytic, and electronic properties of ultrathin layers adsorbed on metal substrates in UHV conditions.

As concerns the vibrational measurements, the phonon modes of graphene/Pt(111) were probed. We have found that lattice dynamics in quasi-freestanding graphene is similar to those ones of graphite, with well-distinct Kohn anomalies for the highest optical branches at the high-symmetry points of the Brillouin zone.

From experimental phonon dispersions it is possible to draw conclusions about the interaction strength in graphene/metal interfaces. Such investigation is of fundamental importance for graphene-based devices as both electronic and optical excitations can be scattered by phonon states or decay into vibrational excitations.

We have studied water interaction with clean and K-doped quasi-freestanding graphene on Pt(111) at 100 K. On pristine graphene, water adsorption does not occur for sample temperature higher than 130 K. Loss measurements demonstrate that at the lowest coverages water molecules adsorb in the two-leg configuration. For increasing water coverage, we have found that the adsorption of one-leg H_2O takes place. Present results agree with recent theoretical works, which thus provide a satisfactory description of the adsorption geometry at the water/graphene interface, and, in particular, of the water orientation on graphene.

Moreover, we have found that water adsorption on K-modified graphene is dissociative, as evidence by the existence of C-H bending and stretching modes in the vibrational spectrum. This provides a new method for modifying the interfacial properties of graphene by adsorption of atomic and molecular species.

Water exposure at room temperature of MLG/Pt(111) could lead to the formation of C-H bonds. Dehydrogenation is possible upon annealing at 450 K, on the other hand, no dissociation was observed at 100 K. Water dissociation could also afford interesting pathways to produce hydrogen. Moreover, water-induced hydrogenation of graphene should be taken into account in engineering graphene-based devices which should work at atmospheric pressure and at room temperature.

Low-energy collective excitations in graphene are attracting much interest in recent years as they influence many of the peculiar properties of graphene samples, in particular, the dispersion and damping of plasmons in epitaxial graphene. We have found a linear dispersion of the sheet plasmon in MLG on Pt(111), such behaviour is attributed to the nonlocal screening of the plasmon mode of MLG caused by the underlying Pt substrate. Due to its low energy and its linear dispersion, the sheet plasmon is expected to play an important role in graphene dynamics. The π plasmon in MLG/Pt(111) has a quadratic dispersion, as in graphite but in contrast with results for MLG/6H-SiC(0001). We ascribe these results to the peculiar electronic properties of the MLG/Pt(111) interface. The system MLG/Pt(111) was characterized by a number of experimental techniques, indicating very weak interaction with the substrate, crucial for preservation of the outstanding intrinsic properties of graphene. It should be expected that the weak hybridization between graphene and Pt states and the graphene-Pt distance which resembles the

interlayer distance in graphite would have implied that MLG/Pt(111) behaves as free-standing graphene. On the other hand, our findings indicate that the screening by the underlying Pt substrate turns the dispersion of the π plasmon from linear to quadratic and it reduces plasmon life-time.

Thus, plasmon modes in MLG on Pt(111) could not be described by a model for quasi-twodimensional electron gas, spatially-separated from the supporting substrate. In spite of the weak MLG-Pt interaction, π electrons behaves as an interacting electron gas. Our findings could be important for a more careful tailoring of the properties of graphene applications which are based on the propagation of plasmon modes.

Finally, we have shown that CO adsorbs without appreciable differences on $Pt_3Ni(111)$ and Pt(111). The vibrational results indicate that the first layer of the $Pt_3Ni(111)$ surface is composed of Pt atoms and, moreover, that the presence of Ni atoms in the second layer has modest influence on the C-O chemical bond. On the contrary, the geometrical structure of the $Pt_3Ni(111)$ alloy has a great influence on the oxidation process at high temperature. In particular, for the $Pt_3Ni(111)$ surface, the occupation of the bridge sites of the Pt first layer and the presence of subsurface oxygen (on the Ni atoms) are identified. The population of the bridge sites in $Pt_3Ni(111)$ is further confirmed by the adsorption of CO. In fact, in the oxidized $Pt_3Ni(111)$ surface CO adsorbs only at atop site. On the contrary, on both clean Pt(111) and oxidized Pt(111), CO molecules occupy bridge as well as atop sites.

List of Publications

2010

1) A. Politano, A. R. Marino, G. Chiarello, "CO-promoted formation of the alkali-oxygen bond on Ni(111)", *Journal of Chemical Physics*, 2010, Vol. 132, n. 4, pp. 044706.
2) A. Politano, A. R. Marino, G. Chiarello, "Alkali-promoted stabilization of subsurface oxygen on Cu(111)", *Chemical Physics*, 2010, Vol. 367, n. 1-2, pp. 148-151.

2011

3) A. Politano, A. R. Marino, V. Formoso, G. Chiarello, "The adsorption and co-adsorption of oxygen and carbon monoxide on $Pt_3Ni(111)$: a vibrational study", *Journal of Chemical Physics*, 2011, Vol. 132, n. 4, pp. 044706.
4) A. Politano, A. R. Marino, V. Formoso, D. Farías, R. Miranda, G. Chiarello, "Evidence for acoustic-like plasmons on epitaxial graphene on Pt(111)", *Physical Review B*, 2011, Vol. 84, n.3, pp. 033401
5) A. Politano, A. R. Marino, V. Formoso, G. Chiarello, "Hydrogen bonding at the water/quasi-freestanding graphene interface", *Carbon*, Vol. 49, n. 15, pp. 5180-5184
6) A. Politano, A. R. Marino, G. Chiarello, "Phonon dispersion of quasi-freestanding graphene on Pt(111)", *Journal of Physics: Condensed Matter*, INVITED, in press
7) A. Politano, A. R. Marino, V. Formoso, G. Chiarello, "Water adsorption on graphene/Pt(111) at room temperature: a vibrational investigation", *AIP Advances*, 2011, Vol. 1, n. 4, pp. 042130.

8) A. Politano, A. R. Marino, V. Formoso, G. Chiarello, "Evidence of Kohn anomalies in quasi-freestanding graphene on Pt(111)", *Carbon*, 2012, Vol. 50, n. 2, pp. 734-736.

9) A. Politano, A. R. Marino, V. Formoso, D. Farías, R. Miranda, G. Chiarello, "Quadratic dispersion and damping processes of π plasmon in monolayer graphene on Pt(111)", *Plasmonics*, in press.

UNDER REVIEW

9) "Probing the initial steps of water interaction with epitaxial graphene", submitted to *Angewandte Chemie*

10) "Elastic properties of a macroscopical graphene sample from angle-resolved vibrational experiments on phonon dispersion", submitted to *Nano Letters*

11) "Evidence of charge carrier-acoustic plasmon coupling in epitaxial graphene on Pt(111) by angle-resolved vibrational experiments", submitted to *Physical Review Letters*

IN PREPARATION

13) "Raman spectroscopy, scanning electron microscopy, and electron energy loss investigation of graphene/Pt(111)", *in preparation*

14) "Plasmon confinement in graphene/Ru(0001)", *in preparation*

15) "Ethylene interaction with $Pt_3Ni(111)$", *in preparation*

16) "Plasmonic modes at graphene", *review in preparation*

Collaborations

A. Politano, D. Farias,

(Universidad Autonoma de Madrid, Spain)

R. Miranda,

(IMDEA NanocienciaNanociencia, Madrid, Spain)

E. Cazzanelli,

(Liquid Crystal Laboratory Laboratory, Unical)

A. Principi,

(Scuola Normale Superiore,Pisa)

V. Silkin,

(Donostia International Physics Center,

San Sebastian, Spain).

Bibliography

[1] K. S. Novoselov, A. K. Geim, S. V. Morozov, D. Jiang, Y. Zhang, S. V. Dubonos, I. V. Grigorieva and A. A. Firsov, Electric Field Effect in Atomically Thin Carbon Films, Science 306 (2004) 666.

[2] T. Aizawa, Y. Hwang, W. Hayami, R. Souda, S. Otani and Y. Ishizawa, Phonon dispersion of monolayer graphite on Pt(111) and NbC surfaces: bond softening and interface structures, Surf. Sci. 260 (1992) 311.

[3] T. Aizawa, R. Souda, Y. Ishizawa, H. Hirano, T. Yamada, K.-I. Tanaka and C. Oshima, Phonon dispersion in monolayer graphite formed on Ni(111) and Ni(001), Surf. Sci. 237 (1990) 194.

[4] T. Aizawa, R. Souda, S. Otani, Y. Ishizawa and C. Oshima, Bond softening in monolayer graphite formed on transition-metal carbide surfaces, Phys. Rev. B 42 (1990) 11469.

[5] Y. Gamo, A. Nagashima, M. Wakabayashi, M. Terai and C. Oshima, Atomic structure of monolayer graphite formed on Ni(111), Surf. Sci. 374 (1997) 61.

[6] A. M. Shikin, D. Farías, V. K. Adamchuk and K. H. Rieder, Surface phonon dispersion of a graphite monolayer adsorbed on Ni(111) and its modification caused by intercalation of Yb, La and Cu layers, Surf. Sci. 424 (1999) 155.

[7] A. M. Shikin, D. Farías and K. H. Rieder, Phonon stiffening induced by copper intercalation in monolayer graphite on Ni(111), Europhys. Lett. 44 (1998) 44.

[8] C. Berger, Z. Song, T. Li, X. Li, A. Y. Ogbazghi, R. Feng, Z. Dai, A. N. Marchenkov, E. H. Conrad, P. N. First and W. A. de Heer, Ultrathin Epitaxial Graphite: 2D Electron Gas Properties and a Route toward Graphene-based Nanoelectronics, J. Phys. Chem. B 108 (2004) 19912.

[9] A. Du, Z. Zhu and S. C. Smith, Multifunctional Porous Graphene for Nanoelectronics and Hydrogen Storage: New Properties Revealed by First Principle Calculations, J. Am. Chem. Soc. 132 (2010) 2876.

[10] R. A. Nistor, D. M. Newns and G. J. Martyna, The Role of Chemistry in Graphene Doping for Carbon-Based Electronics, ACS Nano 5 (2011) 3096.

[11] M. Sprinkle, P. Soukiassian, W. A. De Heer, C. Berger and E. H. Conrad, Epitaxial graphene: The material for graphene electronics, Phys. Status Solidi RRL 3 (2009) A91.

[12] R. S. Sundaram, M. Steiner, H.-Y. Chiu, M. Engel, A. A. Bol, R. Krupke, M. Burghard, K. Kern and P. Avouris, The Graphene–Gold Interface and Its Implications for Nanoelectronics, Nano Lett. 11 (2011) 3833.

[13] Z. Wei, D. Wang, S. Kim, S.-Y. Kim, Y. Hu, M. K. Yakes, A. R. Laracuente, Z. Dai, S. R. Marder, C. Berger, W. P. King, W. A. de Heer, P. E. Sheehan and E. Riedo, Nanoscale Tunable Reduction of Graphene Oxide for Graphene Electronics, Science 328 (2010) 1373.
[14] R. M. Westervelt, Graphene Nanoelectronics, Science 320 (2008) 324.
[15] X. Wu, M. Sprinkle, X. Li, F. Ming, C. Berger and W. A. de Heer, Epitaxial-Graphene/Graphene-Oxide Junction: An Essential Step towards Epitaxial Graphene Electronics, Phys. Rev. Lett. 101 (2008) 026801.
[16] K. S. Kim, Y. Zhao, H. Jang, S. Y. Lee, J. M. Kim, K. S. Kim, J.-H. Ahn, P. Kim, J.-Y. Choi and B. H. Hong, Large-scale pattern growth of graphene films for stretchable transparent electrodes, Nature 457 (2009) 706.
[17] X. Li, Y. Zhu, W. Cai, M. Borysiak, B. Han, D. Chen, R. D. Piner, L. Colomba and R. S. Ruoff, Transfer of large-area graphene films for high-performance transparent conductive electrodes, Nano Lett. 9 (2009) 4359.
[18] R. R. Nair, P. Blake, J. R. Blake, R. Zan, S. Anissimova, U. Bangert, A. P. Golovanov, S. V. Morozov, A. K. Geim, K. S. Novoselov and T. Latychevskaia, Graphene as a transparent conductive support for studying biological molecules by transmission electron microscopy, Appl. Phys. Lett. 97 (2010) 153102.
[19] Y. Cao, S. Liu, Q. Shen, K. Yan, P. Li, J. Xu, D. Yu, M. L. Steigerwald, C. Nuckolls, Z. Liu and X. Guo, High-Performance Photoresponsive Organic Nanotransistors with Single-Layer Graphenes as Two-Dimensional Electrodes, Adv. Funct. Mater. 19 (2009) 2743.
[20] M. D. Stoller, S. Park, Y. Zhu, J. An and R. S. Ruoff, Graphene-Based Ultracapacitors, Nano Lett. 8 (2008) 3498.
[21] Y. Wang, Z. Shi, Y. Huang, Y. Ma, C. Wang, M. Chen and Y. Chen, Supercapacitor Devices Based on Graphene Materials, J. Phys. Chem. C 113 (2009) 13103.
[22] Z. Cheng, Q. Li, Z. Li, Q. Zhou and Y. Fang, Suspended Graphene Sensors with Improved Signal and Reduced Noise, Nano Lett. 10 (2010) 1864.
[23] V. Dua, S. P. Surwade, S. Ammu, S. R. Agnihotra, S. Jain, K. E. Roberts, S. Park, R. S. Ruoff and S. K. Manohar, All-Organic Vapor Sensor Using Inkjet-Printed Reduced Graphene Oxide, Angew. Chem. 49 (2010) 2154.
[24] J. H. Jung, D. S. Cheon, F. Liu, K. B. Lee and T. S. Seo, A Graphene Oxide Based Immuno-biosensor for Pathogen Detection, Angew. Chem. 49 (2010) 5708.
[25] G. Lu, L. E. Ocola and J. Chen, Reduced graphene oxide for room-temperature gas sensors, Nanotechnology 20 (2009) 445502.

[26] W. R. Yang, K. R. Ratinac, S. P. Ringer, P. Thordarson, J. J. Gooding and F. Braet, Carbon Nanomaterials in Biosensors: Should You Use Nanotubes or Graphene?, Angew. Chem. 49 (2010) 2114.
[27] F. Schedin, A. K. Geim, S. V. Morozov, E. W. Hill, P. Blake, M. I. Katsnelson and K. S. Novoselov, Detection of individual gas molecules adsorbed on graphene, Nat. Mater. 6 (2007) 652.
[28] P. J. Hale, S. M. Hornett, J. Moger, D. W. Horsell and E. Hendry, Hot phonon decay in supported and suspended exfoliated graphene, Phys. Rev. B 83 (2011) 121404.
[29] E. D. Grayfer, A. S. Nazarov, V. G. Makotchenko, S. J. Kim and V. E. Fedorov, Chemically modified graphene sheets by functionalization of highly exfoliated graphite, J. Mater. Chem. 21 (2011) 3410.
[30] P. Laaksonen, M. Kainlauri, T. Laaksonen, A. Shchepetov, H. Jiang, J. Ahopelto and M. B. Linder, Interfacial Engineering by Proteins: Exfoliation and Functionalization of Graphene by Hydrophobins, Angew. Chem. 49 (2010) 4946.
[31] S. Vadukumpully, J. Paul and S. Valiyaveettil, Cationic surfactant mediated exfoliation of graphite into graphene flakes, Carbon 47 (2009) 3288.
[32] M. Lotya, Y. Hernandez, P. J. King, R. J. Smith, V. Nicolosi, L. S. Karlsson, F. M. Blighe, S. De, Z. Wang, I. T. McGovern, G. S. Duesberg and J. N. Coleman, Liquid Phase Production of Graphene by Exfoliation of Graphite in Surfactant/Water Solutions, J. Am. Chem. Soc. 131 (2009) 3611.
[33] A. B. Bourlinos, V. Georgakilas, R. Zboril, T. A. Sterioti and A. K. Stubos, Liquid-Phase Exfoliation of Graphite Towards Solubilized Graphenes, Small 5 (2009) 1841.
[34] Y. Hernandez, V. Nicolosi, M. Lotya, F. M. Blighe, Z. Sun, S. De, I. T. McGovern, B. Holland, M. Byrne, Y. K. Gun'ko, J. J. Boland, P. Niraj, G. Duesberg, S. Krishnamurthy, R. Goodhue, J. Hutchison, V. Scardaci, A. C. Ferrari and J. N. Coleman, High-yield production of graphene by liquid-phase exfoliation of graphite, Nat. Nanotechnol. 3 (2008) 563.
[35] D. L. Miller, K. D. Kubista, G. M. Rutter, M. Ruan, W. A. de Heer, P. N. First and J. A. Stroscio, Observing the Quantization of Zero Mass Carriers in Graphene, Science 324 (2009) 924.
[36] S. Watcharinyanon, C. Virojanadara and L. I. Johansson, Rb and Cs deposition on epitaxial graphene grown on 6H-SiC(0001), Surf. Sci. 605 (2011) 1918.
[37] F. Speck, The quasi-free-standing nature of graphene on H-saturated SiC(0001), Appl. Phys. Lett. 99 (2011) 122106.
[38] K. V. Emtsev, A. A. Zakharov, C. Coletti, S. Forti and U. Starke, Ambipolar doping in quasifree epitaxial graphene on SiC(0001) controlled by Ge intercalation, Phys. Rev. B 84 (2011) 125423.

[39] C. Virojanadara, A. A. Zakharov, R. Yakimova and L. I. Johansson, Buffer layer free large area bi-layer graphene on SiC(0001), Surf. Sci. 604 (2010) L4.
[40] J. Robinson, X. Weng, K. Trumbull, R. Cavalero, M. Wetherington, E. Frantz, M. LaBella, Z. Hughes, M. Fanton and D. Snyder, Nucleation of epitaxial graphene on SiC(0001), ACS Nano 4 (2010) 153.
[41] C. Riedl, C. Coletti and U. Starke, Structural and electronic properties of epitaxial graphene on SiC(0001): a review of growth, characterization, transfer doping and hydrogen intercalation, J. Phys. D: Appl. Phys. 43 (2010) 374009.
[42] R. M. Tromp and J. B. Hannon, Thermodynamics and Kinetics of Graphene Growth on SiC(0001), Phys. Rev. Lett. 102 (2009) 106104.
[43] G. F. Sun, J. F. Jia, Q. K. Xue and L. Li, Atomic-scale imaging and manipulation of ridges on epitaxial graphene on 6H-SiC(0001), Nanotechnology 20 (2009) 355701.
[44] M. L. Bolen, S. E. Harrison, L. B. Biedermann and M. A. Capano, Graphene formation mechanisms on 4H-SiC(0001), Phys. Rev. B 80 (2009) 115433.
[45] H. Hibino, S. Mizuno, H. Kageshima, M. Nagase and H. Yamaguchi, Stacking domains of epitaxial few-layer graphene on SiC(0001), Phys. Rev. B 80 (2009) 085406.
[46] C. Virojanadara, M. Syväjarvi, R. Yakimova, L. I. Johansson, A. A. Zakharov and T. Balasubramanian, Homogeneous large-area graphene layer growth on 6H -SiC(0001), Phys. Rev. B 78 (2008) 245403.
[47] P. Lauffer, K. V. Emtsev, R. Graupner, T. Seyller, L. Ley, S. A. Reshanov and H. B. Weber, Atomic and electronic structure of few-layer graphene on SiC(0001) studied with scanning tunneling microscopy and spectroscopy, Phys. Rev. B 77 (2008) 155426.
[48] N. Ferralis, M. Roya and C. Carraro, Evidence of Structural Strain in Epitaxial Graphene Layers on 6H-SiC(0001), Phys. Rev. Lett. 101 (2008) 156801.
[49] C. Riedl, A. A. Zakharov and U. Starke, Precise in situ thickness analysis of epitaxial graphene layers on SiC(0001) using low-energy electron diffraction and angle resolved ultraviolet photoelectron spectroscopy, Appl. Phys. Lett. 93 (2008) 033106.
[50] T. Ohta, F. El Gabaly, A. Bostwick, J. L. McChesney, K. V. Emtsev, A. K. Schmid, T. Seyller, K. Horn and E. Rotenberg, Morphology of graphene thin film growth on SiC(0001), New J. Phys. 10 (2008) 023034.
[51] A. Bostwick, J. McChesney, T. Ohta, E. Rotenberg, T. Seyller and K. Horn, Experimental studies of the electronic structure of graphene, Prog. Surf. Sci. 84 (2009) 380.

[52] T. Ohta, A. Bostwick, T. Seyller, K. Horn and E. Rotenberg, Controlling the electronic structure of bilayer graphene, Science 313 (2006) 951.
[53] S. Shivaraman, R. A. Barton, X. Yu, J. Alden, L. Herman, M. S. V. Chandrashekhar, J. Park, P. L. McEuen, J. M. Parpia, H. G. Craighead and M. G. Spencer, Free-standing epitaxial graphene, Nano Lett. 9 (2009) 3100.
[54] X. Wu, Y. Hu, M. Ruan, N. K. Madiomanana, J. Hankinson, M. Sprinkle, C. Berger and W. A. De Heer, Half integer quantum Hall effect in high mobility single layer epitaxial graphene, Appl. Phys. Lett. 95 (2009) 223108.
[55] A. Zangwill and D. D. Vvedensky, Novel Growth Mechanism of Epitaxial Graphene on Metals, Nano Lett. 11 (2011) 2092.
[56] M. Losurdo, M. M. Giangregorio, P. Capezzuto and G. Bruno, Ellipsometry as a Real-Time Optical Tool for Monitoring and Understanding Graphene Growth on Metals, J. Phys. Chem. C 115 (2011) 21804.
[57] P. A. Khomyakov, G. Giovannetti, P. C. Rusu, G. Brocks, J. van Den Brink and P. J. Kelly, First-principles study of the interaction and charge transfer between graphene and metals, Phys. Rev. B 79 (2009) 195425.
[58] A. Politano, A. R. Marino, V. Formoso and G. Chiarello, Evidence of Kohn anomalies in quasi-freestanding graphene on Pt(111), Carbon 50 (2012) 734.
[59] A. Politano, A. R. Marino, V. Formoso, D. Farías, R. Miranda and G. Chiarello, Evidence for acoustic-like plasmons on epitaxial graphene on Pt(111), Phys. Rev. B 84 (2011) 033401.
[60] A. Politano, A. R. Marino, V. Formoso and G. Chiarello, Hydrogen bonding at the water/quasi-freestanding graphene interface, Carbon 49 (2011) 5180.
[61] A. Politano, B. Borca, M. Minniti, J. J. Hinarejos, A. L. Vázquez de Parga, D. Farías and R. Miranda, Helium reflectivity and Debye temperature of graphene grown epitaxially on Ru(0001), Phys. Rev. B 84 (2011) 035450.
[62] B. Borca, S. Barja, M. Garnica, M. Minniti, A. Politano, J. M. Rodriguez-García, J. J. Hinarejos, D. Farías, A. L. Vázquez de Parga and R. Miranda, Electronic and geometric corrugation of periodically rippled, self-nanostructured graphene epitaxially grown on Ru(0001), New J. Phys. 12 (2010) 093018.
[63] D. Martoccia, M. Björck, C. M. Schlepütz, T. Brugger, S. A. Pauli, B. D. Patterson, T. Greber and P. R. Willmott, Graphene on Ru(0001): a corrugated and chiral structure, New J. Phys. 12 (2010) 043028.
[64] D. Martoccia, P. R. Willmott, T. Brugger, M. Björck, S. Günther, C. M. Schlepütz, A. Cervellino, S. A. Pauli, B. D. Patterson, S. Marchini, J.

Wintterlin, W. Moritz and T. Greber, Graphene on Ru(0001): A 25×25 supercell, Phys. Rev. Lett. 101 (2008) 126102.
[65] J. Coraux, A. T. N'Diaye, M. Engler, C. Busse, D. Wall, N. Buckanie, F. J. Meyer Zu Heringdorf, R. van Gastel, B. Poelsema and T. Michely, Growth of graphene on Ir(111), New J. Phys. 11 (2009) 023006.
[66] Y. Cui, Q. Fu and X. Bao, Dynamic observation of layer-by-layer growth and removal of graphene on Ru(0001), Phys. Chem. Chem. Phys. 12 (2010) 5053.
[67] Y. Cui, Q. Fu, H. Zhang, D. Tan and X. Bao, Dynamic characterization of graphene growth and etching by oxygen on Ru(0001) by photoemission electron microscopy, J. Phys. Chem. C 113 (2009) 20365.
[68] M. Gao, Y. Pan, L. Huang, H. Hu, L. Z. Zhang, H. M. Guo, S. X. Du and H. J. Gao, Epitaxial growth and structural property of graphene on Pt(111), Appl. Phys. Lett. 98 (2011) 033101.
[69] A. Grüneis, K. Kummer and D. V. Vyalikh, Dynamics of graphene growth on a metal surface: A time-dependent photoemission study, New J. Phys. 11 (2009) 073050.
[70] S. Günther, S. Dänhardt, B. Wang, M. L. Bocquet, S. Schmitt and J. Wintterlin, Single Terrace Growth of Graphene on a Metal Surface, Nano Lett. 11 (2011) 1895.
[71] H. Hattab, A. T. N'Diaye, D. Wall, G. Jnawali, J. Coraux, C. Busse, R. van Gastel, B. Poelsema, T. Michely, F. J. M. z. Heringdorf and M. H.-v. Hoegen, Growth temperature dependent graphene alignment on Ir(111), Appl. Phys. Lett. 98 (2011) 141903.
[72] L. Jayeeta, T. S. Miller, A. J. Ross, L. Adamska, I. I. Oleynik and M. Batzill, Graphene growth and stability at nickel surfaces, New J. Phys. 13 (2011) 025001.
[73] B. J. Kang, J. H. Mun, C. Y. Hwang and B. J. Cho, Monolayer graphene growth on sputtered thin film platinum, J. Appl. Phys. 106 (2009) 104309.
[74] S.-Y. Kwon, C. V. Ciobanu, V. Petrova, V. B. Shenoy, J. Bareño, V. Gambin, I. Petrov and S. Kodambaka, Growth of Semiconducting Graphene on Palladium, Nano Lett. 9 (2009) 3985.
[75] P. Lacovig, M. Pozzo, D. Alfè, P. Vilmercati, A. Baraldi and S. Lizzit, Growth of dome-shaped carbon nanoislands on Ir(111): The intermediate between carbidic clusters and quasi-free-standing graphene, Phys. Rev. Lett. 103 (2009) 166101.
[76] K. F. McCarty, P. J. Feibelman, E. Loginova and N. C. Bartelt, Kinetics and thermodynamics of carbon segregation and graphene growth on Ru(0001), Carbon 47 (2009) 1806.
[77] G. Otero, C. Gonzalez, A. L. Pinardi, P. Merino, S. Gardonio, S. Lizzit, M. Blanco-Rey, K. Van de Ruit, C. F. J. Flipse, J. Méndez, P. L. de Andrés and

J. A. Martín-Gago, Ordered Vacancy Network Induced by the Growth of Epitaxial Graphene on Pt(111), Phys. Rev. Lett. 105 (2010) 216102.
[78] H. J. Park, J. Meyer, S. Roth and V. Skákalová, Growth and properties of few-layer graphene prepared by chemical vapor deposition, Carbon 48 (2010) 1088.
[79] M. Sicot, S. Bouvron, O. Zander, U. Rudiger, Y. S. Dedkov and M. Fonin, Nucleation and growth of nickel nanoclusters on graphene Moiré on Rh(111), Appl. Phys. Lett. 96 (2010) 093115.
[80] E. Starodub, S. Maier, I. Stass, N. C. Bartelt, P. J. Feibelman, M. Salmeron and K. F. McCarty, Graphene growth by metal etching on Ru(0001), Phys. Rev. B 80 (2009) 235422.
[81] P. Sutter, J. T. Sadowski and E. Sutter, Graphene on Pt(111): Growth and substrate interaction, Phys. Rev. B 80 (2009) 245411.
[82] P. W. Sutter, P. M. Albrecht and E. A. Sutter, Graphene growth on epitaxial Ru thin films on sapphire, Appl. Phys. Lett. 97 (2010) 213101.
[83] H. Zhang, Q. Fu, Y. Cui, D. Tan and X. Bao, Growth mechanism of graphene on Ru(0001) and O_2 adsorption on the graphene/Ru(0001) surface, J. Phys. Chem. C 113 (2009) 8296.
[84] D. Stradi, S. Barja, C. Díaz, M. Garnica, B. Borca, J. J. Hinarejos, D. Sánchez-Portal, M. Alcamí, A. Arnau, A. L. Vázquez de Parga, R. Miranda and F. Martín, Role of Dispersion Forces in the Structure of Graphene Monolayers on Ru Surfaces, Phys. Rev. Lett. 106 (2011) 186102.
[85] L. Schimka, J. Harl, A. Stroppa, A. Grüneis, M. Marsman, F. Mittendorfer and G. Kresse, Accurate surface and adsorption energies from many-body perturbation theory, Nat. Mater. 9 (2010) 741.
[86] A. Hodgson and S. Haq, Water adsorption and the wetting of metal surfaces, Surf. Sci. Rep. 64 (2009) 381.
[87] K. J. Andersson, F. Calle-Vallejo, J. Rossmeisl and I. Chorkendorff, Adsorption-driven surface segregation of the less reactive alloy component, J. Am. Chem. Soc. 131 (2009) 2404.
[88] J. Snyder, T. Fujita, M. W. Chen and J. Erlebacher, Oxygen reduction in nanoporous metal-ionic liquid composite electrocatalysts, Nat. Mater. 9 (2010) 904.
[89] K. J. Andersson and I. Chorkendorff, On the stability of the CO adsorption-induced and self-organized CuPt surface alloy, Surf. Sci. 604 (2010) 1733.
[90] A. Siani, B. Captain, R. D. Adams, O. S. Alexeev and M. D. Amiridis, Synthesis and Structural Characterization of SiO_2-Supported PtFe Catalysts Prepared from $PtFe_2(C_8H_{12})(CO)_8$, Top. Catal. 54 (2011) 1.

[91] M. Wagner, A. Stroppa, F. Mittendorfer, M. G. Ramsey, S. Surnev and F. P. Netzer, Electronic structure of bimetallic Ni-Rh nanowires, Surf. Sci. 604 (2010) 1406.
[92] F. Studt, F. Abild-Pedersen, T. Bligaard, R. Z. Sorensen, C. H. Christensen and J. K. Nørskov, Identification of non-precious metal alloy catalysts for selective hydrogenation of acetylene, Science 320 (2008) 1320.
[93] H. Ibach and D. L. Mills, Electron Energy Loss Spectroscopy and Surface Vibrations, San Francisco, Academic Press, 1982.
[94] H. Lüth, Surfaces and interfaces of solid materials, Berlin, Springer, 1995.
[95] D. V. Chakarov, L. Österlund and B. Kasemo, Interaction of water with potassium on graphite: A HREELS study, J. Electron Spectrosc. Relat. Phenom. 64-65 (1993) 279.
[96] L. Savio, L. Vattuone, M. Rocca, F. Buatier de Mongeot, G. Comelli, A. Baraldi, S. Lizzit and G. Paolucci, Formation of channels for oxygen migration towards subsurface sites by CO oxidation and growth of the surface oxide phase on Ag(001), Surf. Sci. 506 (2002) 213.
[97] F. Solymosi, Oxidation of hydrocarbon fragments on metal single crystals and on supported metals, J. Mol. Catal. A: Chem. 131 (1998) 121.
[98] A. Politano and G. Chiarello, Enhancement of hydrolysis in alkali ultrathin layers on metal substrates in the presence of electron confinement, Chem. Phys. Lett. 494 (2010) 84.
[99] A. Politano, V. Formoso and G. Chiarello, Temperature effects on alkali-promoted CO dissociation on Ni(111), Surf. Sci. 602 (2008) 2096.
[100] A. Politano, V. Formoso and G. Chiarello, Alkali-promoted CO dissociation on Cu(111) and Ni(111) at room temperature, J. Chem. Phys. 129 (2008) 164703.
[101] A. Politano, V. Formoso and G. Chiarello, Chemical Reactions at Clean and Alkali-Doped Mismatched Metal/Metal Interfaces, J. Phys. Chem. C 113 (2009) 316.
[102] A. Politano, A. R. Marino and G. Chiarello, CO-promoted formation of the alkali-oxygen bond on Ni(111), J. Chem. Phys. 132 (2010) 044706.
[103] A. Politano, V. Formoso and G. Chiarello, Mechanisms Leading to Alkali Oxidation on Metal Surfaces, J. Phys. Chem. C 112 (2008) 17772.
[104] A. Politano and G. Chiarello, Vibrational Investigation of Catalyst Surfaces: Change of the Adsorption Site of CO Molecules upon Coadsorption, J. Phys. Chem. C 115 (2011) 13541.
[105] A. Politano, V. Formoso, R. G. Agostino, E. Colavita and G. Chiarello, Influence of CO adsorption on the alkali-substrate bond studied by high-resolution electron energy loss spectroscopy, Phys. Rev. B 76 (2007) 233403.

[106] A. Politano, V. Formoso, R. G. Agostino, E. Colavita and G. Chiarello, Evidences of alkali-induced softening of the oxygen-substrate bond, J. Chem. Phys. 128 (2008) 074703.
[107] A. Politano and G. Chiarello, Low-energy bulk plasmon of nickel, Solid State Sci. 12 (2010) 2096.
[108] A. Politano, R. G. Agostino, E. Colavita, V. Formoso and G. Chiarello, Collective Excitations in Nanoscale Thin Alkali Films: Na/Cu(111), J. Nanosci. Nanotechnol. 9 (2009) 3932.
[109] A. Politano, V. Formoso and G. Chiarello, Dispersion and Damping of Gold Surface Plasmon, Plasmonics 3 (2008) 165.
[110] A. Politano, R. G. Agostino, E. Colavita, V. Formoso and G. Chiarello, Purely quadratic dispersion of surface plasmon in Ag/Ni(111): the influence of electron confinement, Phys. Status Solidi Rapid Res. Lett. (RRL) 2 (2008) 86.
[111] A. Politano and G. Chiarello, Tuning the lifetime of the surface plasmon upon sputtering, Phys. Status Solidi Rapid Res. Lett. (RRL) 3 (2009) 136.
[112] A. Politano, G. Chiarello, V. Formoso, R. G. Agostino and E. Colavita, Plasmon of Shockley surface states in Cu(111) : A high-resolution electron energy loss spectroscopy study, Phys. Rev. B 74 (2006) 081401.
[113] A. Politano, V. Formoso and G. Chiarello, Annealing effects on the plasmonic excitations of metal/metal interfaces, Appl. Surf. Sci. 255 (2009) 6038.
[114] A. Politano, V. Formoso and G. Chiarello, Damping of the surface plasmon in clean and K-modified Ag thin films, J. Electron Spectrosc. Relat. Phenom. 173 (2009) 12.
[115] A. Politano, V. Formoso and G. Chiarello, Dispersion and damping of surface plasmon in Ag thin films grown on Cu(111) and Ni(111), Superlattices Microstruct. 46 (2009) 137.
[116] A. Politano, V. Formoso and G. Chiarello, Plasmonic Modes Confined in Nanoscale Thin Silver Films Deposited onto Metallic Substrates J. Nanosci. Nanotechnol. 10 (2010) 1313.
[117] H. Ibach, M. Balden and S. Lehwald, Recent advances in electron energy loss spectroscopy of surface vibrations, J. Chem. Soc., Faraday Trans. 92 (1996) 4771.
[118] H. Ibach, Electron energy loss spectroscopy with resolution below 1 meV, J. Electron Spectrosc. Relat. Phenom. 64-65 (1993) 819.
[119] G. Benedek, G. Brusdeylins, V. Senz, J. G. Skofronick, J. P. Toennies, F. Traeger and R. Vollmer, Helium atom scattering study of the surface structure and dynamics of in situ cleaved MgO(001) single crystals, Phys. Rev. B 64 (2001) 125421.

[120] G. Benedek, J. Ellis, N. S. Luo, A. Reichmuth, P. Ruggerone and J. P. Toennies, Enhanced Helium-Atom Scattering from Longitudinal Surface Phonons in Cu(001), Phys. Rev. B 48 (1993) 4917.
[121] G. Benedek, J. Ellis, A. Reichmuth, P. Ruggerone, H. Schief and J. P. Toennies, Organ-Pipe Modes of Sodium Epitaxial Multilayers on Cu(001) Observed by Inelastic Helium-Atom Scattering, Phys. Rev. Lett. 69 (1992) 2951.
[122] G. Benedek, R. Gerlach, A. Glebov, G. Lange, S. Miret-Artes, J. G. Skofronick and J. P. Toennies, Focused inelastic resonances in the scattering of He atoms from NaCl(001), Phys. Rev. B 53 (1996) 11211.
[123] G. Benedek, N. S. Luo, P. Ruggerone, A. Reichmuth and J. P. Toennies, Vibrational Diagnostics of the Epitaxial-Growth of Ultrathin Films of Sodium on Cu(001), Mater. Sci. Eng., B 23 (1994) 123.
[124] G. Benedek and J. P. Toennies, Helium Atom Scattering Spectroscopy of Surface Phonons - Genesis and Achievements, Surf. Sci. 299 (1994) 587.
[125] F. M. Hoffmann and M. D. Weisel, Characterization of potassium promoter states under CO hydrogenation conditions on Ru(001): an in situ study with FT-IRAS, Surf. Sci. 269-270 (1992) 495.
[126] I. Villegas, N. Kizhakevariam and M. J. Weaver, Infrared spectroscopy of model electrochemical interfaces in ultrahigh vacuum: some implications for ionic and chemisorbate solvation at electrode surfaces, Surf. Sci. 335 (1995) 300.
[127] M. Nakamura and M. Ito, Infrared spectroscopic study of water coadsorbed with Na on the Ru(001) surface, Surf. Sci. 502-503 (2002) 144.
[128] I. Nakamura, H. Hamada and T. Fujitani, Adsorption and decomposition of NO on K-deposited Pd(111), Surf. Sci. 544 (2003) 45.
[129] K. Watanabe, N. Takagi and Y. Matsumoto, Mode-selective excitation of coherent surface phonons on alkali-covered metal surfaces, Phys. Chem. Chem. Phys. 7 (2005) 2697.
[130] Y. Matsumoto, K. Watanabe and N. Takagi, Excitation mechanism and ultrafast vibrational wavepacket dynamics of alkali-metal atoms on Pt(111), Surf. Sci. 593 (2005) 110.
[131] V. G. Bordo, G. Marowsky, J. Zhang and H. G. Rubahn, Resonant effects in optical second-harmonic generation from alkali covered Si(111)7×7, Europhys. Lett. 69 (2005) 61.
[132] F. Balzer and H. G. Rubahn, Interference effects in the optical second harmonic generation from ultrathin alkali films, Opt. Commun. 185 (2000) 493.
[133] H. Ibach, M. Etzkorn and J. Kirschner, Electron spectrometers for inelastic scattering from magnetic surface excitations, Surf. Interface Anal. 38 (2006) 1615.

[134] H. Ibach, D. Bruchmann, R. Vollmer, M. Etzkorn, P. S. A. Kumar and J. Kirschner, A novel spectrometer for spin-polarized electron energy-loss spectroscopy, Rev. Sci. Instrum. 74 (2003) 4089.
[135] M. Rocca, Low-Energy EELS Investigation of Surface Electronic Excitations on Metals, Surf. Sci. Rep. 22 (1995) 1.
[136] D. L. Mills, The scattering of low energy electrons by electric field fluctuations near crystal surfaces, Surf. Sci. 48 (1975) 59.
[137] P. A. Thiry, M. Liehr, J. J. Pireaux and R. Caudano, Investigation of Interfaces by High-Resolution Electron-Energy Loss Spectroscopy, Surf. Sci. 189 (1987) 373.
[138] L. De Broglie, Waves and quanta, Nature 112 (1923) 540.
[139] C. Davisson and L. H. Germer, Diffraction of Electrons by a Crystal of Nickel, Phys. Rev. 30 (1927) 705.
[140] C. Davisson and L. H. Germer, The Scattering of Electrons by a Single Crystal of Nickel, Nature 119 (1927) 558.
[141] G. Ertl and J. Küppers, Low Energy Electrons and Surface Chemistry, Weinheim, VCH, 1985.
[142] N. W. Ashcroft and N. D. Mermin, Solid State Physics, Philadelphia, Saunders College Publishing, 1976.
[143] A. H. Castro Neto, F. Guinea, N. M. R. Peres, K. S. Novoselov and A. K. Geim, The electronic properties of graphene, Rev. Mod. Phys. 81 (2009) 109.
[144] A. K. Geim and K. S. Novoselov, The rise of graphene, Nat. Mater. 6 (2007) 183.
[145] K. Novoselov, Graphene: Mind the gap, Nat. Mater. 6 (2007) 720.
[146] K. S. Novoselov, Nobel Lecture: Graphene: Materials in the Flatland, Rev. Mod. Phys. 83 (2011) 837.
[147] N. D. Mermin, Crystalline Order in Two Dimensions, Phys. Rev. 176 (1968) 250.
[148] X. Fan, R. Nouchi and K. Tanigaki, Effect of Charge Puddles and Ripples on the Chemical Reactivity of Single Layer Graphene Supported by SiO_2/Si Substrate, J. Phys. Chem. C (2011) null.
[149] A. Fasolino, J. H. Los and M. I. Katsnelson, Intrinsic ripples in graphene, Nat. Mater. 6 (2007) 858.
[150] R. Miranda and A. L. Vázquez de Parga, GRAPHENE Surfing ripples towards new devices, Nat. Nanotechnol. 4 (2009) 549.
[151] A. L. Vázquez de Parga, F. Calleja, B. Borca, M. C. G. Passeggi, J. J. Hinarejos, F. Guinea and R. Miranda, Periodically rippled graphene: Growth and spatially resolved electronic structure, Phys. Rev. Lett. 100 (2008) 056807.
[152] P. R. Wallace, The Band Theory of Graphite, Phys. Rev. 71 (1947) 622.

[153] N. Nemec, D. Tománek and G. Cuniberti, Contact Dependence of Carrier Injection in Carbon Nanotubes: An Ab Initio Study, Phys. Rev. Lett. 96 (2006) 076802.
[154] N. Nemec, D. Tománek and G. Cuniberti, Modeling extended contacts for nanotube and graphene devices, Phys. Rev. B 77 (2008) 125420.
[155] G. Giovannetti, P. A. Khomyakov, G. Brocks, V. M. Karpan, J. van den Brink and P. J. Kelly, Doping Graphene with Metal Contacts, Phys. Rev. Lett. 101 (2008) 026803.
[156] B. Huard, N. Stander, J. A. Sulpizio and D. Goldhaber-Gordon, Evidence of the role of contacts on the observed electron-hole asymmetry in graphene, Phys. Rev. B 78 (2008) 121402.
[157] A. T. N'Diaye, S. Bleikamp, P. J. Feibelman and T. Michely, Two-Dimensional Ir Cluster Lattice on a Graphene Moiré on Ir(111), Phys. Rev. Lett. 97 (2006) 215501.
[158] A. T. N'Diaye, J. Coraux, T. N. Plasa, C. Busse and T. Michely, Structure of epitaxial graphene on Ir(111), New J. Phys. 10 (2008) 043033.
[159] I. Pletikosić, M. Kralj, P. Pervan, R. Brako, J. Coraux, A. T. N'Diaye, C. Busse and T. Michely, Dirac cones and minigaps for graphene on Ir(111), Phys. Rev. Lett. 102 (2009) 056808.
[160] K. V. Emtsev, A. Bostwick, K. Horn, J. Jobst, G. L. Kellogg, L. Ley, J. L. McChesney, T. Ohta, S. A. Reshanov, J. Rohrl, E. Rotenberg, A. K. Schmid, D. Waldmann, H. B. Weber and T. Seyller, Towards wafer-size graphene layers by atmospheric pressure graphitization of silicon carbide, Nat. Mater. 8 (2009) 203.
[161] C. Coletti, K. V. Emtsev, A. A. Zakharov, T. Ouisse, D. Chaussende and U. Starke, Large area quasi-free standing monolayer graphene on 3C-SiC(111), Appl. Phys. Lett. 99 (2011) 081904.
[162] C. Riedl, C. Coletti, T. Iwasaki, A. A. Zakharov and U. Starke, Quasi-free-standing epitaxial graphene on SiC obtained by hydrogen intercalation, Phys. Rev. Lett. 103 (2009) 246804.
[163] D. C. Elias, R. R. Nair, T. M. G. Mohiuddin, S. V. Morozov, P. Blake, M. P. Halsall, A. C. Ferrari, D. W. Boukhvalov, M. I. Katsnelson, A. K. Geim and K. S. Novoselov, Control of graphene's properties by reversible hydrogenation: Evidence for graphane, Science 323 (2009) 610.
[164] A. K. Geim, Graphene: Status and prospects, Science 324 (2009) 1530.
[165] N. Levy, S. A. Burke, K. L. Meaker, M. Panlasigui, A. Zettl, F. Guinea, A. H. Castro Neto and M. F. Crommie, Strain-Induced Pseudo–Magnetic Fields Greater Than 300 Tesla in Graphene Nanobubbles, Science 329 (2010) 544.

[166] G. M. Rutter, J. N. Crain, N. P. Guisinger, T. Li, P. N. First and J. A. Stroscio, Scattering and Interference in Epitaxial Graphene, Science 317 (2007) 219.
[167] F. Wang, Y. Zhang, C. Tian, C. Girit, A. Zettl, M. Crommie and Y. R. Shen, Gate-Variable Optical Transitions in Graphene, Science 320 (2008) 206.
[168] S. Garaj, W. Hubbard, A. Reina, J. Kong, D. Branton and J. A. Golovchenko, Graphene as a subnanometre trans-electrode membrane, Nature 467 (2010) 190.
[169] K. S. Novoselov, A. K. Geim, S. V. Morozov, D. Jiang, M. I. Katsnelson, I. V. Grigorieva, S. V. Dubonos and A. A. Firsov, Two-dimensional gas of massless Dirac fermions in graphene, Nature 438 (2005) 197.
[170] Y. Zhang, T. T. Tang, C. Girit, Z. Hao, M. C. Martin, A. Zettl, M. F. Crommie, Y. R. Shen and F. Wang, Direct observation of a widely tunable bandgap in bilayer graphene, Nature 459 (2009) 820.
[171] Y. Yamada, C. Sugawara, Y. Satake, Y. Yokoyama, R. Okada, T. Nakayama, M. Sasaki, T. Kondo, J. Oh, J. Nakamura and W. W. Hayes, He/Ar-atom scattering from molecular monolayers: C_{60}/Pt(111) and graphene/Pt(111), J. Phys.: Condens. Matter 22 (2010) 304010.
[172] A. B. Preobrajenski, M. L. Ng, A. S. Vinogradov and N. Mårtensson, Controlling graphene corrugation on lattice-mismatched substrates, Phys. Rev. B 78 (2008) 073401.
[173] B. Wang, M. L. Bocquet, S. Marchini, S. Günther and J. Wintterlin, Chemical origin of a graphene moiré overlayer on Ru(0001), Phys. Chem. Chem. Phys. 10 (2008) 3530.
[174] W. Moritz, B. Wang, M. L. Bocquet, T. Brugger, T. Greber, J. Wintterlin and S. Günther, Structure Determination of the Coincidence Phase of Graphene on Ru(0001), Phys. Rev. Lett. 104 (2010) 136102.
[175] V. Chis and G. Benedek, Phonon-Induced Surface Charge Density Oscillations in Quantum Wells: A First-Principles Study of the (2 × 2)-K Overlayer on Be(0001), J. Phys. Chem. A 115 (2011) 7242.
[176] A. Allard and L. Wirtz, Graphene on Metallic Substrates: Suppression of the Kohn Anomalies in the Phonon Dispersion, Nano Lett. 10 (2010) 4335.
[177] D. K. Efetov and P. Kim, Controlling electron-phonon interactions in graphene at ultrahigh carrier densities, Phys. Rev. Lett. 105 (2010) 256805.
[178] L. J. Karssemeijer and A. Fasolino, Phonons of graphene and graphitic materials derived from the empirical potential LCBOPII, Surf. Sci. 605 (2011) 1611.
[179] H. Yanagisawa, T. Tanaka, Y. Ishida, M. Matsue, E. Rokuta, S. Otani and C. Oshima, Analysis of phonons in graphene sheets by means of HREELS measurement and ab initio calculation, Surf. Interface Anal. 37 (2005) 133.

[180] D. Farías, K. H. Rieder, A. M. Shikin, V. K. Adamchuk, T. Tanaka and C. Oshima, Modification of the surface phonon dispersion of a graphite monolayer adsorbed on Ni(111) caused by intercalation of Yb, Cu and Ag, Surf. Sci. 454 (2000) 437.
[181] J. H. Seol, I. Jo, A. L. Moore, L. Lindsay, Z. H. Aitken, M. T. Pettes, X. Li, Z. Yao, R. Huang, D. Broido, N. Mingo, R. S. Ruoff and L. Shi, Two-Dimensional Phonon Transport in Supported Graphene, Science 328 (2010) 213.
[182] Z. Hartmut, Phonons in layered compounds, J. Phys.: Condens. Matter 13 (2001) 7679.
[183] V. Perebeinos and J. Tersoff, Valence force model for phonons in graphene and carbon nanotubes, Phys. Rev. B 79 (2009) 241409.
[184] J. Maultzsch, S. Reich, C. Thomsen, H. Requardt and P. Ordejón, Phonon Dispersion in Graphite, Phys. Rev. Lett. 92 (2004) 075501.
[185] D. Farías, A. M. Shikin, K. H. Rieder and Y. S. Dedkov, Synthesis of a weakly bonded graphite monolayer on Ni(111) by intercalation of silver, J. Phys.: Cond. Matt. 11 (1999) 8453.
[186] S. Viola Kusminskiy, D. K. Campbell and A. H. Castro Neto, Lenosky's energy and the phonon dispersion of graphene, Phys. Rev. B 80 (2009) 035401.
[187] W. Kohn, Image of the Fermi Surface in the Vibration Spectrum of a Metal, Phys. Rev. Lett. 2 (1959) 393.
[188] S. Piscanec, M. Lazzeri, F. Mauri, A. C. Ferrari and J. Robertson, Kohn Anomalies and Electron-Phonon Interactions in Graphite, Phys. Rev. Lett. 93 (2004) 185503.
[189] M. Lazzeri and F. Mauri, Nonadiabatic Kohn Anomaly in a Doped Graphene Monolayer, Phys. Rev. Lett. 97 (2006) 266407.
[190] G. Cicero, J. C. Grossman, E. Schwegler, F. Gygi and G. Galli, Water confined in nanotubes and between graphene sheets: A first principle study, J. Am. Chem. Soc. 130 (2008) 1871.
[191] D. Donadio, G. Cicero, E. Schwegler, M. Sharma and G. Galli, Electronic Effects in the IR Spectrum of Water under Confinement, J. Phys. Chem. B 113 (2009) 4170.
[192] M. Sharma, D. Donadio, E. Schwegler and G. Galli, Probing Properties of Water under Confinement: Infrared Spectra, Nano Lett. 8 (2008) 2959.
[193] T. Werder, J. H. Walther, R. L. Jaffe, T. Halicioglu and P. Koumoutsakos, On the Water−Carbon Interaction for Use in Molecular Dynamics Simulations of Graphite and Carbon Nanotubes, J. Phys. Chem. B 107 (2003) 1345.

[194] A. Ambrosetti and P. L. Silvestrelli, Adsorption of Rare-Gas Atoms and Water on Graphite and Graphene by van der Waals-Corrected Density Functional Theory, J. Phys. Chem. C 115 (2011) 3695.
[195] M. C. Gordillo and J. Martí, Structure of water adsorbed on a single graphene sheet, Phys. Rev. B 78 (2008) 075432.
[196] M. C. Gordillo and J. Martí, Water on graphene surfaces, J. Phys.: Condens. Matter 22 (2010) 284111.
[197] M. C. Gordillo and J. Martí, Effect of Surface Roughness on the Static and Dynamic Properties of Water Adsorbed on Graphene, J. Phys. Chem. B 114 (2010) 4583.
[198] G. R. Jenness, O. Karalti and K. D. Jordan, Benchmark calculations of water-acene interaction energies: Extrapolation to the water-graphene limit and assessment of dispersion-corrected DFT methods, Phys. Chem. Chem. Phys. 12 (2010) 6375.
[199] O. Leenaerts, B. Partoens and F. M. Peeters, Water on graphene: Hydrophobicity and dipole moment using density functional theory, Phys. Rev. B 79 (2009) 235440.
[200] J. Martí, J. Sala and E. Guàrdia, Molecular dynamics simulations of water confined in graphene nanochannels: From ambient to supercritical environments, J. Mol. Liq. 153 (2010) 72.
[201] J. H. Park and N. R. Aluru, Ordering-Induced Fast Diffusion of Nanoscale Water Film on Graphene, J. Phys. Chem. C 114 (2010) 2595.
[202] M. E. Suk and N. R. Aluru, Water Transport through Ultrathin Graphene, J. Phys. Chem. Lett. 1 (2010) 1590.
[203] E. Voloshina, D. Usvyat, M. Schutz, Y. Dedkov and B. Paulus, On the physisorption of water on graphene: a CCSD(T) study, Phys. Chem. Chem. Phys. 13 (2011) 12041.
[204] H. Ibach, Physics of Surfaces and Interfaces, Berlin, Springer, 2006.
[205] B. C. Stipe, M. A. Rezaei and W. Ho, Single-molecule vibrational spectroscopy and microscopy, Science 280 (1998) 1732.
[206] A. Politano, R. G. Agostino, E. Colavita, V. Formoso, L. Tenuta and G. Chiarello, Nature of the alkali surface bond at low coverages investigated by vibrational measurements, J. Phys. Chem. C 112 (2008) 6977.
[207] A. Politano, R. G. Agostino, V. Formoso and G. Chiarello, Short-range interactions in Na coadsorption with CO and O on Ni(111), ChemPhysChem 9 (2008) 1189.
[208] A. Politano and G. Chiarello, O_2 dissociation in Na-modified gold ultrathin layer on Cu(111), Gold Bull. 43 (2010) 267.
[209] A. Politano, A. R. Marino and G. Chiarello, Alkali-promoted stabilization of subsurface oxygen on Cu(111), Chem. Phys. 367 (2010) 148.

[210] N. Nilius, T. M. Wallis and W. Ho, Vibrational spectroscopy and imaging of single molecules: Bonding of CO to single palladium atoms on NiAl(110), J. Chem. Phys. 117 (2002) 10947.
[211] M. C. Tsai, U. Seip, I. C. Bassignana, J. Küppers and G. Ertl, A vibrational spectroscopy study on the interaction of N_2 with clean and K-promoted Fe(111) surfaces: π-bonded dinitrogen as precursor for dissociation, Surf. Sci. 155 (1985) A269.
[212] A. Lopez, T. Bitzer, T. Heller and N. V. Richardson, Functional group selectivity in adsorption of 4-aminobenzoic acid on clean and Na modified Si(100)-2×1 surfaces, Surf. Sci. 480 (2001) 65.
[213] M. Rubeš, P. Nachtigall, J. Vondrášek and O. Bludský, Structure and Stability of the Water−Graphite Complexes, J. Phys. Chem. C 113 (2009) 8412.
[214] J. Ma, A. Michaelides, D. Alfé, L. Schimka, G. Kresse and E. Wang, Adsorption and diffusion of water on graphene from first principles, Phys. Rev. B 84 (2011) 033402.
[215] M. A. Henderson, The interaction of water with solid surfaces: fundamental aspects revisited, Surf. Sci. Rep. 46 (2002) 1.
[216] S. Meng, L. F. Xu, E. G. Wang and S. Gao, Vibrational Recognition of Hydrogen-Bonded Water Networks on a Metal Surface, Phys. Rev. Lett. 89 (2002) 176104.
[217] D. J. Mann and M. D. Halls, Water Alignment and Proton Conduction inside Carbon Nanotubes, Phys. Rev. Lett. 90 (2003) 195503.
[218] C. S. Lin, R. Q. Zhang, S. T. Lee, M. Elstner, T. Frauenheim and L. J. Wan, Simulation of Water Cluster Assembly on a Graphite Surface, J. Phys. Chem. B 109 (2005) 14183.
[219] G. A. Kimmel, J. Matthiesen, M. Baer, C. J. Mundy, N. G. Petrik, R. S. Smith, Z. Dohnálek and B. D. Kay, No confinement needed: Observation of a metastable hydrophobic wetting two-layer ice on graphene, J. Am. Chem. Soc. 131 (2009) 12838.
[220] T. O. Wehling, A. I. Lichtenstein and M. I. Katsnelson, First-principles studies of water adsorption on graphene: The role of the substrate, Appl. Phys. Lett. 93 (2008) 202110.
[221] K. S. Novoselov, A. K. Geim, S. V. Morozov, D. Jiang, Y. Zhang, S. V. Dubonos, I. V. Grigorieva and A. A. Firsov, Electric field in atomically thin carbon films, Science 306 (2004) 666.
[222] D. Marchenko, A. Varykhalov, A. Rybkin, A. M. Shikin and O. Rader, Atmospheric stability and doping protection of noble-metal intercalated graphene on Ni(111), Appl. Phys. Lett. 98 (2011) 122111.
[223] F. Yavari, C. Kritzinger, C. Gaire, L. Song, H. Gulapalli, T. Borca-Tasciuc, P. M. Ajayan and N. Koratkar, Tunable Bandgap in Graphene by the Controlled Adsorption of Water Molecules, Small 6 (2010) 2535.

[224] B. D. Thoms and J. E. Butler, HREELS scattering mechanism from diamond surfaces, Phys. Rev. B 50 (1994) 17450.
[225] A. Horn, J. Biener, A. Schenk, C. Lutterloh and J. Küppers, H/D exchange reaction at graphitic CH groups by thermal H(D) atoms, Surf. Sci. 331-333 (1995) 178.
[226] G. Lee and E. W. Plummer, High-resolution electron energy loss spectroscopy study on chemisorption of hydrogen on Cu(111), Surf. Sci. 498 (2002) 229.
[227] E. Cadelano, P. L. Palla, S. Giordano and L. Colombo, Elastic properties of hydrogenated graphene, Phys. Rev. B 82 (2010) 235414.
[228] M. K. Kostov, E. E. Santiso, A. M. George, K. E. Gubbins and M. B. Nardelli, Dissociation of Water on Defective Carbon Substrates, Phys. Rev. Lett. 95 (2005) 136105.
[229] A. Allouche and Y. Ferro, Dissociative adsorption of small molecules at vacancies on the graphite (0001) surface, Carbon 44 (2006) 3320.
[230] P. Cabrera-Sanfelix and G. R. Darling, Dissociative adsorption of water at vacancy defects in graphite, J. Phys. Chem. C 111 (2007) 18258.
[231] S. Meng and S. Gao, Formation and interaction of hydrated alkali metal ions at the graphite-water interface, J. Chem. Phys. 125 (2006) 014708.
[232] A. Bostwick, T. Ohta, J. L. McChesney, K. V. Emtsev, F. Speck, T. Seyller, K. Horn, S. D. Kevan and E. Rotenberg, The interaction of quasi-particles in graphene with chemical dopants, New J. Phys. 12 (2010) 125014.
[233] S. Meng, D. Chakarov, B. Kasemo and S. Gao, Two-dimensional hydration shells of alkali metal ions at a hydrophobic surface, J. Chem. Phys. 121 (2004) 12572.
[234] E. Starodub, A. Bostwick, L. Moreschini, S. Nie, F. E. Gabaly, K. F. McCarty and E. Rotenberg, In-plane orientation effects on the electronic structure, stability, and Raman scattering of monolayer graphene on Ir(111), Phys. Rev. B 83 (2011) 125428.
[235] C. Mellita and F. Sharon, Alkali metal adsorption on graphite: a review, J. Phys.: Condens. Matter 17 (2005) R995.
[236] T. Langer, J. Baringhaus, H. Pfnür, H. W. Schumacher and C. Tegenkamp, Plasmon damping below the Landau regime: the role of defects in epitaxial graphene, New J. Phys. 12 (2010) 033017.
[237] C. Tegenkamp, H. Pfnür, T. Langer, J. Baringhaus and H. W. Schumacher, Plasmon electron–hole resonance in epitaxial graphene, J. Phys.: Condens. Matter 23 (2011) 012001.
[238] T. Langer, D. F. Förster, C. Busse, T. Michely, H. Pfnür and C. Tegenkamp, Sheet plasmons in modulated graphene on Ir(111), New J. Phys. 13 (2011) 053006.

[239] A. Bostwick, F. Speck, T. Seyller, K. Horn, M. Polini, R. Asgari, A. H. MacDonald and E. Rotenberg, Observation of Plasmarons in Quasi-Freestanding Doped Graphene, Science 328 (2010) 999.
[240] S. Yuan, R. Roldán and M. I. Katsnelson, Excitation spectrum and high-energy plasmons in single-layer and multilayer graphene, Phys. Rev. B 84 (2011) 035439.
[241] J. Yan, K. S. Thygesen and K. W. Jacobsen, Nonlocal Screening of Plasmons in Graphene by Semiconducting and Metallic Substrates: First-Principles Calculations, Phys. Rev. Lett. 106 (2011) 146803.
[242] C. E. P. Villegas and M. R. S. Tavares, Substrate interaction effects on optical and acoustical plasmons in bi-waveguides based on graphene, Diamond Relat. Mater. 20 (2011) 170.
[243] K. A. Velizhanin and A. Efimov, Probing plasmons in graphene by resonance energy transfer, Phys. Rev. B 84 (2011) 085401.
[244] S. Y. Shin, N. D. Kim, J. G. Kim, K. S. Kim, D. Y. Noh and J. W. Chung, Control of the π plasmon in a single layer graphene by charge doping, Appl. Phys. Lett. 99 (2011) 082110.
[245] S. Y. Shin, C. G. Hwang, S. J. Sung, N. D. Kim, H. S. Kim and J. W. Chung, Observation of intrinsic intraband π-plasmon excitation of a single-layer graphene, Phys. Rev. B 83 (2011) 161403.
[246] A. Principi, R. Asgari and M. Polini, Acoustic plasmons and composite hole-acoustic plasmon satellite bands in graphene on a metal gate, Solid State Commun. 151 (2011) 1627.
[247] L. Ju, B. Geng, J. Horng, C. Girit, M. Martin, Z. Hao, H. A. Bechtel, X. Liang, A. Zettl, Y. R. Shen and F. Wang, Graphene plasmonics for tunable terahertz metamaterials, Nat. Nanotechnol. 6 (2011) 630.
[248] V. B. Jovanović, I. Radović, D. Borka and Z. L. Mišković, High-energy plasmon spectroscopy of freestanding multilayer graphene, Phys. Rev. B 84 (2011) 155416.
[249] M. Jablan, M. Soljačić and H. Buljan, Unconventional plasmon-phonon coupling in graphene, Phys. Rev. B 83 (2011) 161409.
[250] Y. Gao and Z. Yuan, Anisotropic low-energy plasmon excitations in doped graphene: An ab initio study, Solid State Commun. 151 (2011) 1009.
[251] A. A. Dubinov, V. Y. Aleshkin, V. Mitin, T. Otsuji and V. Ryzhii, Terahertz surface plasmons in optically pumped graphene structures, J. Phys.: Condens. Matter 23 (2011) 145302.
[252] S. H. Abedinpour, G. Vignale, A. Principi, M. Polini, W.-K. Tse and A. H. MacDonald, Drude weight, plasmon dispersion, and ac conductivity in doped graphene sheets, Phys. Rev. B 84 (2011) 045429.
[253] N. J. M. Horing, Linear Graphene Plasmons, IEEE Trans. Nanotechnol. 9 (2010) 679.

[254] M. Gao, Y. Pan, C. Zhang, H. Hu, R. Yang, H. Lu, J. Cai, S. Du, F. Liu and H. J. Gao, Tunable interfacial properties of epitaxial graphene on metal substrates, Appl. Phys. Lett. 96 (2010) 053109.
[255] F. Stern, Polarizability of a Two-Dimensional Electron Gas, Phys. Rev. Lett. 18 (1967) 546.
[256] T. Nagao, T. Hildebrandt, M. Henzler and S. Hasegawa, Two-dimensional plasmon in a surface-state band, Surf. Sci. 493 (2001) 680.
[257] T. Nagao, T. Hildebrandt, M. Henzler and S. Hasegawa, Dispersion and damping of a two-dimensional plasmon in a metallic surface-state band, Phys. Rev. Lett. 86 (2001) 5747.
[258] Y. Chen, J. C. Hermanson and G. J. Lapeyre, Coupled plasmon and phonon in the accumulation layer of InAs(110) cleaved surfaces, Phys. Rev. B 39 (1989) 12682.
[259] B. Diaconescu, K. Pohl, L. Vattuone, L. Savio, P. Hofmann, V. M. Silkin, J. M. Pitarke, E. V. Chulkov, P. M. Echenique, D. Farías and M. Rocca, Low-energy acoustic plasmons at metal surfaces, Nature 448 (2007) 57.
[260] S. J. Park and R. E. Palmer, Acoustic Plasmon on the Au(111) Surface, Phys. Rev. Lett. 105 (2010) 016801.
[261] K. Pohl, B. Diaconescu, G. Vercelli, L. Vattuone, V. M. Silkin, E. V. Chulkov, P. M. Echenique and M. Rocca, Acoustic surface plasmon on Cu(111), Europhys. Lett. 90 (2010) 57006.
[262] E. H. Hwang and S. Das Sarma, Dielectric function, screening, and plasmons in two-dimensional graphene, Phys. Rev. B 75 (2007) 205418.
[263] E. H. Hwang, R. Sensarma and S. Das Sarma, Plasmon-phonon coupling in graphene, Phys. Rev. B 82 (2010) 195406.
[264] M. Polini, R. Asgari, G. Borghi, Y. Barlas, T. Pereg-Barnea and A. H. MacDonald, Plasmons and the spectral function of graphene, Phys. Rev. B 77 (2008) 081411.
[265] Y. Liu and R. F. Willis, Plasmon-phonon strongly coupled mode in epitaxial graphene, Phys. Rev. B 81 (2010) 081406.
[266] J. Lu, K. P. Loh, H. Huang, W. Chen and A. T. S. Wee, Plasmon dispersion on epitaxial graphene studied using high-resolution electron energy-loss spectroscopy, Phys. Rev. B 80 (2009) 113410.
[267] V. M. Silkin, A. Garcia-Lekue, J. M. Pitarke, E. V. Chulkov, E. Zaremba and P. M. Echenique, Novel low-energy collective excitation at metal surfaces, Europhys. Lett. 66 (2004) 260.
[268] V. M. Silkin, J. M. Pitarke, E. V. Chulkov and P. M. Echenique, Acoustic surface plasmons in the noble metals Cu, Ag, and Au, Phys. Rev. B 72 (2005) 115435.
[269] N. J. M. Horing, Aspects of the theory of graphene, Philos. Trans. R. Soc. A 368 (2010) 5525.

[270] M. van Schilfgaarde and M. I. Katsnelson, First-principles theory of nonlocal screening in graphene, Phys. Rev. B 83 (2011) 081409.
[271] J. M. Pitarke, V. U. Nazarov, V. M. Silkin, E. V. Chulkov, E. Zaremba and P. M. Echenique, Theory of acoustic surface plasmons, Phys. Rev. B 70 (2004) 205403.
[272] B. Borca, F. Calleja, J. J. Hinarejos, A. L. Vázquez de Parga and R. Miranda, Reactivity of periodically rippled graphene grown on Ru(0001), J. Phys.: Cond. Matt. 21 (2009) 134002.
[273] Y. Liu, R. F. Willis, K. V. Emtsev and T. Seyller, Plasmon dispersion and damping in electrically isolated two-dimensional charge sheets, Phys. Rev. B 78 (2008) 201403.
[274] J. Sun, J. B. Hannon, R. M. Tromp, P. Johari, A. A. Bol, V. B. Shenoy and K. Pohl, Spatially-Resolved Structure and Electronic Properties of Graphene on Polycrystalline Ni, ACS Nano 4 (2010) 7073.
[275] R. Rosei, S. Modesti, F. Sette, C. Quaresima, A. Savoia and P. Perfetti, Electronic structure of carbidic and graphitic carbon on Ni(111), Phys. Rev. B 29 (1984) 3416.
[276] A. V. Generalov and Y. S. Dedkov, EELS study of the epitaxial graphene/Ni(111) and graphene/Au/Ni(111) systems, Carbon 50 (2012) 183.
[277] C. Kramberger, R. Hambach, C. Giorgetti, M. H. Rümmeli, M. Knupfer, J. Fink, B. Büchner, L. Reining, E. Einarsson, S. Maruyama, F. Sottile, K. Hannewald, V. Olevano, A. G. Marinopoulos and T. Pichler, Linear plasmon dispersion in single-wall carbon nanotubes and the collective excitation spectrum of graphene, Phys. Rev. Lett. 100 (2008) 196803.
[278] N. Papageorgiou, M. Portail and J. M. Layet, Dispersion of the interband π electronic excitation of highly oriented pyrolytic graphite measured by high resolution electron energy loss spectroscopy, Surf. Sci. 454-456 (2000) 462.
[279] X. Liu, T. Pichler, M. Knupfer, M. S. Golden, J. Fink, D. A. Walters, M. J. Casavant, J. Schmidt and R. E. Smalley, An electron energy-loss study of the structural and electronic properties of magnetically aligned single wall carbon nanotubes, Synth. Met. 121 (2001) 1183.
[280] U. Diebold, A. Preisinger, P. Schattschneider and P. Varga, Angle resolved electron energy loss spectroscopy on graphite, Surf. Sci. 197 (1988) 430.
[281] U. Büchner, Wave-Vector Dependence of the Electron Energy Losses of Boron Nitride and Graphite, Phys. Status Solidi B 81 (1977) 227.
[282] K. Zeppenfeld, Wavelength dependence and spatial dispersion of the dielectric constant in graphite by electron spectroscopy, Opt. Commun. 1 (1969) 119.

[283] J. J. Ritsko and M. J. Rice, Plasmon Spectra of Ferric-Chloride-Intercalated Graphite, Phys. Rev. Lett. 42 (1979) 666.
[284] D. Pines, Elementary Excitations in Solids, New York, Benjamin, 1964.
[285] M. P. López-Sancho, M. A. H. Vozmediano and F. Guinea, Transverse transport in graphite, Eur. Phys. J.-Spec. Top. 148 (2007) 73.
[286] M. Dion, H. Rydberg, E. Schröder, D. C. Langreth and B. I. Lundqvist, Van der Waals Density Functional for General Geometries, Phys. Rev. Lett. 92 (2004) 246401.
[287] J. Nilsson, A. H. Castro Neto, N. M. R. Peres and F. Guinea, Electron-electron interactions and the phase diagram of a graphene bilayer, Phys. Rev. B 73 (2006) 214418.
[288] Z. Yuan and S. Gao, Landau damping and lifetime oscillation of surface plasmons in metallic thin films studied in a jellium slab model, Surf. Sci. 602 (2008) 460.
[289] S. Y. Zhou, G. H. Gweon, A. V. Fedorov, P. N. First, W. A. de Heer, D. H. Lee, F. Guinea, A. H. Castro Neto and A. Lanzara, Substrate-induced bandgap opening in epitaxial graphene, Nat. Mater. 6 (2007) 770.
[290] A. G. Marinopoulos, L. Reining, A. Rubio and V. Olevano, Ab initio study of the optical absorption and wave-vector-dependent dielectric response of graphite, Phys. Rev. B 69 (2004) 245419.
[291] M. Marsman, J. Paier, A. Stroppa and G. Kresse, Hybrid functionals applied to extended systems, J. Phys.: Cond. Matt. 20 (2008) 064201.
[292] A. Stroppa, F. Mittendorfer, J. N. Andersen, G. Parteder, F. Allegretti, S. Surnev and F. P. Netzer, Adsorption and Dissociation of CO on Bare and Ni-Decorated Stepped Rh(553) Surfaces, J. Phys. Chem. C 113 (2009) 942.
[293] A. Stroppa, K. Termentzidis, J. Paier, G. Kresse and J. Hafner, CO adsorption on metal surfaces: A hybrid functional study with plane-wave basis set, Phys. Rev. B 76 (2007) 195440.
[294] S. Meng, E. G. Wang, C. Frischkorn, M. Wolf and S. Gao, Consistent picture for the wetting structure of water/Ru(0001), Chem. Phys. Lett. 402 (2005) 384.
[295] S. Meng, E. G. Wang and S. Gao, Water adsorption on metal surfaces: A general picture from density functional theory studies, Phys. Rev. B 69 (2004) 195404.
[296] G. Chiarello, D. Robba, G. De Michele and F. Parmigiani, An X-ray Photoelectron-Spectroscopy Study of the Vanadia Titania Catalysts, Appl. Surf. Sci. 64 (1993) 91.
[297] A. Stroppa and G. Kresse, The shortcomings of semi-local and hybrid functionals: what we can learn from surface science studies, New J. Phys. 10 (2008) 063020.

[298] H. P. Koch, P. Singnurkar, R. Schennach, A. Stroppa and F. Mittendorfer, A RAIRS, TPD, and DFT study of carbon monoxide adsorption on stepped Rh(553), J. Phys. Chem. C 112 (2008) 806.
[299] F. Besenbacher, I. Chorkendorff, B. S. Clausen, B. Hammer, A. M. Molenbroek, J. K. Nørskov and I. Stensgaard, Design of a surface alloy catalyst for steam reforming, Science 279 (1998) 1913.
[300] J. G. Chen, C. A. Menning and M. B. Zellner, Monolayer bimetallic surfaces: Experimental and theoretical studies of trends in electronic and chemical properties, Surf. Sci. Rep. 63 (2008) 201.
[301] A. Baraldi, L. Bianchettin, S. De Gironcoli, E. Vesselli, S. Lizzit, L. Petaccia, G. Comelli and R. Rosei, Enhanced chemical reactivity of under-coordinated atoms at Pt-Rh bimetallic surfaces: A spectroscopic characterization, J. Phys. Chem. C 115 (2011) 3378.
[302] H. Baltruschat and S. Ernst, Molecular adsorbates at single-crystal platinum-group metals and bimetallic surfaces, ChemPhysChem 12 (2011) 56.
[303] J. H. Meng, C. A. Menning, M. B. Zellner and J. G. Chen, Effects of bimetallic modification on the decomposition of CH_3OH and H_2O on Pt/W(110) bimetallic surfaces, Surf. Sci. 604 (2010) 1845.
[304] C. A. Menning and J. G. Chen, General trend for adsorbate-induced segregation of subsurface metal atoms in bimetallic surfaces, J. Chem. Phys. 130 (2009) 174709.
[305] O. Skoplyak, C. A. Menning, M. A. Barteau and J. G. Chen, Experimental and theoretical study of reactivity trends for methanol on CoPt (111) and NiPt (111) bimetallic surfaces, J. Chem. Phys. 127 (2007) 114707.
[306] H. Ren, M. P. Humbert, C. A. Menning, J. G. Chen, Y. Shu, U. G. Singh and W. C. Cheng, Inhibition of coking and CO poisoning of Pt catalysts by the formation of Au/Pt bimetallic surfaces, Appl. Catal., A 375 (2010) 303.
[307] O. R. Inderwildi, S. J. Jenkins and D. A. King, When adding an unreactive metal enhances catalytic activity: NOx decomposition over silver-rhodium bimetallic surfaces, Surf. Sci. 601 (2007) L103.
[308] J. Greeley and M. Mavrikakis, Alloy catalysts designed from first principles, Nat. Mater. 3 (2004) 810.
[309] J. Greeley, I. E. L. Stephens, A. S. Bondarenko, T. P. Johansson, H. A. Hansen, T. F. Jaramillo, J. Rossmeisl, I. Chorkendorff and J. K. Nørskov, Alloys of platinum and early transition metals as oxygen reduction electrocatalysts, Nature Chem. 1 (2009) 552.
[310] H.-Y. Su, X.-H. Bao and W.-X. Li, Modulating the reactivity of Ni-containing Pt(111)-skin catalysts by density functional theory calculations, J. Chem. Phys. 128 (2008) 194707.

[311] N. M. Marković and P. N. Ross, Surface science studies of model fuel cell electrocatalysts, Surf. Sci. Rep. 45 (2002) 117.
[312] V. R. Stamenković, B. Fowler, B. S. Mun, G. Wang, P. N. Ross, C. A. Lucas and N. M. Marković, Improved oxygen reduction activity on $Pt_3Ni(111)$ via increased surface site availability, Science 315 (2007) 493.
[313] R. Subbaraman, D. Strmcnik, A. P. Paulikas, V. R. Stamenković and N. M. Marković, Oxygen reduction reaction at three-phase interfaces, ChemPhysChem 11 (2010) 2825.
[314] T. H. Yu, Y. Sha, B. V. Merinov and W. A. Goddard III, Improved non-Pt alloys for the oxygen reduction reaction at fuel cell cathodes predicted from quantum mechanics, J. Phys. Chem. C 114 (2010) 11527.
[315] Z. Yang, J. Wang and X. Yu, The adsorption, diffusion and dissociation of O_2 on Pt-skin $Pt_3Ni(111)$: A density functional theory study, Chem. Phys. Lett. 499 (2010) 83.
[316] C. A. Menning and J. G. Chen, Thermodynamics and kinetics of oxygen-induced segregation of 3d metals in Pt--3d--Pt(111) and Pt--3d--Pt(100) bimetallic structures, J. Chem. Phys. 128 (2008) 164703.
[317] V. Stamenković, B. S. Mun, K. J. J. Mayrhofer, P. N. Ross, N. M. Marković, J. Rossmeisl, J. Greeley and J. K. Nørskov, Changing the activity of electrocatalysts for oxygen reduction by tuning the surface electronic structure, Angew. Chem. 45 (2006) 2897.
[318] R. B. Hoyle, A. T. Anghel, M. R. E. Proctor and D. A. King, Pattern formation during the oxidation of CO on Pt{100}: A mesoscopic model, Phys. Rev. Lett. 98 (2007) 226102.
[319] L. Grabow, Y. Xu and M. Mavrikakis, Lattice strain effects on CO oxidation on Pt(111), Phys. Chem. Chem. Phys. 8 (2006) 3369.
[320] J. C. Davies, R. M. Nielsen, L. B. Thomsen, I. Chorkendorff, Á. Logadóttir, Z. Łodziana, J. K. Nørskov, W. X. Li, B. Hammer, S. R. Longwitz, J. Schnadt, E. K. Vestergaard, R. T. Vang and F. Besenbacher, CO desorption rate dependence on CO partial pressure over platinum fuel cell catalysts, Fuel Cells 4 (2004) 309.
[321] N. R. Avery, Electron energy loss spectroscopic study of CO on Pt(111), J. Chem. Phys. 74 (1981) 4202.
[322] A. M. Baro and H. Ibach, New study of CO adsorption at low temperature (90 K) on Pt (111) by EELS, J. Chem. Phys. 71 (1979) 4812.
[323] S. Ohnishi and N. Watari, Cluster-model study of CO adsorption on the Pt(111) surface, Phys. Rev. B 49 (1994) 14619.
[324] X. Su, P. S. Cremer, Y. R. Shen and G. A. Somorjai, Pressure Dependence (10^{-10}-700 Torr) of the Vibrational Spectra of Adsorbed CO on Pt(111) Studied by Sum Frequency Generation, Phys. Rev. Lett. 77 (1996) 3858.

[325] W. D. Mieher, L. J. Whitman and W. Ho, A time resolved electron energy loss spectroscopy study of CO on Pt(111): Adsorption site occupations versus coverage and temperature, J. Chem. Phys. 91 (1989) 3228.
[326] C. Klünker, M. Balden, S. Lehwald and W. Daum, CO stretching vibrations on Pt(111) and Pt(110) studied by sumfrequency generation, Surf. Sci. 360 (1996) 104.
[327] V. R. Stamenković, B. S. Mun, K. J. J. Mayrhofer, P. N. Ross and N. M. Marković, Effect of Surface Composition on Electronic Structure, Stability, and Electrocatalytic Properties of Pt-Transition Metal Alloys: Pt-Skin versus Pt-Skeleton Surfaces, J. Am. Chem. Soc. 128 (2006) 8813.
[328] J. X. Wang, H. Inada, L. Wu, Y. Zhu, Y. Choi, P. Liu, W.-P. Zhou and R. R. Adzic, Oxygen Reduction on Well-Defined Core−Shell Nanocatalysts: Particle Size, Facet, and Pt Shell Thickness Effects, J. Am. Chem. Soc. 131 (2009) 17298.
[329] B. S. Mun, M. Watanabe, M. Rossi, V. Stamenković, N. M. Marković and P. N. Ross Jr, The study of surface segregation, structure, and valence band density of states of Pt_3Ni(100), (110), and (111) crystals, Surf. Rev. Lett. 13 (2006) 697.
[330] Y. Ma and P. B. Balbuena, Surface properties and dissolution trends of Pt_3M alloys in the presence of adsorbates, J. Phys. Chem. C 112 (2008) 14520.
[331] Y. Ma and P. B. Balbuena, Pt surface segregation in bimetallic Pt_3M alloys: A density functional theory study, Surf. Sci. 602 (2008) 107.
[332] D. Pillay and M. D. Johannes, Effect of S on Pt(111) and Pt_3Ni(111) surfaces: A first principles study, J. Phys. Chem. C 112 (2008) 1544.
[333] V. Stamenković, T. J. Schmidt, P. N. Ross and N. M. Marković, Surface segregation effects in electrocatalysis: Kinetics of oxygen reduction reaction on polycrystalline Pt_3Ni alloy surfaces, J. Electroanal. Chem. 554-555 (2003) 191.
[334] D. Pillay and M. D. Johannes, Comparison of sulfur interaction with hydrogen on Pt(111), Ni(111) and Pt_3Ni(111) surfaces: The effect of intermetallic bonding, Surf. Sci. 602 (2008) 2752.
[335] Y. N. Sun, Z. H. Qin, M. Lewandowski, S. Kaya, S. Shaikhutdinov and H. J. Freund, When an encapsulating oxide layer promotes reaction on noble metals: Dewetting and in situ formation of an "inverted" FeO_x/Pt catalyst, Catal. Lett. 126 (2008) 31.
[336] W. Weiss and W. Ranke, Surface chemistry and catalysis on well-defined epitaxial iron-oxide layers, Prog. Surf. Sci. 70 (2002) 1.
[337] J. Wang, C. Y. Fan, K. Jacobi and G. Ertl, The kinetics of CO oxidation on RuO_2(110): Bridging the pressure gap, J. Phys. Chem. B 106 (2002) 3422.

[338] H. Wang and W. F. Schneider, Nature and role of surface carbonates and bicarbonates in CO oxidation over RuO2, Phys. Chem. Chem. Phys. 12 (2010) 6367.
[339] J. Knudsen, L. R. Merte, G. Peng, R. T. Vang, A. Resta, E. Lægsgaard, J. N. Andersen, M. Mavrikakis and F. Besenbacher, Low-Temperature CO Oxidation on Ni(111) and on a Au/Ni(111) Surface Alloy, ACS Nano 4 (2010) 4380.
[340] H. Steininger, S. Lehwald and H. Ibach, Adsorption of oxygen on Pt(111), Surf. Sci. 123 (1982) 1.
[341] J. L. Gland, B. A. Sexton and G. B. Fisher, Oxygen interactions with the Pt(111) surface, Surf. Sci. 95 (1980) 587.
[342] C. A. Menning, H. H. Hwu and J. G. Chen, Experimental and Theoretical Investigation of the Stability of Pt−3d−Pt(111) Bimetallic Surfaces under Oxygen Environment, J. Phys. Chem. B 110 (2006) 15471.
[343] H. Ibach and D. Bruchmann, Observation of Surface Phonons on Ni(111) by Electron Energy-Loss Spectroscopy, Phys. Rev. Lett. 44 (1980) 36.
[344] Y. D. Kim, A. P. Seitsonen, S. Wendt, J. Wang, C. Fan, K. Jacobi, H. Over and G. Ertl, Characterization of various oxygen species on an oxide surface: RuO_2(110), J. Phys. Chem. B 105 (2001) 3752.
[345] G. Benedek, F. Buatier de Mongeot, U. Valbusa and M. Rocca, Formation of d-holes in the initial stages of the oxidation of Ag(001), Europhys. Lett. 53 (2001) 544.
[346] P. T. Sprunger, Y. Okawa, F. Besenbacher, I. Stensgaard and K. Tanaka, STM investigation of the coadsorption and reaction of oxygen and hydrogen on Ni(110), Surf. Sci. 344 (1995) 98.
[347] G. Chiarello, A. Cupolillo, C. Giallombardo, R. G. Agostino, V. Formoso, D. Pacilé, L. Papagno and E. Colavita, Co-adsorption of oxygen and carbon monoxide on Ni(111), Surf. Sci. 536 (2003) 33.